Establishment of murine 3D bronchioalveolar lung organoids from adult somatic stem cells for organ development and disease modeling

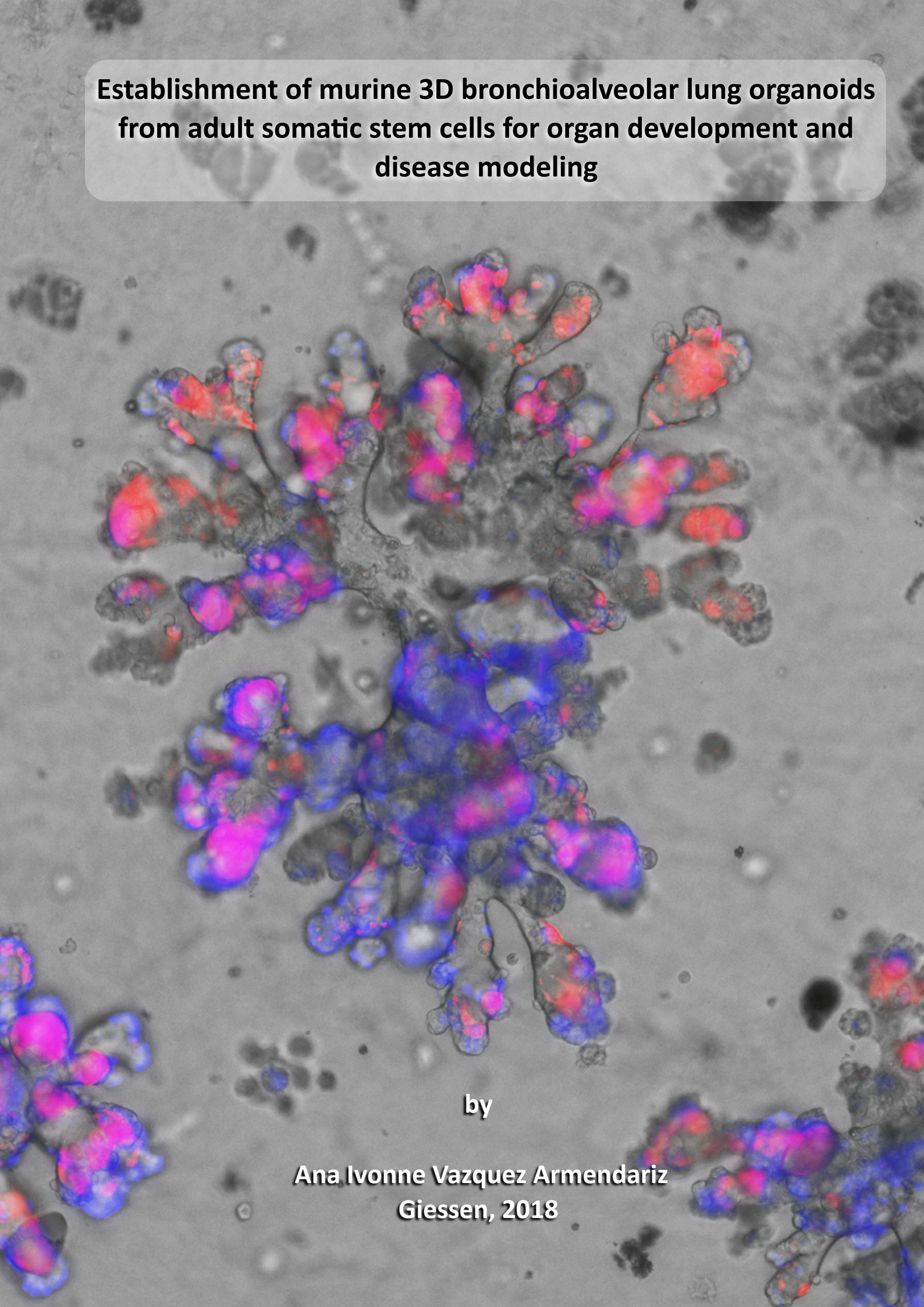

by

Ana Ivonne Vazquez Armendariz
Giessen, 2018

Establishment of murine 3D bronchioalveolar lung organoids from adult somatic stem cells for organ development and disease modeling

Inaugural dissertation

submitted to the Faculty of Medicine
in partial fulfillment of the requirements for the Doctor in Philosophy (PhD)

by

Ana Ivonne Vázquez Armendariz
born in Monterrey, México

Gießen, 2018

From the Department of Internal Medicine II of the
Justus-Liebig-University Gießen

Director: Prof. Dr. Werner Seeger

1. Supervisor and Committee Member: Prof. Dr. med. Susanne Herold, PhD
2. Supervisor and Committee Member: Prof. Dr. rer. nat. Michael Martin
Committee Member (Chair): Prof. Dr. Norbert Weißmann
Committee Member: Prof. Dr. med. Matthias Ochs

Date of Doctoral Defense:
26th of September 2018

TABLE OF CONTENTS

1. INTRODUCTION

1.1. Gross anatomy of the mammalian lung

The lung is a complex and highly specialized multicellular organ which main function is the process of gas exchange to release carbon dioxide (CO_2) and oxygenate the blood. Mouse models have shown to be relevant tools for a better understanding of the complicated cellular and molecular mechanisms underlying processes during lung homeostasis and disease. Nevertheless, the translation to humans involves thorough validation due to the explicit functional and physiological differences between species[1]. For instance, there are clear differences in respiratory frequency, total lung capacity, and tidal volume between mice and men. Additionally, the murine right lung is divided into four lobes - cranial, middle, caudal, and accessory - while the left lung has only one lobe. In contrast, the human right lung consists of three lobes: upper, middle, and lower, separated by the oblique and horizontal fissures, whereas the left lung is divided into upper and lower lobe by the oblique fissure[1,2].

Despite these differences, two comparable structural and functional compartments have been identified in the lower respiratory tract of both species: the conducting tract and the respiratory zone (Fig. 1-1). The conducting tract is comprised of the airways including the trachea, bronchi, and bronchioles which serve as air conducting structures. Beginning with the trachea, every conducting airway splits by bifurcation. In this process, the trachea subdivides into two main primary bronchi entering the left and right lung and continue to branch in a dichotomous (men) or monopodial (mice) pattern[3]. During dichotomous branching, the parental segment symmetrically divides giving rise to two smaller segments, whereas during asymmetrical monopodial branching, a larger parent segment progressively divides into smaller daughter segments. In both instances, continuous branching gives rise to the bronchial tree, which includes 17 to 21 and 13 to 17 airway generations in

men and mice, respectively. In men, cartilage rings are present in the intralobar bronchi but become continuously thinner with each division and slowly transition into bronchioles deprived of cartilage. In mice, this distinction between bronchi and bronchioles is not observed as cartilage rings are only present in the extrapulmonary airways[1,2,4]. Terminal bronchioles represent the most distal components of the conducting tract.

The respiratory zone encompasses the respiratory bronchioles, alveolar ducts, and alveolar sacs, the latter representing the functional respiratory units of the lung. In contrast to humans, mice generally do not have respiratory bronchioles and consequently most of the terminal bronchioles directly proceed into alveolar ducts lined by alveoli. At the end of the respiratory zone, the alveoli cluster to form alveolar sacs with gas exchange occurring through capillaries carrying blood from other parts of the body[1,2]. The total number of alveoli has been estimated to be around 486 million (men) and 4.2 million (mice) per adult lung providing in humans a vast surface area of approx. 143 m^2 for gas exchange[5,6].

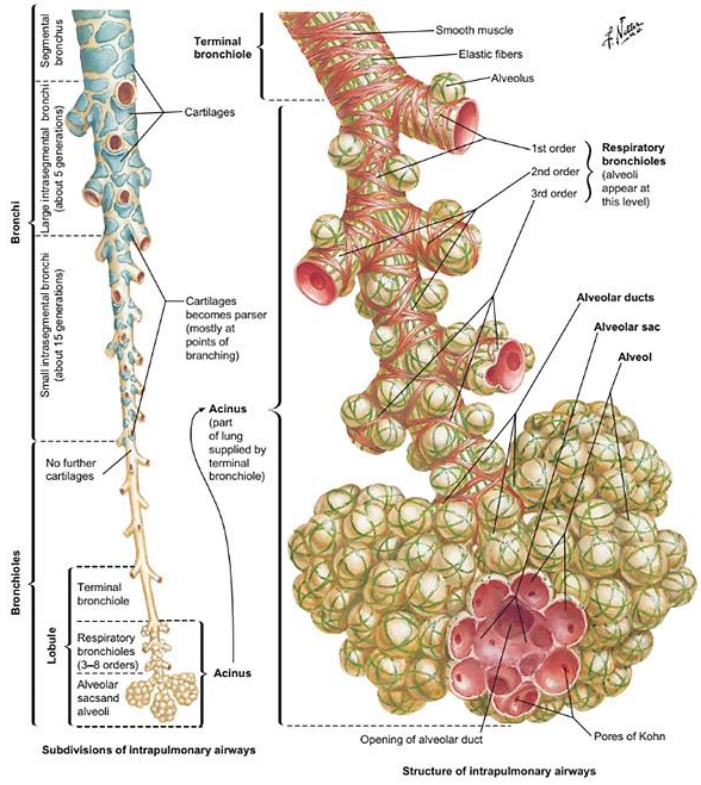

Figure 1-1. Lower respiratory tract[1]. The lower respiratory tract includes the trachea, bronchi, bronchioles and alveoli. In the lung, each bronchus divides into bronchi and continues to branch into smaller airways (bronchioles). The bronchioles end in the alveoli which form alveolar sacs. Image reproduced from Frank Netter, Atlas of human anatomy, 4th Edition, page 204 (2006).

1.2. Cellular and molecular basis of lung development

During development, the lung undergoes successive and morphologically distinct stages to achieve functionality. Lung development in mice begins at embryonic day (E) 9.5 (approx. day 28 in men) in the anterior foregut endoderm from where two primary buds arise[8,9]. In contrast, the trachea develops from a portion of the ventral foregut that separates from the dorsal portion, which will form the esophagus[10]. Human and murine lung development is divided into five overlapping stages based on sequential branching morphogenesis and mediated by signals coming from the surrounding mesenchyme: embryonic, pseudoglandular, canalicular, saccular, and alveolar (Fig. 1-2)[11,12]. Several mesenchymal signals regulate early embryonic cell fate decisions including the following signalling pathways: FGF, EGF, BMP, TGF-β, WNT, hedgehog, retinoic acid, and Notch[11,13]. The expression of these signals varies significantly along the proximal-distal axis; consequently, interference with any of these pathways severely impairs lung development processes, resulting in abnormal phenotypes[14–16].

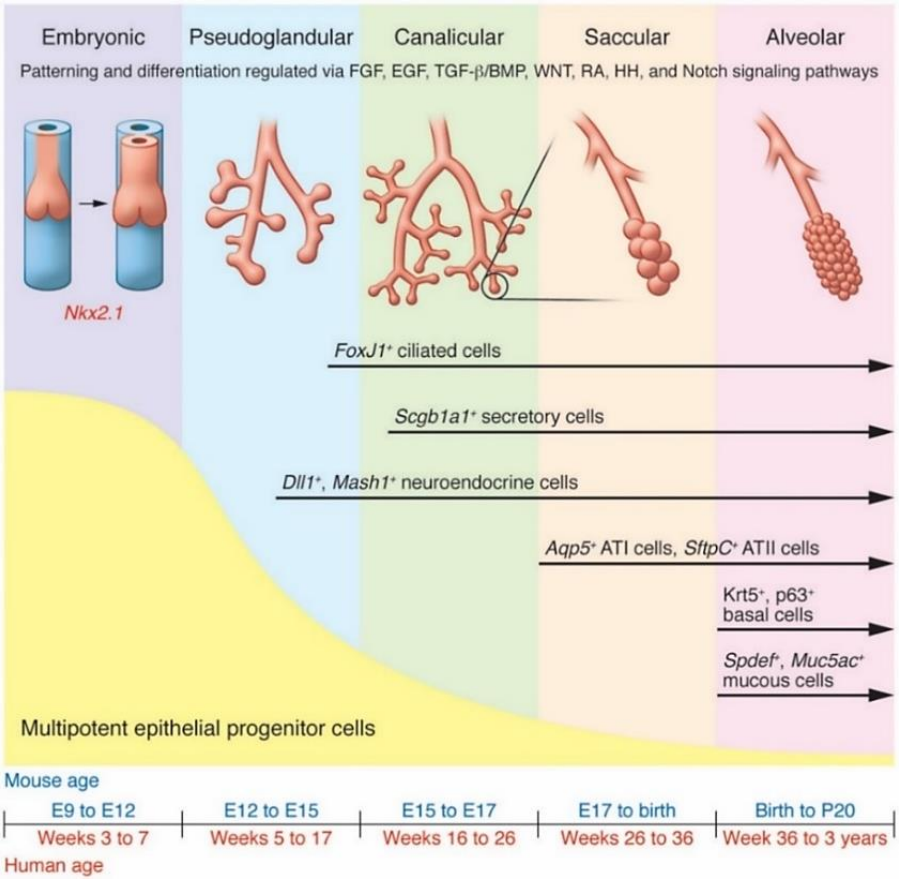

Figure 1-2. Embryonic, fetal, and postnatal development of the lung[17]**.** Lung development in mouse and human consists of five overlying stages: embryonic, pseudoglandular, canalicular, saccular, and alveolar. As branching progresses, epithelial progenitors give rise to epithelial cells with differentiated characteristics while gradually becoming more lineage restricted. FGF, Fibroblast growth factors; EGF, epidermal growth factor; TGF-β; transforming growth factor-beta; BMP, bone morphogenic protein; HH, hedgehog; RA, retinoic acid. Image reproduced from Rackley, C. R. *et al*. *J. Clin. Invest.* 122, 2724–30 (2012).

At the embryonic stage, the endoderm undertakes progressive cell fate decisions giving rise to epithelial progenitor cells with progressive lineage restriction. The exact timing for epithelial progenitor cell appearance is highly dependent on the region and cell type. During this period, local expression of the transcription factor Nkx2.1 is an early indicator of lung specification marking the ventral boundary in the anterior foregut where the trachea and primary lung buds appear[9,18,19]. Then, lung buds undergo several rounds of elongation and branching in a highly fixed pattern, creating a complex tree-like structure[20]. Interestingly, FGF10-deficient mice exhibit a severe main stem bronchi formation defect[3,21]. These data suggest that branching morphogenesis considerably relies on the local expression of FGF10 by the mesenchyme and its receptor expression, FGFR2, in the endoderm.

During the pseudoglandular stage, epithelial cells undergo proximal-to-distal differentiation. For instance, differentiated Foxj1-expressing ciliated cells and pulmonary neuroendocrine cells appear first in the proximal conducting airways and are found subsequently in distal regions of the airways[22,23]. Moreover, while expression of the transcription factor SOX2 characterizes proximal progenitors that differentiate into neuroendocrine, secretory, ciliated, and mucosal cells, distal progenitors located in the tips of the expanding tubes are defined by expression of SOX9 and ID2[24,25].

The following canalicular phase is characterized by additional peripheral branching, branch elongation and widening of distal airspaces[12]. Notably, capillaries begin to assemble around the airspaces and their contact with the overlying cuboidal epithelium induces epithelial flattening, providing the basis for formation of the first primitive air-blood barriers. Expression of secretoglobin 1A1 (SCGB1A1), a marker for secretory club cells, starts in the canalicular stage but functional club cells capable of protein secretion do not appear until the postnatal stage[22].

As lung development continues, the acinar epithelium begins its differentiation into alveolar epithelial type I cells (AECI), and the surfactant-producing type II cells (AECII)[26,27]. In the beginning of the saccular stage, airways end in large smooth-walled cylindrical structures, termed terminal saccules, which become more complex as gestational age progresses with continuous distal growth and subdivisions of airspaces. Finally, during the alveolar period, final maturation of the lung is achieved with most of the alveoli established and gas exchange surface area vastly increasing due to secondary septation. Alveolarization starts before birth in humans while, in mice, this process occurs exclusively postnatally[28,29]. Of note, basal and mucous cells emerge last during development and generally appear just prior to birth[30].

1.3. Cellular composition of the respiratory epithelium

The adult lung is an extremely intricate organ comprised of over 40 different unique cell types which provide multiple region-specific functions including formation of a physical barrier against inhaled pathogens, synthesis of host-defense compounds such as antimicrobial proteins and mucins, removal of pathogens and particles through mucociliary clearance, crosstalk with immune cells by cytokine and chemokine release, establishment of a thin air-blood interface to enable gas exchange, and production and secretion of pulmonary surfactant to reduce alveolar surface tension[9,31].

To achieve these and other crucial functions, the cellular composition of the lung epithelium varies along its proximal to distal axis (Fig. 1-3). In the lower respiratory tract of mice, the trachea, the two main bronchi, and the upper regions of the intralobar airways are lined by pseudostratified columnar epithelium comprised of club, ciliated, pulmonary neuroendocrine cells, and basal cells, interspersed by submucosal glands underneath the airway epithelium surface[32,33]. A major function of the secretory cells of the lower respiratory tract is the establishment of a defensive mucous layer on the epithelial cell surface to confine inhaled pathogens. In contrast to humans, goblet cells are scarce in the pseudostratified columnar epithelium of mice[4,34]. Also in humans, basal cell numbers gradually decrease towards the distal part of the bronchiolar tree whereas murine simple columnar epithelium in the intralobar bronchioles is already deprived of basal cells[17].

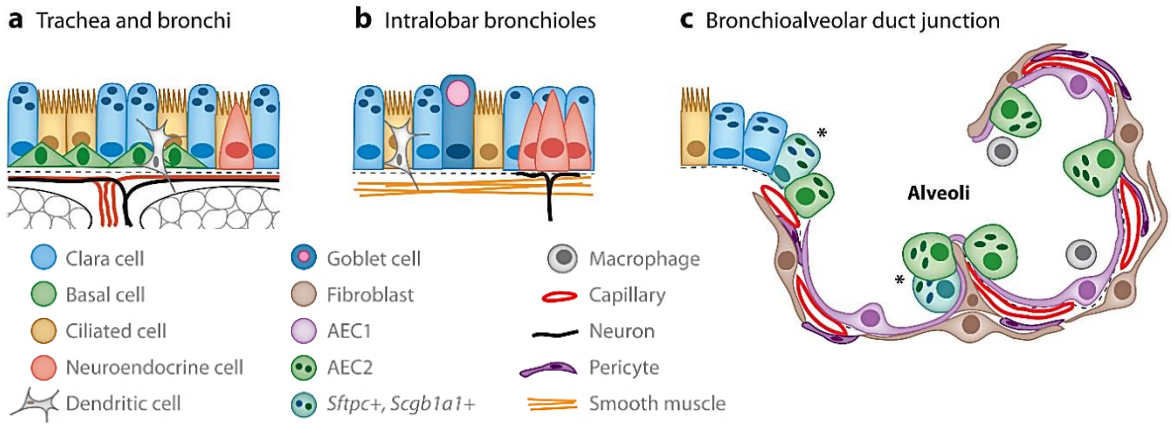

Figure 1-3. Cell components of the murine respiratory system[35]. (a) Tracheobronchial airways are formed by pseudostratified epithelium harbouring basal, ciliated, and secretory club cells. (b) Intralobar bronchioles are lined by a simple columnar epithelium containing ciliated and club cells. (c) The alveoli are lined by squamous AECI and cuboidal AECII. $SFTPC^{+}SCGB1A1^{+}$ bronchioalveolar stem cells are present in the bronchoalveolar duct junction and alveoli. AEC are closely associated with mesenchymal cells such as fibroblasts and endothelial cells. Image reproduced from Rock, J. R. & Hogan, B. L. M. *et al*. *Annu. Rev. Cell Dev. Biol.* 27, 493–512 (2011).

As described before, the trachea bifurcates into two main bronchi which subsequently subdivide into smaller bronchioles. At this point, the epithelium gradually turns into a simple columnar epithelium containing ciliated and secretory cells (club and globet cells) which drive removal of inhaled microorganisms and particulates by mucociliary clearance[35–37]. In contrast with the scarce pulmonary neuroendocrine cells found in the proximal airways, pulmonary neuroendocrine cells in the intralobar airways aggregate in structures termed neuroepithelial bodies. Pulmonary neuroendocrine cells are in contact with sensory nerve fibres and are thought to react to stimuli such as hypoxia and release bioactive substances (e.g. serotonin, calcitonin, and bombesin) which may in part regulate the immune response of epithelial cells, flow of air and blood, lung growth and development[32,34].

In the terminal bronchioles, the columnar epithelium is replaced by alveoli comprised of flat squamous AECI and cuboidal AECII. AECI account for about 95% of the total surface area of the lung however only represent a minor fraction of the total cell number in the alveoli due to their flattened squamous shape[38]. AECI are the prime sites for gas exchange and regulate fluid clearance[39]. Of note, AECII secrete pulmonary surfactant, a complex mixture of lipids, such as phosphatidylcholine and neutral lipids, and associated proteins: surfactant protein A, B, C, and D. Pulmonary surfactant is stored inside intracellular organelles, called lamellar bodies, and plays a critical role in reducing alveolar surface tension to prevent alveolar collapse at low pressures and providing host defense by binding of surfactant collectins to the surface of microbes which causes microbe aggregation, thereby enhancing pathogen uptake and killing by alveolar macrophages[40,41].

Besides the epithelium, the lung contains other cell types such as endothelium of veins, arteries, capillaries, and lymphatic vessels as well as pericytes, fibroblasts, vascular and airway smooth muscle cells, myofibroblasts, lipocytes, and mesothelium. These cells interact directly with the respiratory epithelium

modulating lung development, homeostasis, and repair[9,42–46]. For instance, epithelial platelet-derived growth factor α is required for the recruitment of smooth muscle cell progenitors to the distal tips of the airways, where they differentiate and deposit elastin to promote alveolarization[44].

1.4. Lung injury and regeneration

1.4.1. Epithelial progenitor/stem cells in the adult lung

Despite the slow epithelial turnover in the lung under homeostatic conditions, numerous studies have shown that to regain lung homeostasis and functionality following injury, region-specific epithelial stem/progenitor populations that reside in niches along the proximal-distal axis of the respiratory tree become activated and exhibit a remarkable capacity to self-renew, proliferate and differentiate into more specialized cells to restore the respiratory epithelium (Fig.1-4)[31,47–51].

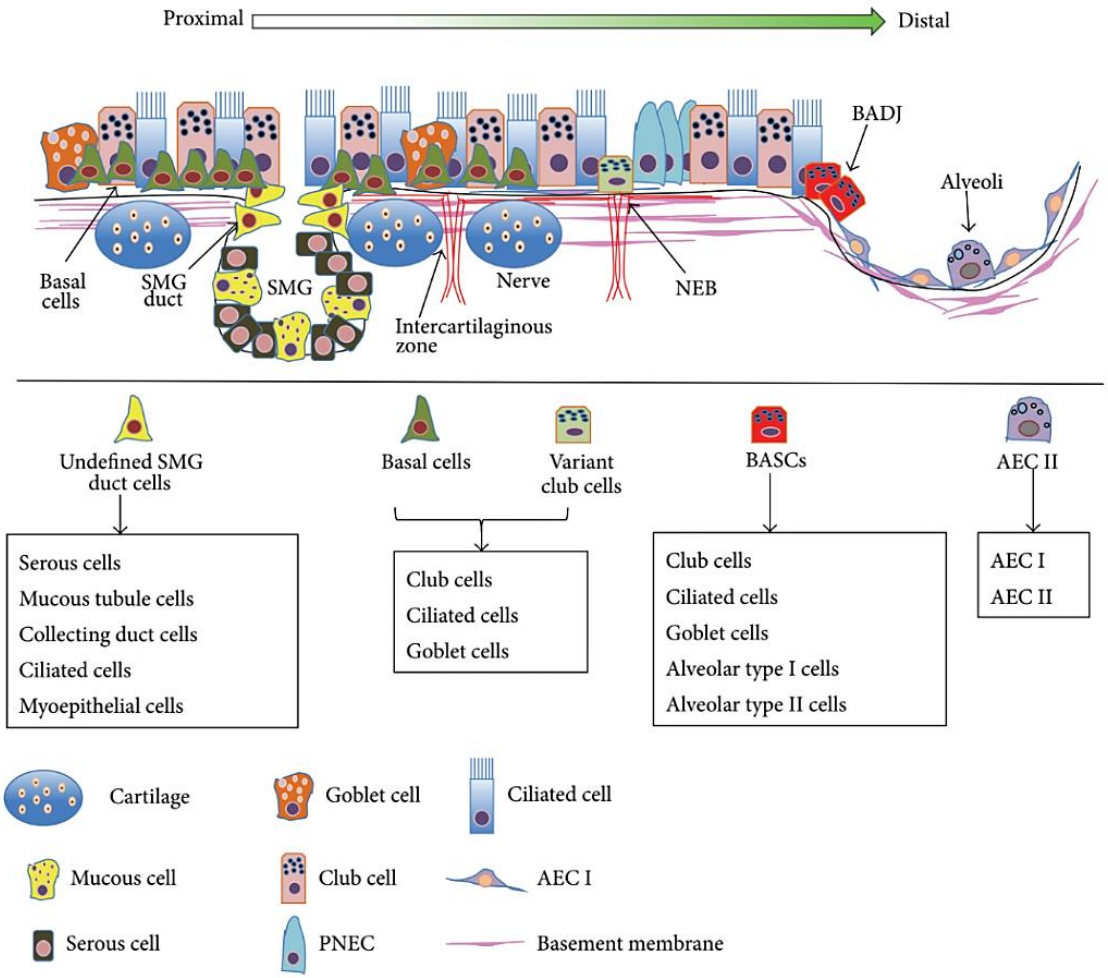

Figure 1-4. Stem/progenitor cells in the adult mouse lung[47]**.** Location, distribution, and differentiation of potential lung epithelial stem/progenitor cells along the proximal-distal axis of the respiratory epithelium. SMG, airway submucosal gland; NEB, neuroepithelial bodies; BADJ, bronchoalveolar duct junction; BASC, bronchioalveolar stem cells; PNEC, pulmonary neuroendocrine cells. Image reproduced from Li, F., He, J*., et al. Stem Cells Int.* 2015, 1–11 (2015).

Multiple stem/progenitor cell populations in the lung with different extent of plasticity or lineage commitment have been recently identified, and we have just begun to understand their lineage relations, differentiation potential, and their capacity to contribute to lung repair after injury. During normal turnover and upon injury, a subset of basal cells in the trachea and main stem bronchi has been described as the dominant epithelial stem cell type responsible for the regeneration of all main epithelial cell types in the pseudostratified epithelium including ciliated, goblet, and club cells[52–54]. Basal stem cells are characterized by expression of the cellular surface markers transcription factor transformation-related protein 63 (P63), cytokeratin 5 (KRT5), cytokeratin 14 (KRT14), and Aquaporin 3 (AQP3). This has been demonstrated by lineage tracing approaches with KRT5-CreERT2 mice in which $KRT5^-$ expressing basal cells could differentiate into club and ciliated cells during both steady state and repair[4]. Accordingly, nerve growth factor receptor (NGFR) and integrin alpha 6 (itgα6) were identified as potential cellular markers for the isolation of human basal cells with stem cell properties[48]. Additionally, a region-specific itgα6^{bright}Sca-1 (stem cells antigen-1)$^+$ALDH1 (aldehyde dehydrogenase-1)$^+$ basal cell subset showed self-renewal potential *in vitro* and participated in epithelial maintenance of the airways and in injury repair upon naphthalene treatment *in vivo*[53]. Besides basal cells, submucosal glands found in the trachea contain a fairly uncharacterized stem/progenitor cell population which has the ability to regenerate not only submucosal glands tubules and ducts but also the surrounding epithelium[50,55]. Also, along the proximal-distal axis of the airways, secretory club cells display progenitor potential by providing not only long-term

maintenance but also by contributing to bronchiolar epithelium renewal after injury[37]. Notably, lineage-tracing with SCGB1A1-CreERTM mice during homeostasis proved that SCGB1A1-expressing secretory club cells give rise to ciliated cells, although the contribution of club cells to basal cell regeneration was relatively low. Nevertheless, after ablation of $KRT5^+$ cells, a fraction of SCGB1A1-positive secretory cells dedifferentiate into basal-like stem cells with self-renewal and differentiation properties[56].

Numerous studies have recognized another subpopulation of $SCGB1A1^+$ cells, termed variant club (vClub) cells, which are resistant to toxic agents, lack CyP450-2F2 – a relevant xenobiotic-metabolizing enzyme – and show stem cell properties including the capacity for self-renewal and contribute to club and ciliated cell replenishment[49,57,58]. Besides the bronchial airways, vClub cells located at the bronchoalveolar duct junction of the distal bronchioles were shown to restore the airway epithelium following depletion of club cells by naphthalene *in vivo*[59].

Other bronchiolar progenitors include cell subsets that are enriched by flow cytometry based on their differential cell surface expression of EpCAM and Sca-1, and their autofluorescence (AF) characteristics. In response to naphthalene, a $CD45^-CD31^-CD34^-EpCAM^+Sca\text{-}1^{low}AF^{low}$ cell population was resistant and highly proliferative while $CD45^-CD31^-CD34^-EpCAM^+Sca\text{-}1^{low}AF^{high}$ cells were described as regular naphthalene-sensitive club cells[60]. In a similar study, epithelial progenitors isolated by FACS based on $EpCAM^{hi}$itgα6 integrin beta (itgβ)4^+CD24^{low} marker expression exhibited self-renewal potential and gave rise to both airway and alveolar cell lineages *in vitro*[61]. Following severe H1N1 influenza infection, two rare epithelial stem/progenitor cells of the distal airways, lineage-negative epithelial stem/progenitors (LNEP) and distal airway stem cells (DASC), become activated and migrate to the sites of injury within alveoli to support lung repair. LNEP are defined by the surface marker signature itgβ$4^+CD200^+CD14^+$ whereas DASC co-express P63

and KRT5. Transplantation of LNEP and DASC into influenza-infected mice, not only showed a substantial engraftment of these stem cells into the injured lungs but also differentiated into bronchiolar and alveolar epithelial cell lineages[62–65].

At the bronchioalveolar duct junction (BADJ), the bronchioalveolar stem cells (BASC) represent another important stem/progenitor cell population which co-express SCGB1A1 and surfactant protein C (SFTPC) and can differentiate into club cells, AECII, and AECI *in vitro*[51,59]. For instance, BASC were able to regenerate the respiratory epithelium following lung injury induced by exposure to influenza virus, naphthalene, and bleomycin[66,67]. Diverse cell surface markers have been identified for the isolation and identification of BASC including Sca-1, CD24, and itgα6β4[51,60,68–72]. Moreover, BASC were also enriched in a $EpCAM^{+}Sca\text{-}1^{low}CD24^{low}$ cell subpopulation[70]. In line, a distal epithelial stem/progenitor cell fraction ($EpCAM^{+}Sca\text{-}1^{low}itg\alpha6\beta4^{+}CD24^{low}$) was found capable of self-renewal and gave rise to airway and alveolar epithelial cells[71].

In the alveoli, a subpopulation of AECII have been referred to as stem/progenitor cells for squamous AECI in the adult lung by *in vitro* cell proliferation and clonogenic assays, *in vivo* epithelial injury repair, and lineage tracing analysis[4,73–77]. In addition, expression of itgα6β4 might represent a potential biomarker for stem/progenitor cells since an AECII subset containing SFTPC-$itg\alpha6\beta4^{+}$ cells was discovered in the alveolar epithelium and contributed to AECI generation in the alveoli *ex vivo*[78].

Proximal

Distal

Stem/progenitor cell	Marker expression
Basal cells	P63, KRT5, KRT14, NGFR, AQP3
Duct cells	KRT5, KRT14, KRT18
Club cells	SCGB1A1, CYP2F2^{hi}
vClub cells	SCGB1A1, CYP2F2^{-}
Bronchiolar progenitors	EpCAM^{+}Sca-1^{low}AF^{low}
Multipotent epithelial progenitors	EpCAM^{hi}itgα6β4^{+}CD24^{low}
LNEP	itgβ4, CD200, CD14, ΔNp63
DASC	P63, KRT5, KRT6
BASC	SCGB1A1, SFTPC, Sca-1, CD34
integrinα6β4 progenitors	itgα6, itgβ4
AECII	SFTPC

Table 1-1. Putative stem/progenitor cell populations of the adult murine lung epithelium[31]. Markers used to define the different stem/progenitor cells along the proximal-distal axis of the murine lung. LNEP, lineage-negative epithelial stem/progenitors; DASC, distal airway stem cells; BASC, bronchioalveolar stem cells. Modified from Kotton, D. N. & Morrisey, E. E. *et al. Nat Med* 20**,** 822–832 (2014).

Although less well-characterized, several cellular markers have been identified for the isolation of human lung stem cells including AQP3, c-kit, NGFR, itgα6, Lgr6, HTII-280, ICAM-1[4,48,50,52,73,79–81]. For instance, a subset of basal cells and AECII isolated by FACS analysis of NGFR/itgα6 and HTII-280 expression, respectively, were identified as potential human lung stem cells[48,73]. Similarly, c-kit^{+} cells and E-Cad/Lgr6^{+} cells were recognized as human stem cells due to their capacity for self-renewal and differentiation *in vitro* and *in vivo*[80,82]. However, mainly due to lack of lineage tracing methodologies in the human system, none of these markers were found to robustly define a human lung stem cell giving rise to differentiated epithelial cells in the human lung.

Overall, the identification of several self-renewing stem/progenitor cell populations highlights the complexity of the cellular networks involved in lung epithelial repair. For instance, distinct stem/progenitor cell population(s) are activated upon regenerative signals depending on the injury type, severity, and affected region (Table 1-1). Nonetheless, some of the characterized stem/progenitor candidates may at least to some extent represent the same cell types, phenotypic variants or subpopulations of a single cell population. For example, this could be the case for the LNEP and DASC that arise upon influenza infection, and BADJ-associated vClub cells and BASC that endure naphthalene injury.

1.4.2. Epithelial progenitor/stem cells niches in the adult lung

Stem cell niches refer to local tissue-specific microenvironments that maintain or activate stem cells during homeostasis or upon injury, respectively. Distinct stem cell niches have been discovered in the adult lung providing signals for maintenance, proliferation, and differentiation of epithelial progenitor/stem cells[83]. As described by our laboratory and others, FGF10 has recently been suggested to play a dominant role in the crosstalk between mesenchymal and epithelial cells in the developing lung and in response to injury[84,85]. Communication among lung stem cells and their niches yields an effective system vital for retaining stem cell potential that contributes to cell fate and migration decisions[33,55,86]. Through multiple murine injury models and lineage tracing approaches, six putative stem cell niches have been identified in the adult lung including the duct of submucosal glands, surface basal cells in the intercartilaginous zone underlying the proximal airways[4,48,87], neuroepithelial bodies residing in the bronchi and bronchioles[57,76,86,88], BADJ regions[51,59,60,68,70], and the alveolar epithelium[73,77,89].

Numerous data have demonstrated that BADJ is the stem cell niche for BASC, which are capable to regenerate both airway and alveoli lineages after injury. During lineage tracing analysis with SCGB1A1-reporter mice, SCGB1A1-labeled cells failed

to promote alveolar repair following hyperoxia-induced lung injury[49]. Nonetheless, upon murine lung injury with influenza virus infection, naphthalene, or bleomycin exposure, BASC were capable of self-renewal and repair of the epithelium *in vivo* and gave rise to club cells and AEC *ex vivo*[66,67]. These studies suggest that the potential of BASC to regenerate injured respiratory epithelium might be injury-specific and rely on distinct microenvironmental cues at BADJ.

At the end of the respiratory tree, AECII have been proposed as the major stem/progenitor cells responsible for self-renewal and regeneration of AECI following injury although AECII are not capable to give rise to other distal or proximal cells[4,73–77]. It has been suggested that primary platelet-derived growth factor receptor alpha^{+} (PDGFRα) lung resident cells include a population of lipofibroblasts which reside in close proximity to AECII. Lipofibroblasts may play a significant role in epithelial-mesenchymal crosstalk during alveolar development and serve as a stem cell niche in the lung[73,90].

1.4.3. Role of tissue-resident alveolar macrophages during lung development and repair

Two major classes of lung macrophages have been recognized, tissue resident alveolar macrophages (TR-Mac) and interstitial macrophages. During embryogenesis, fetal TR-Mac F4/80^{int}CD11b^{hi}Ly6c^{+} derived from embryonic progenitors coming from the yolk sac reach the developing lung at E10.5[91–94]. Despite the dogma that tissue macrophages constitutively derive from monocytes, recent publications using monocyte fate mapping, parabiosis, and adoptive transfer strategies have shown that, tissue macrophages, including TR-Mac, are capable to proliferate and self-renew independently of circulating monocytes[95–97].

Due to the localization in the alveolar lumen, TR-Mac are the first line of defense against air-borne pathogens including bacteria, fungi, and viruses mainly by clearance through phagocytosis of infected cells[98–102]. Besides phagocytosis of foreign particles, TR-Mac are also essential for surfactant catabolism. In this regard, the growth factor GM-CSF (granulocyte-macrophage colony stimulating factor) has been shown to be vital for TR-Mac maturation through activation of the nuclear receptor PPAR-γ which also drives cholesterol metabolism, β-oxidation of fatty acids, lipid transport, storage and degradation[103].

1.4.4. Growth factors driving lung generation and regeneration

Growth factors are small proteins that diffuse through short distances and induce diverse cellular responses through activation of different signaling pathways. During lung development, growth factors such as FGF10[21], VEGF[104], PDGF[105], and TGFβ[106] play a crucial role in branching morphogenesis, cell proliferation and differentiation. Furthermore, after lung injury, growth factor responses activate repair mechanisms aimed to restore lung homeostasis[107,108]. For instance, hyperoxia-induced injury in mice increases FGF7 and FGF2 levels in the lung, promoting AECII proliferation and enabling repair of the damaged epithelium[108].

As mentioned in the previous section, GM-CSF is a growth factor essential for differentiation and function of myeloid cells. In the lung, GM-CSF is involved in several cell functions including antiviral and antimicrobial responses, and surfactant metabolism[109–111]. Besides being produced by myeloid cells, GM-CSF is highly released by AECII under inflammatory conditions[112]. Moreover, after viral infection, AEC-derived GM-CSF has been shown to promote epithelial repair and restoration of barrier function by proliferation of AECII[113]. Based on these observations, it is of great interest to investigate the role of GM-CSF on proliferation and differentiation of distal lung stem/progenitor cell populations during lung homeostasis and after injury.

1.4.5. Lung organoid systems to model lung development and disease

Modern technology has led to the identification and characterization of several stem/progenitor cells crucial for organ development and regeneration in mammals. Nonetheless, several cellular and molecular processes can not be easily studied *in vivo* and traditional 2D *in vitro* cultures lack the conditions necessary to study distinct features involved in organ formation and regeneration, such as intercellular crosstalk and cell polarization. Consequently, three-dimensional (3D) culture systems have recently emerged as a valuable platform for the better understanding of organogenesis and disease processes *in vitro*[114]. The term "organoids" refers to 3D structures derived from single stem cells which differentiate into organ-specific cells types that self-organize to form a structure resembling the cellular organization and functionality of the organ of origin[115]. Notably, these systems can be used to study embryonic developmental mechanisms, model tissue during homeostasis and disease, and define and characterize stem cell-niche interactions[116,117].

Organoids can originate from three main stem cell sources: embryonic stem cells, induced pluripotent stem cells (iPSC) and adult somatic stem cells[115,118]. Using different protocols it is now possible to produce tissue-specific organoids derived from human and/or murine mammary gland[119], bone[120], small intestine[121,122], stomach[123,124], colon[125], liver[126,127], pancreas[128], retina[129], brain[130], thyroid[131], heart[132], prostate[133], and lung[48,73,134,135]. Therefore, 3D organoid models have recently developed as a powerful technology for *in vitro* modeling of development and disease, as well as for drug discovery[136,137].

Regarding the lung, organoid models have been developed to visualize and study processes of generation and regeneration of the lung with the future vision to translate the knowledge gained from these models into therapeutic strategies. Some of the adult epithelial progenitor/stem cells described in section 1.4.1 can generate organoids which partially reproduce the complexity of lung structures

when cultured in an appropriate microenvironment (Fig. 1-5). One crucial requirement for 3D organoid formation and cell differentiation is the use of hydrogels, such as Matrigel, which contain a mixture of extracellular matrix components[138]. Such extracellular matrix in combination with air-liquid interface culture systems have been shown to boost lung organoid growth, polarization and cell differentiation[48,139,140]. To date, lung organoids are generated in 3D cultures from single stem/progenitor cells by addition of growth factors such as EGF and retinoic acid, or by co-cultivation with feeder cells including fibroblasts, endothelial cells, or smooth muscle cells (Table 1-2)[48,73,134,135].

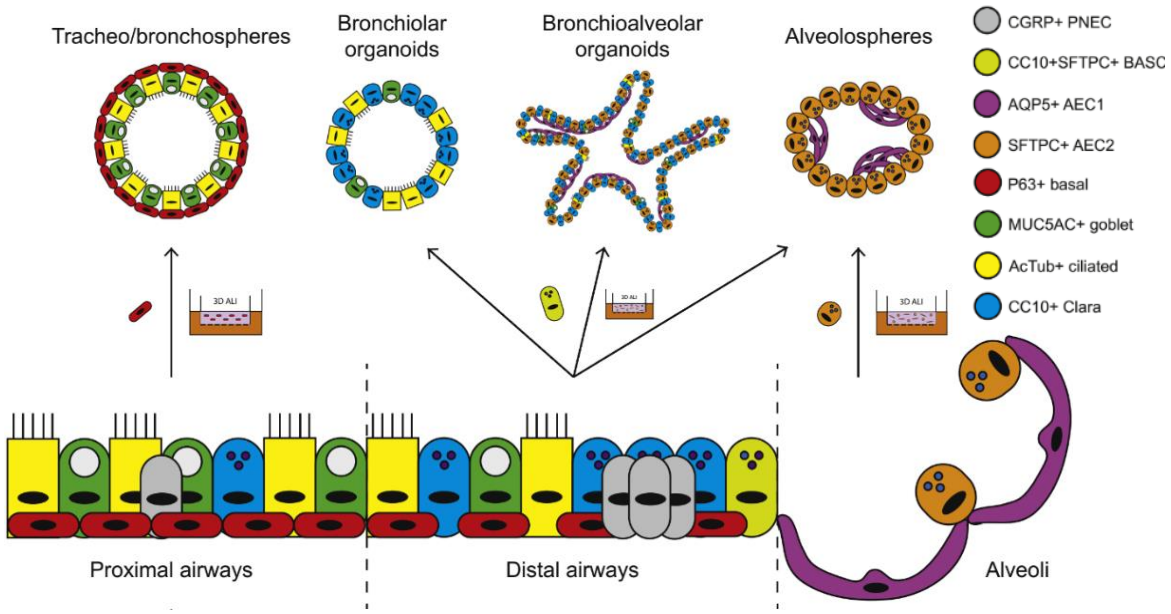

Figure 1-5. Murine lung organoid models[141]. Lung organoids generated from epithelial cells isolated from different respiratory compartments. $P63^{+}$ basal cells are capable of giving rise to trachea/bronchospheres, AECII form alveolospheres while $SCGB1A1^{+}SFTPC^{+}$ BASC generate bronchiolar organoids, bronchioalveolar organoids, and alveolospheres. Image modified from Nadkarni, R. R., Abed, S. & Draper, J. S. *et al. Biochem. Biophys. Res. Commun.* 473**,** 675–682 (2016).

For instance, isolated murine basal cells expressing P63 and NGFR generate organoids termed tracheospheres. After 14 days of culture, these spherical

organoids consist of a $P63^+KRT5^+KRT14^+NGFR^+$ basal cell layer enclosed by another layer of $KRT8^+$ differentiated goblet and ciliated cells on the luminal side[48,142]. Due to its close resemblance with the cell composition of the proximal airways, tracheospheres have been proposed as models for the screening of new drugs and small molecules aimed to treat lung diseases, such as asthma and CF which are associated with inflammation, cellular stress, and a significant increase of secretory cells at the expense of ciliated cells[35]. Using clonal tracheosphere assays derived from Foxj1-GFP transgenic mice in combination with *in vivo* approaches, Tadokoro and colleges found that an increase in IL-6/STAT3 signaling favors basal cell differentiation into ciliated cells rather than secretory cells[54]. In similar studies, treatment with BMP signalling pathway inhibitors led to higher cell proliferation and colony formation efficiency but prevented basal cell differentiation[143,144].

Human basal cells also form organoids named tracheospheres, bronchospheres or nasospheres depending on whether the basal cells are derived from the trachea, large airways or nasal epithelium, respectively. As in murine tracheospheres, these organoids contained $P63^+KRT5^+$ basal cells and functional ciliated and goblet cells[145–147]. In this regard, screening of 5000 different compounds in human bronchospheres identified Notch signaling pathway as a possible regulator of basal cell differentiation. For instance, inhibition of NOTCH1 receptor let to a significant increase in the expression of basal cell markers whereas blocking of NOTCH2 receptor enabled the expression of ciliated markers instead of goblet cell markers[146]. These data not only supported previous observations depicting Notch as a relevant regulator of secretory and ciliated cell differentiation *in vivo*[148,149] but also brought novel information on Notch signaling activation. In addition, using air-liquid interface and organoid cultures, Gao and colleagues identified through CRISPR/Cas9 genome editing of primary human basal cells the role of transcription factor grainyhead-like 2 in regulating barrier function and differentiation of ciliated cells [150].

In diverse studies, secretory club cells capable of forming organoids were isolated by flow cytometry based on the expression of surface cell markers. McQualter and colleagues used the expression signature $EpCAM^{hi}itg\alpha6\beta4^{+}CD24^{low}$ for stem cell isolation and when co-cultured with primary $EpCAM^{-}Sca1^{+}$ lung stromal cells obtained three distinct types of organoids[61]. After 14 days in culture, 46% of the organoids were large and spheric with a single lumen (type A), 35% were small, dense, and lobular (type C) while 19% had a mixed phenotype, with multiple bud-like protrusions (type B). Type A and B organospheres comprised $P63^{+}$ basal cells, $Foxj1^{+}$ ciliated cells, and $Muc5ac^{+}$ goblet cells while these markers were absent in type C colonies. In contrast, type C organospheres contained primarily $SFTPC^{+}$ AECII-like cells whereas in type B colonies $SFTPC^{+}$ AECII were only located at the tips of the buds. Comparable data in which epithelial colonies exhibited three distinct morphologies was observed when SCGB1A1-CreER lineage traced murine cells were co-cultivated with a mouse lung stromal cell line and a TGFβ inhibitor[151].

Similarly, Kim and colleagues characterized a 3D co-culture model of BASC and a heterogeneous population of lung endothelial cells which gave rise to three different kinds of organoid structures defined according to the expression of SCGB1A1 (bronchiolar), SFTPC (alveolar), or both (bronchioalveolar)[152,153]. In this study, the 3D model was used to assess the role of the endothelial-derived BMP4-NFATc1-thrombospondin-1 signalling axis in BASC proliferation. The results indicate the potential of BASC to give rise to both alveolar and airway lineages and suggests that the alveolar differentiation can be augmented by thrombospondin-1 released by endothelial cells[134].

Alveolospheres are generated by co-cultivation of lung stromal cells with AECII isolated from lineage traced-$SFTPC^{+}$ cells or based on AECII surface markers. After 14 days of culture, alveolospheres were composed of two cell levels, an outer layer containing $SFTPC^{+}$ AECII and an internal layer comprised of AECI expressing the

differentiation markers Ager$^+$, PDPN$^+$, and Hopx$^+$[73,154]. In human lungs, AECII are defined based on the cell surface expression of EpCAM$^+$HTII-280$^+$[155]. Nevertheless, alveolospheres do not recapitulate the structural features of the alveolar compartment in the adult lung and neither mouse nor human AECII can be expanded efficiently in culture before seeding in Matrigel.

Human pluripotent stem cells (hPSC) can be obtained from human embryonic stem cells and induced pluripotent stem cells (hiPSC) and are able to self-renew indefinitely in culture while retaining the capacity to differentiate into almost any mature cell type in the human body[156,157]. For instance, hiPSC can be reprogrammed into adult somatic cells by addition of stage-specific growth factors to recapitulate signaling pathways involved in lung development[9,158]. Therefore, hiPSC-derived lung organoids may represent an attractive path for disease modeling. Such an organoid model could be used for drug screening of samples from patients with chronic asthma or CF to assess if epigenetic changes in the progenitors cells alters self-renewal and differentiation functions[159–161]. In this line, following step by step differentiation protocols, it has been possible to redirect murine and human PSC into lung progenitors[159,162,163], mature airway and alveolar cells[164], and to form an organized airway epithelium[161,165–167]. The most effective protocols first generate definitive endoderm, then anterior foregut endoderm, followed by ventral anterior foregut endoderm and NKX2.1$^+$ lung progenitors[168]. Regarding human embryonic stem cells, the pseudoglandular or canalicular phase of the developing lung has been shown to be the best source of progenitors with the potential to give rise to airway and alveolar cell lineages[169,170].

So far, only a few studies have described the generation of lung organoids derived from hPSC *in vitro*. For example, hPSC-derived lung organoids were developed using a Matrigel-coated scaffold and were then transplanted into mice to achieve further airway differentiaiton[171]. Yet, this approach failed to generate alveolar cells implying

the need for more cell-specific protocols. In another study, Carboxypeptidase M (CPM) was identified as a cell-surface marker for ventral anterior foregut endoderm that overlapped with NKX2.1 expression. 3D culture of CPM-expressing cells with alveolar-associated growth factors and human lung fibroblasts gave rise to alveolar epithelial organospheres comprised of NKX2.1 and CPM-expressing cells, along with differentiated cells such as AQP5$^+$ AECI and SFTPC$^+$ AECII[172]. Such alveolar organospheres were comparable in structure and cell composition to alveolospheres generated from AECII in the adult murine lung[73]. In addition, Dye *et al* provided a protocol for hPSCs differentiation into multi-lineage organoids consisting of epithelial and mesenchymal compartments[135]. In this approach, the authors at first followed previous protocols to form organospheres. At this point, the hedgehog signaling pathway was stimulated to enhance NKX2.1 expression allowing organospheres to form complex structures termed human lung organoids (HLO)[135]. HLO developed proximal airway-like epithelial tubules harboring several cell types found in the airways such as basal, ciliated, and club cells. Even though HLO contained distal-like epithelial cells that co-expressed SFTPC/SOX9 and Hopx/SOX9, this model did not generate differentiated AEC.

Lung organoid model	Cell composition or markers	Main organoid-forming cell type	Feeder cell types
Tracheo/broncho-spheres	Basal, ciliated, and goblet cells	Basal cells	HLF, HUVEC
Bronchiolar organoids	Club, ciliated and goblet cells	BASC	LuMEC
Bronchioalveolar organoids	Club, ciliated, goblet, AECI, and AECII	BASC	HLF, HUVEC, LuMEC
Alveolospheres	AECI and AECII	AECII, BASC	PDGFRα$^+$ lung stromal cells, LuMEC
Alveolar organospheres	AECI and AECII	NKK2.1+SFTPC+CPM+ alveolar progenitors	HLF
HLO	NKK2.1, SOX2, SOX9, P63, SCGB1A1, *Muc5ac Hopx,* ECAD, VIM, αSMA	NKK2.1$^+$FOXA2$^+$ CPM$^+$ lung progenitors	hPSC-derived fibroblasts

Table 1-2. Properties of known lung organoid models[141]**.** Lung organoids derived from primary cells and hPSC, organoid cell composition and feeder cells. HUVEC, human umbilical vein endothelial cells; HLF, human lung fibroblasts; LuMEC, primary mouse lung endothelial cells; VIM, vimentin; ECAD, E-Cadherin; CPM, carboxypeptidase M. Modified from Nadkarni, R. R., Abed, S. and Draper, J. S. *et al. Biochem. Biophys. Res. Commun.* 473**,** 675-682 (2016).

Even with the significant advances in 3D culture technology, none of the models formerly described in this chapter recapitulates the structural complexity of the distal lung. Current lung organoid models mostly consist of only epithelial cells, and in rare cases, the mesenchymal compartment. In addition, tissue-resident cells of myeloid origin, which are important mediators of lung development, immune response and tissue regeneration, remain absent.

In this line, epithelial stem/progenitor cells of the distal lung (EpiSPC) with a high proliferative response to influenza A virus (IAV)-induced lung injury have been recently described by our group[85]. Notably, EpiSPC have the capacity to self-renew and form organoids in Matrigel cultures in the presence of FGF10 and HGF. Following orthotopic transplantation into IAV-injured murine lungs, EpiSPC regenerate the distal lung tissue and give rise to AECI, thus demonstrating inherent stem cell properties. Hence, establishment of a lung organoid model that combines EpiSPC and mesenchymal cells to best represent the structural and cellular composition of the distal lung was envisioned.

2. AIMS OF THE WORK

3D organoids currently reported in the literature only recapitulate certain morphological and cellular features of the lung. A model that fully recapitulates the complexity of the proximal and distal compartments of the lung is critically missing.

Therefore, the aims of the present work were:

1. Establishment of a robust protocol for the isolation and 3D co-culture of EpiSPC and lung-resident mesenchymal cells (rMC) to generate lung organoids comprised of well-organized tubular and saccular structures representing the 3D organization of the airways and alveoli, respectively.

2. Successful integration of tissue-resident yolk-sack derived macrophages into the forming lung organoids to complement the system with further relevant lung-resident cell types and allow the study of intercellular cross-talk mechanisms, particularly those driving lung development and repair *in vivo*.

3. Test the applicability of the *in vitro* system to study lung development by using lung organoids derived from BASC and rMC isolated from transgenic animals as well as morpholino addition to inhibit the activity of an important mRNAs or microRNAs involved in the regulation of lung generation.

4. Investigate the impact of growth factors such as GM-CSF on stem/progenitor cell proliferation and differentiation during co-culture conditions to assess key factors known to be involved in alveolar repair following pathogen-induced lung injury and visualize the influence on distinct stages of lung organoid formation.

5. Effective infection of lung organoids with IAV to further study and visualize processes of lung infection, injury and repair at high resolution and at a single-cell level.

3. METHODS

3.1. Mice strains

Wildtype (WT) *C57BL/6* mice were purchased from Charles River Laboratories. *B6.129 [Cg)-Gt(ROSA)26Sor*$^{tm4(ACTB-tdtomato-EGFP)Luo}$*/J]* (mTmG) mice, GM-CSF deficient (GM-CSF$^{-/-}$) *[B6.129S-Csf2*^{tm1Mlg}*/J]* mice and GM-CSF receptor β-deficient (GM-CSFRβ$^{-/-}$) *[B6.129S1-Csf2rb*^{tm1Cgb}*/J]* mice were obtained from Jackson Laboratory. Transgenic mice overexpressing GM-CSF (SPC-GM) in AECII were generated in GM-CSF deficient mice by expression of a chimeric gene containing GM-CSF under control of the human SP-C promoter and were a gift from Dr. Jeffrey Whitsett (University of Cincinnati, OH). Ai9 *[B6.Cg-Gt(ROSA)26Sor*$^{tm9(CAG-tdtomato)Hze}$*/J]* (mT) mice expressing tdTomato after Cre-mediated recombination, PDGFRα^{EGFP} *[B6.129S4-Pdgfra*$^{tm11(EGFP)So}$*/J]* expressing eGFP from the endogenous *Pdgfra* locus (PDGFRα^{GFP}), and TOPGAL *[Tg(TCF/Lef1-lacZ)34Efu/J]* reporter mice were provided by S. Bellusci (ECCPS, University of Giessen, Giessen, Germany). SCGB1A1^{mCherry}SFTPC^{YFP} reporter mice *[B6;129-Sftpc*$^{tm1.1(2A-YFP-2A-tTA-N)Thbr}$*Scgb1a1*$^{tm1.1(2A-mCherry-2A-tTA-C)Thbr}$*]* were generated by T. Braun (Max Planck Institute for Heart and Lung Research, Bad Nauheim, Germany). Mice were housed under pathogen-free conditions.

3.2. Model establishment

3.2.1. Primary murine AEC isolation

Primary murine lung cell isolation was modified from Herold, S. *et al*[173]. Mice were anesthetized with isoflurane inhalation and killed by cervical dislocation. To obtain lung homogenates, 1.5 ml of dispase was installed through the trachea of HBSS perfused lungs followed by lung harvest and 40 min incubation in dispase. Afterwards, the heart and trachea were removed and lungs were homogenized (GentleMACS, MACS Miltenyi Biotech) in DMEM/2.5% HEPES with 0.01% DNase I and filtered subsequently through 100 µm and 40 µm nylon filters. Lung

homogenates were then centrifuged for 10 min with 500 G at 4°C. To remove red blood cells (RBC), cells were resuspended in RBC lysis buffer (0.15 M NH_4Cl, 10 mM $NaHCO_3$, 1 mM EDTA, pH 7.4) for 90 s. Lysis was stopped by addition of DMEM containing 10% FCS and centrifugation with 500 G for 10 min at 4°C. For leukocyte/endothelial cell depletion, homogenates were resuspended in DMEM and incubated with the appropriate volume of biotinylated rat anti-mouse CD45, CD16/32, and CD31 antibodies for 30 min at 37°C. Cells were centrifuged for 10 min with 500 G at 4°C and resuspended in DMEM containing biotin-binding magnetic beads for 30 min with rotation at room temperature (RT) followed by magnetic separation for 15 min at RT. CD45/CD16/32/CD31-negative cells in the flow-through were collected and washed once with DMEM and quantified to be used for further analysis.

3.2.2. EpiSPC and rMC cell sorting

Multicolor flow cytometry and cell sorting were performed on a BD FACS Aria™ III cell sorter using DIVA software (BD Bioscience). For single cell suspension, cell sorting and analysis, cells were pelleted with 500 G, 10 min at 4°C, blocked with gammaglobulins (Sandoglobulin) and stained with the corresponding fluorescence-labeled antibodies for 15 min at 4°C in MACS buffer (PBS, 7.4% EDTA, 0.5% FCS pH 7.2). Cells were washed once with MACS buffer and centrifuged with 500 G for 5 min at 4°C, resuspended in 300-500 µl of MACS buffer and filtered into FACS tubes for cell analysis and sorting using an 85 µm nozzle.

Unless otherwise specified, rMC and EpiSPC-enriched population were isolated with the following antibody cocktail:

Antibody	dilution
CD31 Alexa 488	1:50
CD45 FITC	1:50

CD326 (EpCAM) APC/Cy7	1:50
CD24 PE/Cy7	1:200
Sca-1 PB	1:50

3.2.3. EpiSPC and rMC co-culture

Flow-sorted EpiSPC and rMC were pelleted by centrifugation with 500 G for 5 min at 4°C. Cells were resuspended in EpiSPC medium (α-MEM, 10% FCS, 100 U/ml penicillin, 0.1 mg/ml streptomycin, 2 mM L-glutamine, 1x Insulin-Transferrin-Selenium, 0.0002% heparin) and quantified. For co-cultivation, the cell concentration was adjusted to $5x10^3$ EpiSPC and $3x10^4$ rMC per 25 µl of EpiSPC medium per 12 mm cell culture insert (Millipore). EpiSPC and rMC were mixed and diluted with cold growth factor reduced Matrigel® (Corning) at an 1:1 ratio as described before[85]. Cell suspension was gently mixed, avoiding the formation of bubbles. For each insert, 90 µl of mixed EpiSPC and rMC in Matrigel were added on top of a 0.4 µm filter membrane, placed in a 24-well plate, and incubated for 5 min at 37°C for polymerization of Matrigel. 350 µl of EpiSPC medium were added per well to obtain an air-liquid interface and cultures were incubated at 37°C with 5% CO_2 for three weeks to obtain fully formed lung organoids. Medium was changed three times per week. Given data is representative for three independent experiments.

3.2.3.1. mTmG co-cultures

For clonal expansion experiments, EpiSPC were isolated from WT and mTmG reporter mice, mixed at the ratio of 1:4 and co-cultured with rMC for three weeks. For rMC characterization, rMC were isolated from mTmG reporter mice and co-cultured with WT EpiSPC for three weeks.

3.2.3.2. SCGB1A1^{mCherry}SFTPC^{YFP} co-cultures

SCGB1A1^{+}SPC^{+}, SCGB1A1^{+}SFTPC^{-} and SCGB1A1^{-}SFTPC^{+} cells isolated from an EpiSPC-enriched population were co-cultured with rMC at a concentration of 1×10^3 or 5×10^3 cells per insert. In these experiments, cells were isolated based on the endogenous mCherry and YFP fluorescence and using the following antibodies:

Antibody	dilution
CD31 PB	1:50
CD45 Horizon™ V450	1:50
CD326 (EpCAM) APC/Cy7	1:50
CD24 PE/Cy7	1:200
Sca-1 APC	1:50

3.2.3.3. Co-culture of EpiSPC with PDGFRα^{GFP} rMC

PDGFRα^{GFP} rMC were co-cultured with EpiSPC isolated from WT or mTmG mice. Additionally, rMC were isolated and co-cultured with EpiSPC based on GFP expression: PDGFRα negative, low and high.

The following antibodies were used for PDGFRα^{GFP} rMC isolation:

Antibody	dilution
CD31 PE	1:50
CD45 APC/Cy7	1:50
CD326 (EpCAM) APC/Cy7	1:50
Sca-1 PB	1:50

3.2.3.4. GM-CSF$^{-/-}$ and GM-CSFRβ$^{-/-}$ co-cultures

Sorting of GM-CSF$^{-/-}$ cells was performed as described before in point 3.2.2. After isolation, co-cultures were followed for three weeks and EpiSPC proliferation was assessed by measuring of organoid diameters and quantity.

3.3. Experimental protocols

3.3.1. Organoid IAV infection

For IAV infection of the organoids, EpiSPC/rMC co-cultures were washed once with PBS and infected with mock or 5x10^6 pfu of WT-SC35M, Cre-SC35M$_{NS1_2A_Cre_2A_NEP}$[174] (H7N7, mouse-adapted) or A/PR/8/34 (PR8) (H1N1, mouse-adapted) in 600 µl of ice-cold PBS for 2 h at RT with gentle agitation. After 30 min incubation at 37°C with 5% CO_2, virus-containing PBS was removed and inserts were washed twice with PBS. Inserts were placed in infection medium (α-MEM, 0.2% BSA, 100 U/ml penicillin, 0.1 mg/ml streptomycin, 1x ITS, 2mM L-glutamine, 0.0002% heparin) and incubated for the indicated times. Presented data is representative of three independent experiments.

3.3.2. Organoid dissociation

To assess organoid cell composition and infection, organoids were removed from cell culture inserts by addition of ice-cold PBS and rigorous pipetting, collected in 1.5 ml tubes and centrifuged with 500 G, 10 min at 4°C. Organoids were dissociated by incubation with 200 µl dispase for 30 min at 37°C with mild rotation. Digested organoids were washed once with 1 ml DMEM and twice with MACS buffer and centrifuged with 500 G for 5 min at 4°C. During these steps, organoids were further dissociated into single cells by gentle pipetting, stained with antibodies and analyzed by flow cytometry.

3.3.3. Cell sorting of infected cells

After digestion of IAV and mock-infected organoids, cells were pelleted with 500 G, 10 min at 4°C, blocked with gammaglobulins and stained with the corresponding fluorophore-labeled antibodies for 15 min at 4°C in MACS buffer. Cells were washed once with MACS buffer and centrifuged with 500 G for 5 min at 4°C, stained in 250 µl of MACS buffer containing the secondary antibody against IAV hemagglutinin (HA) for 15 min at 4°C. Cells were washed as stated before, resuspended in 300-500 µl of MACS buffer and filtered into FACS tubes for cell sorting using an 85 µm nozzle.

The following antibodies were used for cell sorting of infected cells:

Antibody	dilution
CD31 Alexa 488	1:50
CD45 FITC	1:50
CD326 (EpCAM) APC/Cy7	1:50
Podoplanin (PDPN) APC	1:20
Hemagglutinin (HA)	1:75
Secondary antibody	
Donkey anti-goat Alexa 647	1:500

3.3.4. Flow cytometry analysis of infected cells

Multicolor flow cytometry was performed on a BD FACS Aria™ III cell sorter using DIVA software. For single cell suspension analysis, cells were pelleted with 500 G, 10 min at 4°C, blocked with gammaglobulins and surface cell markers were stained with the corresponding fluorescence-labeled antibodies for 15 min at 4°C in MACS buffer. Cells were washed as stated before and fixed with 100 µl 1% PFA for 10 min at 4°C in the dark. For evaluation of nucleoprotein (NP) expression, cells were washed and permeabilized with 100 µl 0.2% saponin in PBS for 15 min at 4°C in the dark. Cells were washed again and internal markers were stained with the

corresponding fluorescence-labeled antibodies for 30 min at 4°C. Cells were washed with MACS buffer containing 0.1% Saponin. At last, cells were resuspended in 300 µl of MACS buffer, filtered and transferred to FACS tubes for analysis. Corresponding isotype antibodies were used as negative controls. Given data is representative of three independent experiments.

Antibody mix for infected organoids NP analysis:

Antibody	dilution
Extracellular	
CD326 (EpCAM) APC-eF780	1:100
CD24 PE/Cy7	1:200
Sca-1 PB	1:50
Intracellular	
Viral nucleoprotein (NP) FITC	1:20

3.3.5. Plaque assay

One day before infection MDCK cells (1×10^6 per well) were seeded into a 12-well plate and cultured at 37°C, 5% CO_2. The next day, infection was done in duplicate using cell culture supernatants of 48 h post infection (pi) in 250 µl PBS for 1 h at 37°C. 500 µl of pre-warmed Avicel® overlay medium (MEM, 0.1% BSA, 100 U/ml penicillin, 0.1 mg/ml streptomycin, 0.1% Hepes, 2 µg/ml trypsin (TPCK-treated), 1.25% Avicel) was added. Plates were incubated at 37°C, 5% CO_2 without movement. After 48 h Avicel overlay was removed, cells were fixed with 4% PFA in PBS for 15 min at RT. Cells were washed twice with PBS and permeabilized with 0.3% Triton X-100 in PBS for 15 min at RT. Staining for viral proteins was done using a polyclonal antibody against Influenza A virus (Abcam) in staining buffer (PBS, 10% HS, 0.1% Tween-80) for 1 h at RT. Cells were washed three times with wash buffer (PBS, 0.05% Tween-80) and incubated with horseradish peroxidase-conjugated secondary antibody (Santa Cruz) for 1 h at RT in the dark. Cells were washed four

times with wash buffer. NP staining was visualized using TrueBlue™ peroxidase substrate for up to 30 min. Cells were washed twice with dH_2O to stop the reaction. Stained plaques were counted and represented as a mean. Given data is representative of three independent experiments.

3.3.6. Morpholino transfection

Scrambled morpholino (Scra) control (sequence: 5´-CCTCTTACCTCAGTTA CAATTTATA-3´) and *miR142-3p*-specific morpholino (mo142-3p) (sequence: 5´-TCCATAAAGTAGGAAACACTACACC-3´) (Gene Tools, LLC) were prepared in α-MEM with 0.2% FCS at a concentration of 4 µM. At day 6 of culture, mo142-3p or Scra was applied to co-cultures overnight for three consecutive nights, followed by application for 48 h for days 9 to 11. EpiSPC proliferation was assessed by measuring the organoid diameters on the day of treatment and 5 days later (day 11). Then, treated organoids were removed from Matrigel, digested and flow-sorted based on EpCAM expression. For further experiments, lung organoids were subsequently treated every 24 h with mo142-3p or Scra until day 21 of culture. Branching in lung organoids was assessed by counting the branching points after 15 days of treatment with Scra or mo142-3p using confocal microscopy. Given data is representative of three or four independent experiments.

3.3.7. GM-CSF ELISA

A commercially available ELISA kit (R&D Systems) was used according to the manufacturer's instructions to determine the concentration of GM-CSF in cell culture supernatant. Samples were stored at -80°C and used undiluted for ELISA. Cytokine abundance was quantified by addition of a luminescent substrate and colorimetric detection at 450 nm wavelength in a microplate reader (Bio-Rad). GM-CSF concentration was calculated on basis of samples of known concentration in a standard curve. Given data is representative of three independent experiments.

3.3.8. Anti-GM-CSF mAb treatment

From day 2 of co-culture, medium was replaced by EpiSPC medium containing 50 ng/ml of anti-GM-CSF mAb or isotype control (R&D Systems). EpiSPC proliferation was assessed by measuring organoid diameters and quantity on days 6,8, and 11 of culture. Treatment continued until day 21. Given data is representative of three independent experiments.

3.3.9. Isolation and FACS analysis of TR-Mac

Bronchoalveolar lavage was collected from the lungs of mTmG adult mice with PBS/EDTA. The lavage was centrifuged at 500 G for 5 min at 4°C and cells were resuspended in DMEM medium (10% FCS, 100 U/ml penicillin, 0.1 mg/ml streptomycin, 2 mM L-glutamine). Cells were then plated on non-treated petri dishes for 1 h with 5% CO_2 at 37°C. Medium was removed and adherent cells were washed once with PBS. For cell detachment, tissue-resident alveolar macrophages (TR-Mac) were treated with Accutase for 20 min with 5% CO_2 at 37°C. At last, TR-Mac were collected into a Falcon tube using a cell scraper, centrifuged and resuspended in medium until further analysis.

For flow cytometry analysis, TR-Mac were pelleted with 500 G, 10 min at 4°C, blocked with gammaglobulins and stained with the corresponding fluorescence-labeled antibodies for 15 min at 4°C in MACS buffer. Cells were washed once with MACS buffer and centrifuged with 500 G for 5 min at 4°C, resuspended in 200 µl of MACS buffer and filtered into FACS tubes for cell analysis.

The following antibodies were used for TR-Mac characterization:

Antibody	dilution
Gr1 PE-Cy7	1:100
CD45 Horizon™ V500	1:100

Ly6G APC	1:50
Siglec-F APC-CY7	1:50
CD11c FITC	1:20

3.3.10. *Microinjection of TR-Mac*

On day 14 of culture, microinjection of TR-Mac isolated from mTmG mice into lung organoids was performed using an oil-filled microinjection system (CellTram®Vario) with 10 µm diameter capillary needle (Eppendorf) and DMIL LED microscope (Leica). After microinjection, cultures were kept in the incubator with 5% CO_2 at 37°C until further analysis.

3.3.11. Microscopy

3.3.11.1. Immunofluorescence

Co-cultures were fixed with 4% PFA for 10 min at RT. Cultures were washed with buffer (0.2% BSA/PBS), permeabilized with 0.1% triton/PBS for 5 min and blocked in 5% HS, 2% BSA/PBS for 30 min at RT. For staining, cultures were incubated with primary antibodies over night at 4°C, followed by washing and addition of secondary antibodies for 2 h at RT. For staining of PDGFRα^{GFP} cultures, cultures were not permeabilized. Given data is representative of three independent experiments.

3.3.11.2. LysoTracker, phospholipid and neutral lipid staining

For staining of lamellar bodies, LysoTracker® Red DND-99 (Thermo Scientific) stock solution was diluted in pre-warmed α-MEM according to the manufacturer's instructions. 25 nM LysoTracker was added to co-cultures and incubated for 30-60 min at 37°C. Similarly, for staining of phospholipids, red phospholipidosis detection reagent (Thermo Scientific) was diluted 1:500 in α-MEM and added to EpiSPC/rMC co-cultures for 48 h. For staining of neutral lipids, co-cultures were fixed with 4% PFA for 15 min, washed twice with PBS and stained with 1x of PBS diluted LipidTOX™ red neutral lipid staining solution (Thermo Scientific). After 6 h

incubation at RT, cultures were co-stained with DAPI and mounted in glass slides for imaging. Given data is representative of three independent experiments.

3.3.11.3. β-galactosidase staining

Organoids were fixed with 4% PFA for 5 min at RT, washed once with PBS and incubated with pre-warmed LacZ buffer (5 mM $[Fe(CN)_6]^{3-}$, 5mM $[Fe(CN)_6]^{4-}$, 2 mM $MgCl_2$ in PBS) for 10 min at 37°C. LacZ buffer was replaced with staining solution (1 mg/ml X-Gal in LacZ buffer) and incubated at 37°C until blue staining became visible. Stained cultures were rinsed once with PBS and kept in PBS at 4°C for further analysis. Given data is representative of three independent experiments.

3.3.11.4. Microscopes

Micrographies of co-cultures were taken using the EVOS™ FL Auto Imaging System (Thermo Scientific). A Leica SP8 confocal microscope was used for confocal imaging as indicated in the results section. For live cell imaging of organoid formation, a Leica DMI6000 B microscope was used.

3.3.12. Gene expression analysis

3.3.12.1. RNA isolation

RNA was isolated from flow-sorted cells and organoid cultures using RNeasy Micro Kit or miRNeasy Mini Kit (Qiagen). After cell sorting or organoid dissociation, cells were washed once with PBS (500 G, 5 min at 4°C) and lyzed in 350µl RLT buffer. Samples were then processed according to the manufacturer's instructions. RNA concentration and purity were analyzed by spectrophotometry (Nanovue Plus, GE Healthcare).

3.3.12.2. cDNA synthesis

cDNA was synthesized using M-MLV reverse transcriptase (Invitrogen) and random hexamer primer according to the manufacturer's instructions using 250 ng of total

RNA. For reverse transcription of *miR142-3p* a stem loop reverse primer was used according to the protocol published by Tang and co-workers[175]. All incubation steps were performed in a PeqSTAR thermocycler (Peqlab, Erlangen).

3.3.12.3. Quantitative real-time PCR

Quantitative PCR was performed in a StepOnePlus™ Real-Time PCR System (Thermo Scientific) using SYBR Green (Life Technologies) according to the manufacturer's instructions. The relative gene expression levels were normalized to ribosomal protein subunit S-18 (RPS-18) or 5S rRNA and presented as fold change ($2^{\Delta\Delta Ct}$) or gene expression relative to day 0, Scra, or mock. Given data are representative of three independent experiments.

The following primers were used:

Rps-18	FP 5'-CCGCCATGTCTCTAGTGATCC-3'
	RP 5'-TTGGTGAGGTCGATGTCTGC-3'
***Ifn*β**	FP 5'-GTTACACTGCCTTTGCCATCC-3'
	RP 5'-GTGGAGTTCATCCAGGAGACG-3'
Sftpc	FP 5'-GGAGGAAGGGCATGATACTGG-3'
	RP 5'-TTCTACCGACCCTGTGGATGC-3'
Foxj1	FP 5'-GAGCCAGGCCTCACATTCG-3'
	RP 5'-CGCTGGTAACCCAGACTCC-3'
Muc5ac	FP 5'-AGGACCACTGTATTGCTGGC-3'
	RP 5'-TCCAGAACATGTGTTGGTGC-3'
Hopx	FP 5'-CAACAAGGTCAACAAGCACCC-3'
	RP 5'-GCGCTGCTTAAACCATTTCTGC-3'
NP	FP 5'-ACGAAGGTGGTCCCAAGAGG-3'
	RP 5'-GATTTGGCCCGCAGATGCC-3'
Sox9	FP 5'-GAAGAACGGACAAGCGGAGG-3'
	RP 5'-GATTGCCCAGAGTGCTCGC-3'

Rarb	FP 5'-GGTCTCTCATGAAGCTAGCTATTTATCTG-3'
	RP 5'-CAGTTCTTATCTCGATGGCAAGTG -3'
5S rRNA	FP 5'-TCTCGGAAGCTAAGCAGGGTC-3'
	RP 5'-AGCCTACAGCACCCGGTATTC-3'
miR142-3p	FP 5'-ACTCCAGCTGGGTGTAGTGTTTCCTACTT-3'
	stem loop reverse 5'-CTCAACTGGTGTCGTGGA
	GTCGGCAATTCAGTTGAGTCCATAAA-3'
	universal reverse 5'-TCAACTGGTGTCGTGGAGTCG-3'

3.3.13. IAV infection in vivo experiment

WT, GM-CSF$^{-/-}$ and SPC-GM adult mice were infected with 500 pfu of PR8 applied intratracheally. After 7 days of infection, mice were anesthetized with isoflurane inhalation and killed by cervical dislocation. Lungs were perfused with HBSS followed by intratracheal instillation of 1.5 ml 1:1 TissueTek: 2% PFA/PBS mixture. Lungs were then harvested, embedded in TissueTek:PBS, frozen in liquid nitrogen and stored at -80°C. For immunofluorescence, cryoslices with 5 µm thickness were prepared using a Leica CM 1850 UVcryotome. Before staining, slices were air-dried, fixed with 4% PFA for 20 min at RT, washed with PBS/0.2% BSA, and permeabilized with 0.3% Triton-X-100 for 10 min at RT. Cryoslices were then blocked using 10% HS in PBS for 1 h at RT and stained with SFTPC and ki67 antibodies as described in section 3.3.11.1. Given data are representative of four independent experiments.

3.4. Statistics

All data are given as mean ± SEM. Statistical significance between two groups was estimated using the unpaired Student's t test. For comparison of three groups, ANOVA and post-hoc Tukey's test were performed. Calculations were done with GraphPad Prism 5 (GraphPad Software, Inc.). A P-value lower than 0.05 was considered to be significant.

4. RESULTS

4.1. 3D co-culture of EpiSPC and rMC results in the formation of bronchioalveolar lung organoids

As previously described, EpiSPC are capable to form organoids *in vitro* only when FGF10 and HGF are present in the culture medium[85]. rMC are known to be a source of such growth factors and promote branching morphogenesis and alveolar septation during lung development[3,24,176]. Therefore, the establishment of a lung organoid model combining EpiSPC and rMC to better recapitulate the structural and cellular composition of the lung was envisioned. EpiSPC and rMC for 3D cultures were isolated from leukocyte/endothelial cell-depleted lung homogenate of adult mice by high-speed cell sorting. For this purpose, expression signature for EpiSPC ($EpCAM^{high}CD24^{low}itg\alpha6^{high}itg\beta4^{high}CD200^{+}Sca\text{-}1^{+}$) and rMC ($EpCam^{-}Sca\text{-}1^{+}$) was exploited[85]. After doublet discrimination, EpiSPC and rMC populations were FACS-separated based on the surface expression of $EpCAM^{high}CD24^{low}Sca\text{-}1^{+}$ and $EpCAM^{-}Sca\text{-}1^{+}$, respectively (Fig. 4-1). Following cell sorting, purity of EpiSPC and rMC was approximately 90% and 98%, respectively.

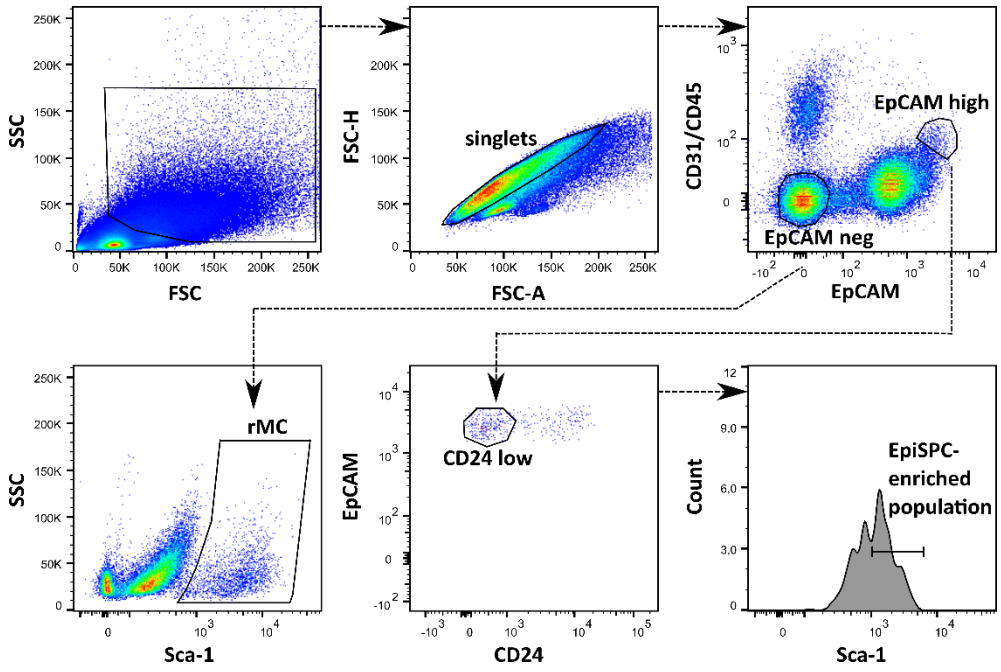

Figure 4-1. EpiSPC and rMC isolation from adult murine lung. Gating strategy for cell sorting of EpiSPC and rMC from CD31/CD45-depleted lung homogenate.

Flow-sorted EpiSPC and rMC were counted and seeded into Matrigel for 3D cultures. Growth and development of lung organoids was monitored over 21 days. EpiSPC proliferated in culture forming colonies between day 4 to 6. After 10 to 11 days in culture, most organoids further increased in size and changed morphology from spherical to diverse asymmetrical forms. By day 21, lung organoids differentiated into bronchioalveolar lung organoids (BALO) characterized by the presence of elongated tubular and multiple saccular structures (Fig. 4-2A and D) representing the airway and alveolar *in situ* morphology, respectively. In addition to BALO, two other types of organoids were found with a much lower incidence (~10% of total organoids per well). These organotypic structures remarkably resembled formerly described bronchiolar organoids[134], termed here bronchiolospheres, and alveolospheres[73]. While during early phases of organoid development colonies are rather similar, mature bronchiolospheres (Fig. 4-2B) and alveolospheres (Fig. 4-2C) did not form defined tubular structures. Notably, bronchiolospheres maintained a disorganized arrangement whereas alveolospheres developed later during culture and were characterized by a compact saccular conformation.

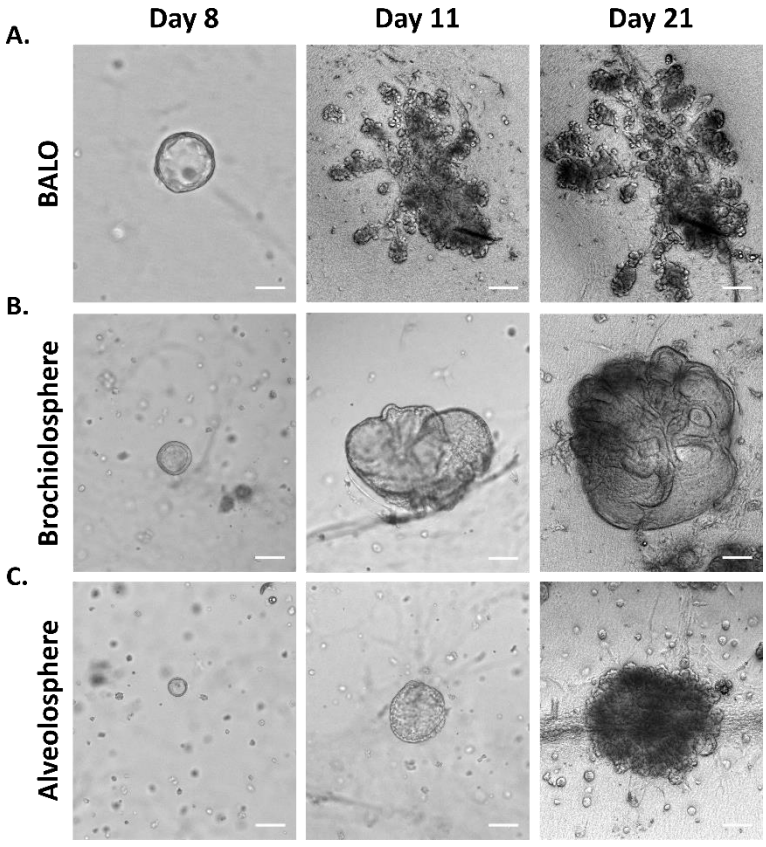

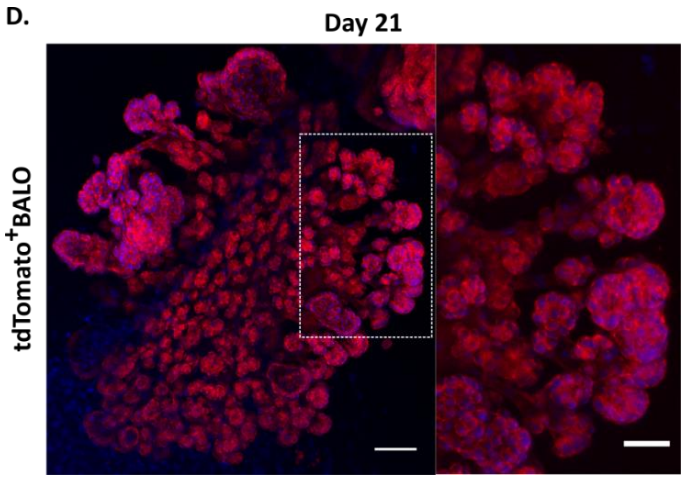

Figure 4-2. Organoid formation during EpiSPC and rMC co-cultivation. EpiSPC formed three distinct lung organoids. Representative images of EpiSPC proliferation and differentiation into (A) BALO, (B) bronchiolosphere, and (C) alveolosphere at day 8, 10 and 21 of culture. Scale bars represent 100 µm. (D) Representative confocal images showing tdTomato^{+} BALO tubular and saccular structures at day 21 of culture. Scale bars represent 100 (left) and 50 (right) µm.

4.2. BALO are generated from single EpiSPC

The term organoid refers to 3D structures derived from a single stem cell population capable to differentiate into organ-specific cells types which self-organize to form a structure resembling the cellular organization of the organ of origin[115,167]. To assess BALO clonality, flow-sorted EpiSPC from WT and mTmG tdTomato (a red fluorescent protein)- expressing mice were mixed at a ratio of 1:4 and co-cultured with rMC. Throughout co-cultivation, only WT or tdTomato^{+} BALO but no mixed phenotypes were observed by microscopy (Fig. 4-3A). Further indication for BALO clonality was obtained by live cell imaging in which growth and development of WT and tdTomato^{+} BALO were monitored from day 15 to 20 and no mixed phenotypes were observed (Fig. 4-3B). Overall, these data confirm the capacity of EpiSPC to expand and differentiate into BALO in the presence of rMC.

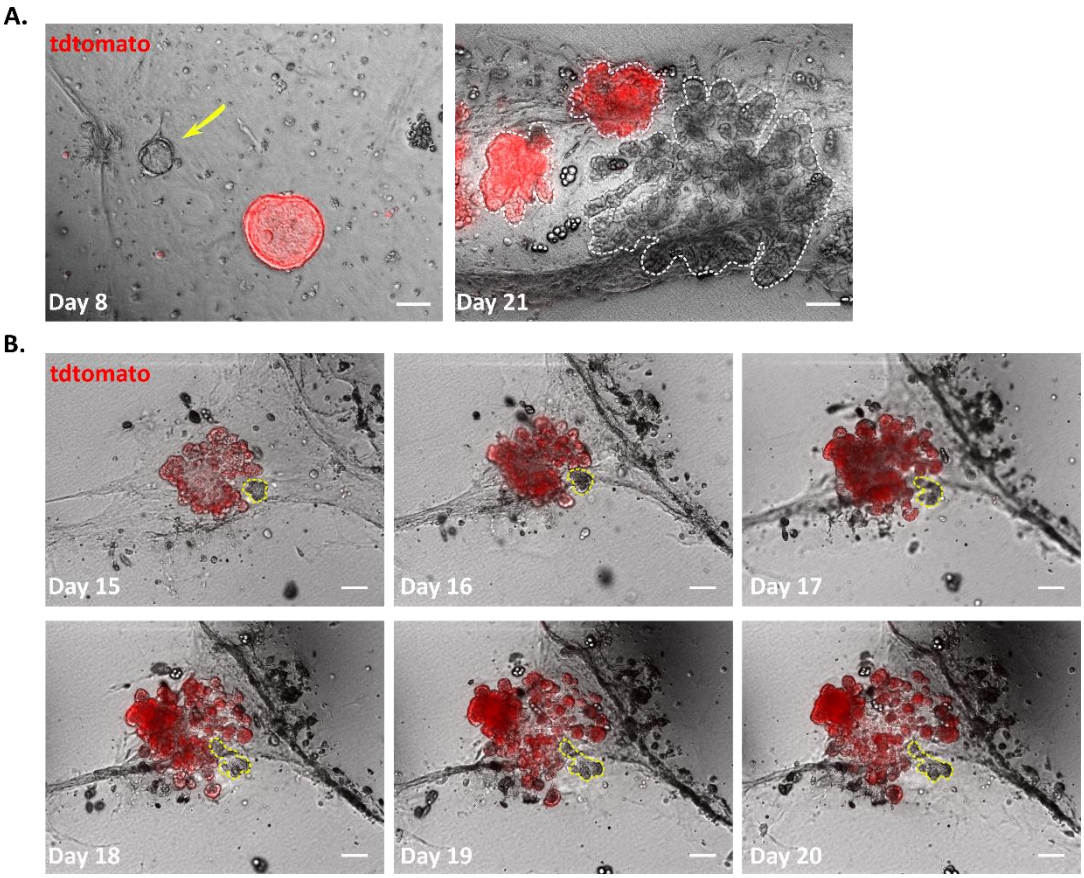

Figure 4-3. BALO clonality. EpiSPC derived from WT or mTmG mice during co-cultivation with rMC gave rise to individual BALO. (A) Representative images of day 8 and 21 BALO (white dashed line) derived from WT (arrow) or mTmG mice. (B) Live cell imaging-derived images of WT (yellow dashed line) and tdTomato^{+} BALO from day 15 to 20 of culture. Scale bars represent 100 µm.

4.3. EpiSPC giving rise to BALO possess a BASC phenotype

In relation to seeded EpiSPC, an average ratio of 1:100 BALO developed after 21 days in culture suggesting that only a small fraction of the sorted EpiSPC population had the capacity to proliferate and generate BALO. As described before, BASC are stem cells located at the BADJ which can self-renew and differentiate into bronchiolar cells and AEC in response to injury (Fig. 1-3). BASC express EpCAM, Sca-1, and co-express SFTPC and SCGB1A1[51], therefore, to investigate if BASC were the progenitor cells within the EpiSPC population giving rise to BALO, a *Scgb1a1*^{mCherry}*Sftpc*^{YFP} double-fluorescent reporter mouse line was used.

EpiSPC were flow-sorted from lung homogenate of *Scgb1a1*^{mCherry}*Sftpc*^{YFP} mice following the same gating strategy as previously described in figure 4-1 (Figure 4-4A). Expression of SCGB1A1 and SFTPC within the EpiSPC population was also analyzed (Figure 4-4B). Remarkably, only about 5% of the EpiSPC population was double-positive for SCGB1A1^{+}SFTPC^{+}. While most cells (95%) were SCGB1A1^{+}SFTPC^{-}, SCGB1A1^{-}SFTPC^{+} cells represented only a minor fraction (<0.5%). Nonetheless, by day 21 of co-culture, mCherry^{+}YFP^{+} BASC-derived BALO accounted for 80% of all organoids suggesting that BALO are derived from BASC (Fig. 4-4C). Bronchiolospheres were composed solely of SCGB1A1^{+} cells and accounted for only 11%, whereas alveolospheres were composed solely of SFTPC^{+} cells and accounted for 9% of all organoids. Of note, the presence of cells with the SCGB1A1^{+}SFTPC^{+} BASC phenotype within the EpiSPC fraction was further confirmed by microscopic analysis of freshly-sorted cells after doublet exclusion (Fig. 4-4D).

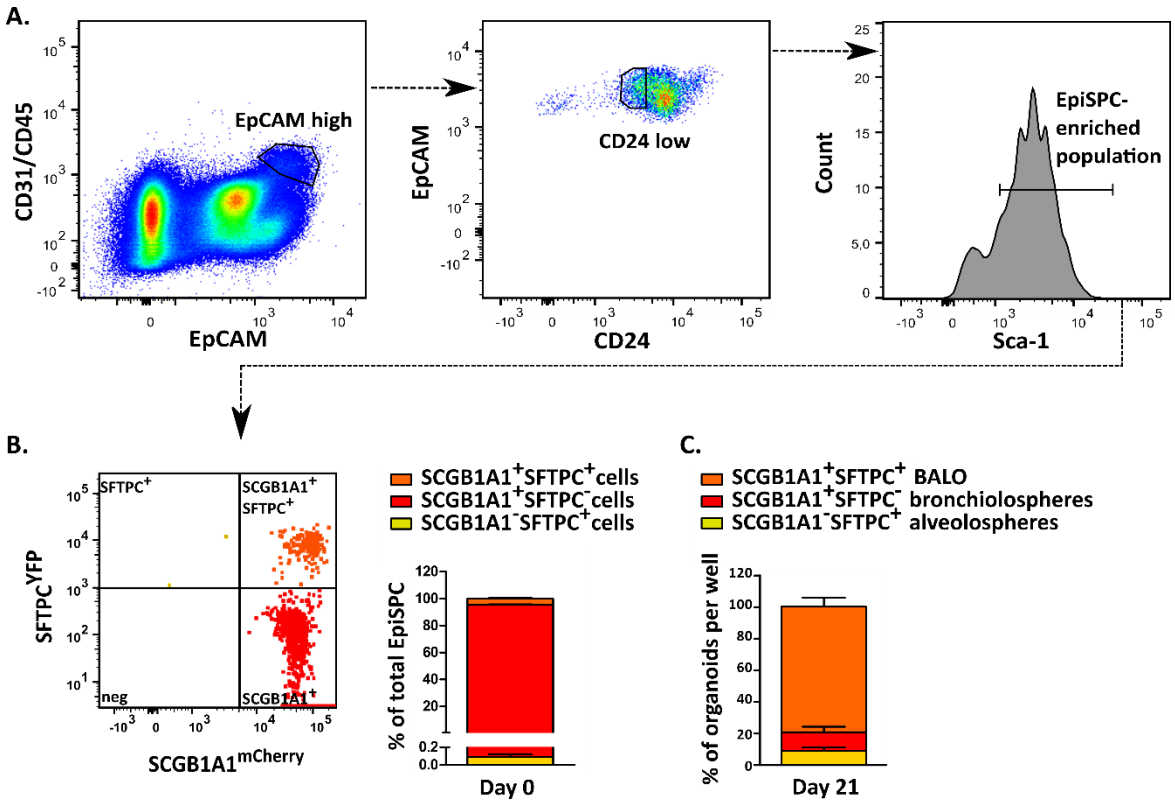

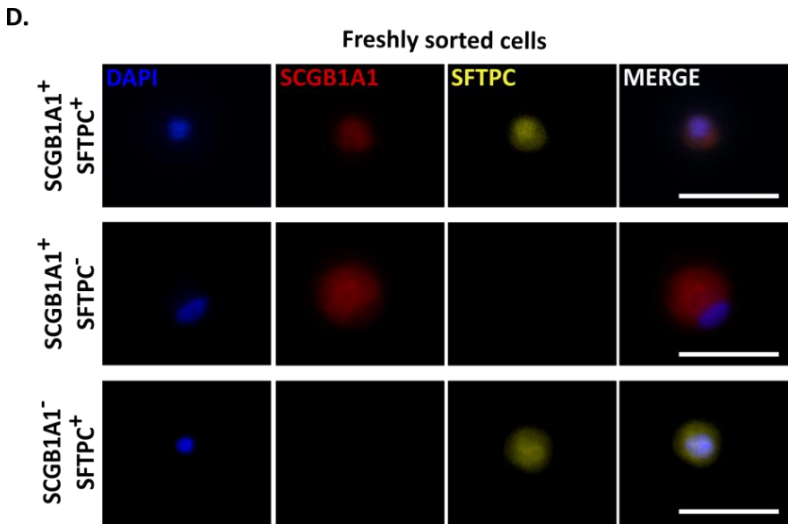

Figure 4-4. Characterization of the sorted EpiSPC population using *Scgb1a*^{mCherry}*Sftpc*^{YFP} double-fluorescent reporter mice. SCGB1A1^{+}SFTPC^{+} EpiSPC differentiated into BALO. (A) Gating strategy for cell sorting of EpiSPC from double-fluorescent reporter mice. (B) Percentage of SCGB1A1^{+}SFTPC^{+}, SCGB1A1^{+}SFTPC^{-} or SCGB1A1^{-}SFTPC^{+} cells within the EpiSPC population in n=4 different experiments and mean ± SEM is depicted. (C) Percentage of SCGB1A1^{+}SFTPC^{+} BALO, SCGB1A1^{+}SFTPC^{-} bronchiolospheres or SCGB1A1^{-}SFTPC^{+} alveolospheres organoids after 21 days in culture in n=4 different experiments and mean ± SEM is depicted. (D) Representative images of freshly sorted SCGB1A1^{+}SFTPC^{+}, SCGB1A1^{+}SFTPC^{-} or SCGB1A1^{-}SFTPC^{+} cells. Scale bars represent 25 µm.

To further demonstrate that BASC is the stem cell population responsible for BALO formation, EpiSPC were flow-sorted according to single or double expression of SCGB1A1 and SFTPC, and developing organoids were followed over time by confocal microscopy (Fig. 4-5). In SCGB1A1^{+}SFTPC^{+} BASC-derived organoids, SCGB1A1^{+} and SFTPC^{+} cells were uniformly distributed within early-stage BALO with only a small fraction of double-positive cells remaining at day 8 of culture. Between days 11 to 21, cells located within BALO-central branches were SCGB1A1^{+} whereas the outer alveolar-like structures were comprised of SFTPC^{+} cells indicating the presence of club cells and AECII, respectively (Fig. 4-5A). In contrast, culture of SCGB1A1 or SFTPC single-positive cells gave rise to bronchiolospheres or alveolospheres, respectively (Fig. 4-5B-C). Notably, SCGB1A1^{+}SFTPC^{-} and SCGB1A1^{-}SFTPC^{+} organoids

remained single positive during culture and never gave rise to BALO. These results confirmed previous morphological observations on growth and differentiation of EpiSPC described in figure 4-2.

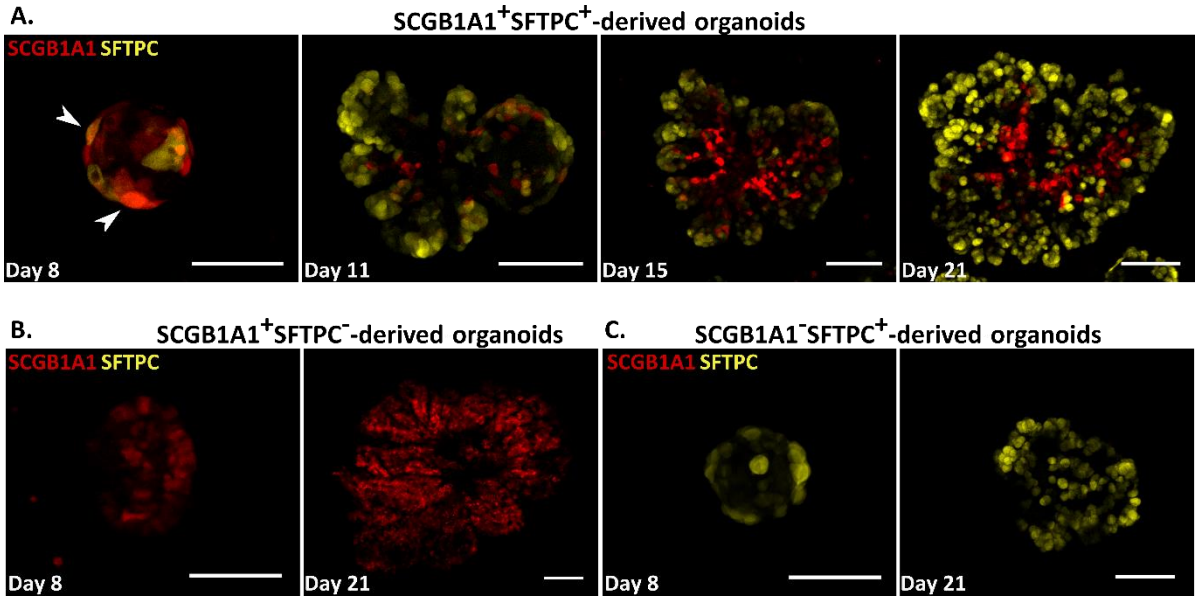

Figure 4-5. SCGB1A1 and SFTPC expression in EpiSPC-derived organoids. Only double-positive EpiSPC gave rise to BALO. Representative confocal images showing endogenous SCGB1A1 and SFTPC expression during (A) BALO, (B) bronchiolosphere, and (C) alveolosphere formation derived from EpiSPC sorted based on their expression of SCGB1A1$^+$SFTPC$^+$, SCGB1A1$^+$SFTPC$^-$ or SCGB1A1$^-$SFTPC$^+$, respectively. Arrowheads indicate SCGB1A1$^+$SFTPC$^+$ co-expressing cells. Scale bars represent 100 µm.

Together, the data indicate that a rare SCGB1A1$^+$SFTPC$^+$ BASC population within the EpiSPC fraction exhibits high stem cell potential and gives rise to BALO containing central SCGB1A1$^+$ tubular and surrounding SFTPC$^+$ saccular structures. Therefore, EpiSPC giving rise to BALO henceforth will be defined as BASC.

4.4 BALO model 3D morphology and cellular composition of the bronchioalveolar compartment

To characterize BALO with respect to their cellular composition, whole lung homogenate from adult mice and freshly sorted BASC and rMC were compared to day 21 digested cultures using flow cytometry (Fig. 4-6A-C). After 21 days of culture, BALO were comprised of a major EpCAM^{+} and a minor EpCAM^{-} cell population. Remarkably, EpCAM^{+} cells consisted of cell fractions identical in lineage marker expression and in frequency as to the murine adult lung, including a major fraction of AECII (94.3±0.2% in BALO and 95±0.1% in lung), low-frequent podoplanin (PDPN)$^{+}$ AECI (5.3±0.6% in BALO and 4.9±0.2% in lung), and EpCAM^{high}CD24^{high} small airway (bronchial) epithelial cells (2.5±1.8% in BALO and 2.2±1% in adult lung). This latter fraction contained also 0.2±0.9% EpCAM^{high}CD24^{low}Sca-1^{+} EpiSPC in BALO, as observed in adult lung 0.5±0.4% (Fig. 4-6B). Moreover, a fraction of the EpCAM^{-} Sca-1^{+} rMC population from freshly sorted cells became EpCAM^{-}Sca-1^{-} after 21 days in culture suggesting differentiation of sorted rMC during culture (44.5±16% in co-cultures and 88.3±2.2% in lung) (Fig. 4-6C). Of note, day 21 co-cultures lack CD45 and CD31-expressing cells. In addition, freshly sorted rMC and BASC were mixed (day 0) and gene expression was compared to cells isolated from complete BALO co-cultures on days 10 and 21. In comparison to day 0, cells from day 21 co-cultures showed significant upregulation of genes for differentiation markers of the adult lung e.g. *Hopx* and *Sftpc* for AECI and AECII and *Foxj1* and *Muc5ac* for ciliated and goblet cells, respectively (Fig. 4-6D).

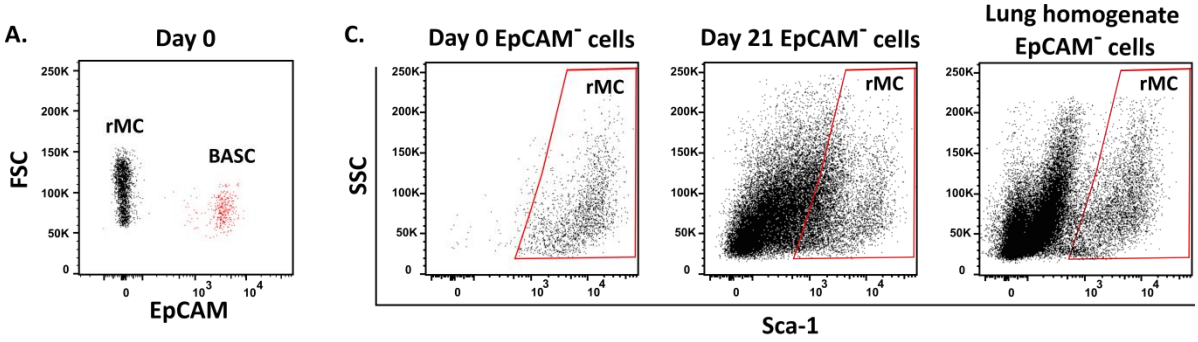

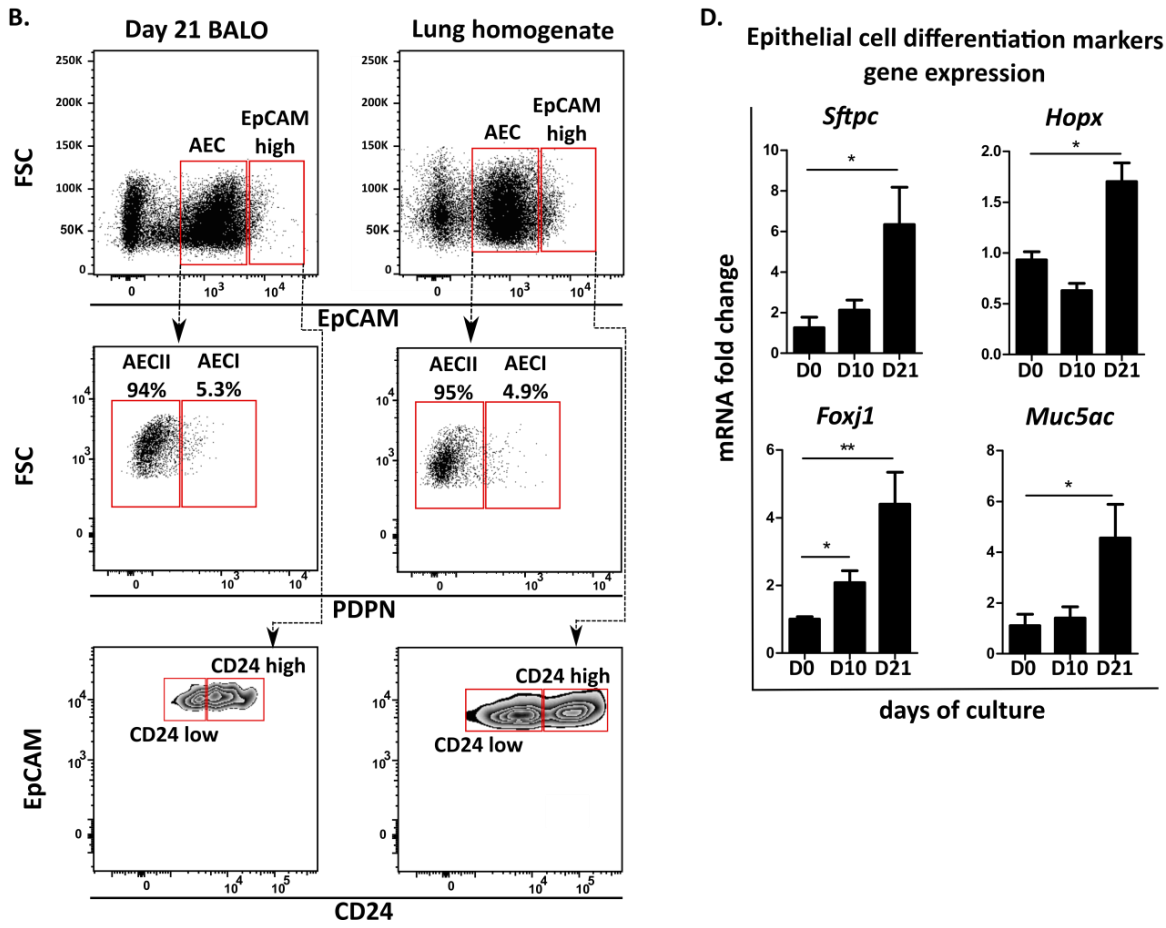

Figure 4-6. Cell composition comparison between lung homogenate from adult mice, freshly sorted BASC/rMC and day 21 BALO cultures. Cells isolated from BALO expressed markers of differentiated cell types of the adult lung. (A) Flow cytometry analysis of the BASC and rMC purity after cell isolation (day 0). (B-C) Flow cytometry analysis of lung cell homogenate from adult mice and day 21 BALO and rMC. (D) Gene expression analysis of *Hopx*, *Sftpc*, *Foxj1*, and *Muc5ac* at day 0, 10 and 21 of culture in n=3 different experiments and mean ± SEM is depicted (P-value <0.05).

To further confirm cell differentiation in BALO, confocal microscopy using fluorescence-labeled markers for airways and alveoli was used (Fig. 4-7A-B). As previously shown in figure 4-5 with organoids derived from SCGB1A1^{+}SFTPC^{+} BASC, central tubular structures within BALO were positive for small airway club marker, SCGB1A1 and peripheral alveolar structures were positive for the AECII marker, SFTPC (Fig. 4-7A). Moreover, BALO were positive for PDPN and β-IV tubulin

representing markers for differentiated alveoli (AECI) and airways (ciliated cells), respectively (Fig. 4-7A-B). Notably, recent stereological analysis has shown that the mean alveolar diameter of the lung alveoli was calculated to be 45.06 µm ± 1.4 in 9 week-old (adult) mice[177]. To compare alveolar morphometry of BALO to mouse lungs, the diameter of the alveolar structures in day 21 BALO were quantified and the results showed similar values to adult mouse lungs (45.17 µm ± 3.5) (Fig. 4-7C).

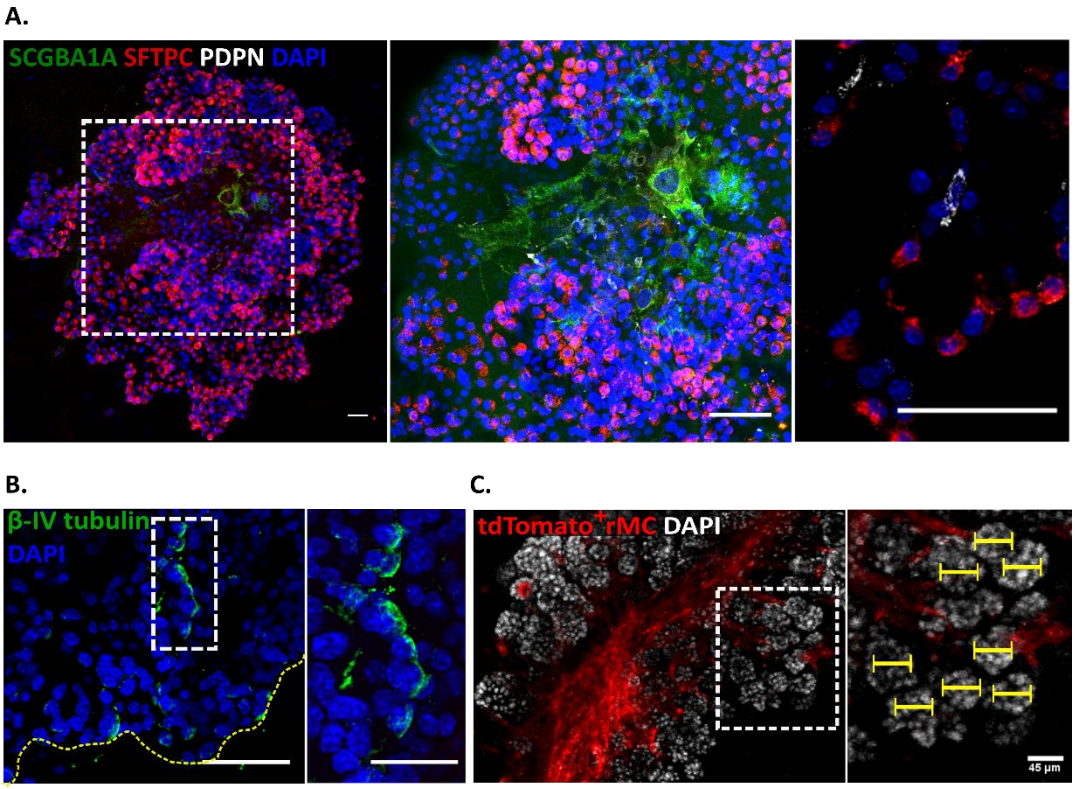

Figure 4-7. Epithelial cell differentiation markers and alveolar morphology in BALO. BALO possess a proximo-distal specification. Representative confocal images of (A) SCGB1A1$^+$, SFTPC$^+$, PDPN$^+$ (arrows), and (B) β-IV tubulin$^+$ cells in day 21 BALO. Scale bars represent 50 (left) and 25 µm (right). (C) Alveolar diameter in BALO was calculated from n=5 BALO in n=3 different experiments, and a representative image of alveolar size quantification is depicted. Yellow lines indicate 45µm.

Since AECII are a main component in BALO, the long-term functionality with respect to surfactant secretion, a factor important to limit surface tension in the lung and a component of innate host defense, was investigated. BALO were stained with LysoTracker dye, a marker for surfactant-containing lamellar bodies in differentiated

AECII, and with LipidTOX for phospholipids as a major component of the pulmonary surfactant at day 56 and 21 of culture, respectively. Compared to bronchiolospheres, alveolar spaces within BALO were highly positive for both, lamellar bodies and phospholipids (Fig. 4-8 A and B). In addition, BALO also stained positive for neutral lipids, another component of the surfactant (Fig. 4-8C).

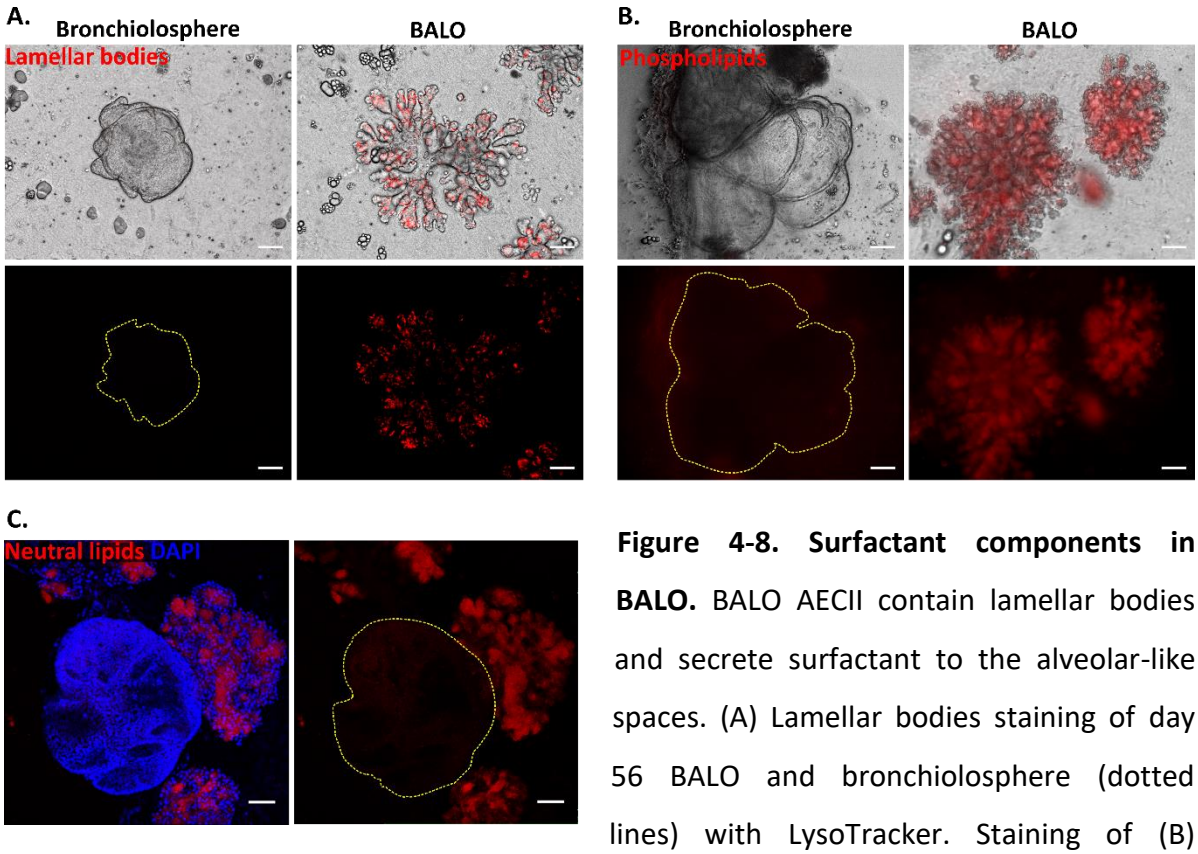

Figure 4-8. Surfactant components in BALO. BALO AECII contain lamellar bodies and secrete surfactant to the alveolar-like spaces. (A) Lamellar bodies staining of day 56 BALO and bronchiolosphere (dotted lines) with LysoTracker. Staining of (B) phospholipids and (C) neutral lipids in day 21 BALO and bronchiolospheres (dotted lines) with LipidTOX. Scale bars represent 100 µm.

In summary, the BALO *in vitro* model meets all described criteria referring to organoid definition published by Lancaster and Knoblich[115]. Accordingly, multiple lung-specific cell types that resemble the *in vivo* context were identified in BALO including spatially restricted cell lineage commitment with organization into defined tubular (bronchial airway) and saccular (alveolar) compartments, and alveolar structures containing functional pulmonary surfactant-secreting AECII.

4.5 Distinct fibroblast subsets develop from EpCAM^{-}Sca-1^{+} rMC within BALO cultures and are indispensable for BALO growth, branching morphogenesis, and cell differentiation

Crosstalk between epithelial and mesenchymal cells is indispensable for branching morphogenesis and cell differentiation during lung development[9]. Hence, in order to assess the relevance of rMC presence during BALO formation, microscopic analysis of rMC expressing tdTomato during co-cultivation with BASC was performed. By day 8 of culture, only a few rMC directly interacted with the developing BALO. However, as culture progressed, rMC incorporated within BALO providing a scaffold for the forming BALO (Fig. 4-9). Remarkably, tdTomato^{+} rMC gave rise to multiple fibroblast cell types, including cells containing lipid inclusions (data not shown) and spindle-shaped cells by day 21 of culture. These results indicate that distinct rMC subpopulations directly interact with epithelial cells throughout BALO development.

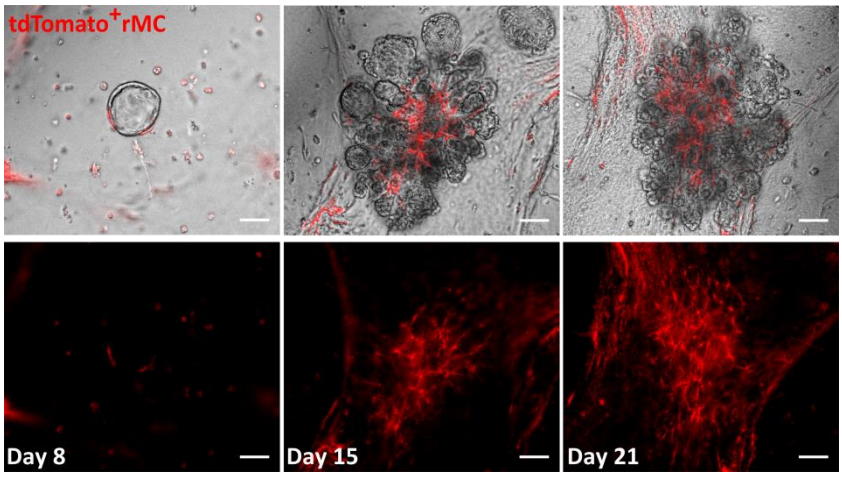

Figure 4-9. rMC are required for BALO formation. rMC are indispensable for organoid development and give rise to diverse cell types during co-cultivation. Time course images of BALO formation during co-cultivation with tdTomato^{+} rMC reveals structural integration of rMC into the developing BALO. Scale bars represent 100 µm.

The high complexity and diversity within the fibroblasts and mesenchymal stem cell populations in the lung has been well documented[9]. Notably, platelet derived

growth factor receptor alpha^{+} (PDGFRα) lung fibroblasts were shown to be crucial for alveolarization and realveolarization[178]. Therefore, to better characterize rMC heterogeneity, PDGFRα^{GFP} reporter mice were employed. Through flow cytometry analysis, two distinct populations were identified within the sorted CD45^{-}CD31^{-} EpCAM^{-}Sca-1^{+} fraction and defined as PDGFRα^{low} and PDGFRα^{high} rMC (Fig. 4-10A). Notably, reciprocal expression of Sca-1 and PDGFRα was observed in rMC, PDGFRα^{high} rMC were Sca-1^{int} while PDGFRα^{low} rMC were Sca-1^{high}. Sorted rMC derived from PDGFRα^{GFP} mice were co-cultured with BASC, and BALO development and GFP expression was monitored for 21 days. Comparable with the observations made on figure 4-9, from days 8 to 21 of culture, PDGFRα^{high} rMC proliferated and were increasingly observed within BALO (Fig. 4-10B-C). These data suggest that the PDGFRα^{high} rMC population is necessary for proper BALO development.

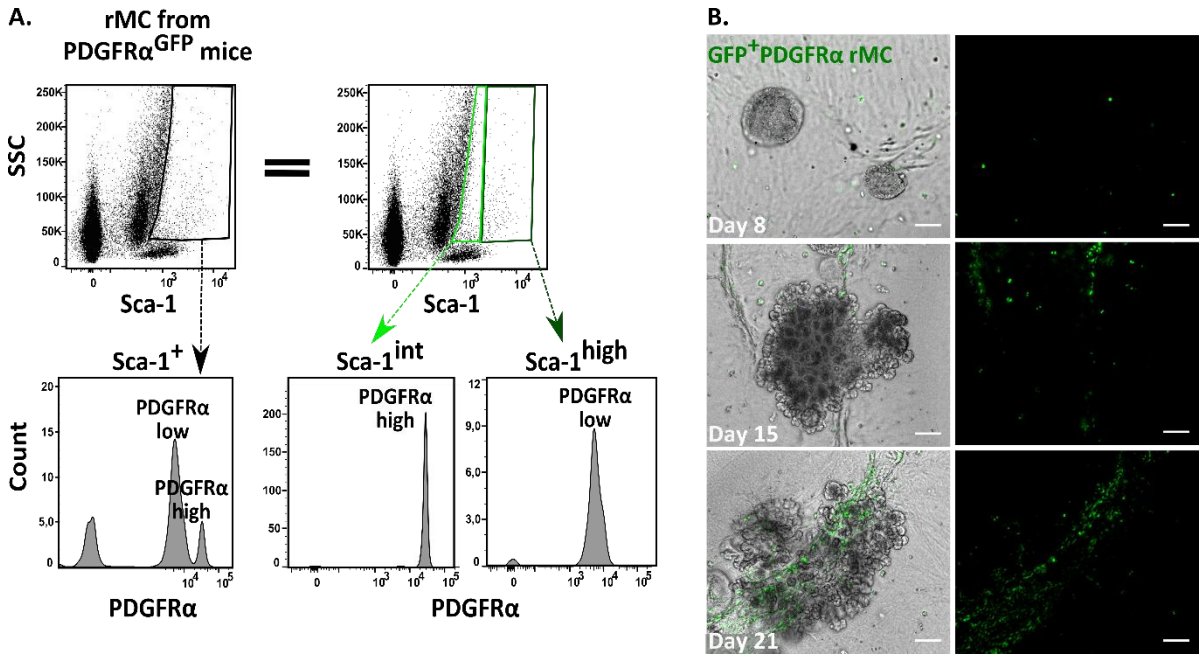

Figure 4-10. PDGFRα expression in the sorted rMC population. rMC differentially express PDGFRα during co-cultivation. (A) Flow cytometry analysis of PDGFRα expression in rMC derived from PDGFRα^{GFP} mice lung homogenates. (B) Time course images of BALO formation during co-cultivation with rMC derived from PDGFRα^{GFP} mice. Scale bars represent 100 µm.

To further define the crucial population(s) within the rMC population necessary for BALO formation, rMC were sorted according to their differential expression of PDGFRα and co-cultured with BASC. Organoid growth and development was monitored by microscopy for 21 days (Fig. 4-11). The PDGFRα^{low} rMC population sustained initial colony outgrowth but did not promote organoid formation whereas PDGFRα^{high}-expressing rMC co-cultivated with BASC failed to support organoid formation (Fig. 4-11A-B). However, culture with both PDGFRα^{high} and PDGFRα^{low} expressing rMC resulted in complete BALO formation indicating that both populations are required for proper organoid growth and development (Fig. 4-11C). Of note, due to the reciprocal expression of Sca-1 and PDGFRα in rMC (see Fig. 4-10A), expression of PDGFRα was dispensable for the rMC gating strategy and Sca-1 was employed as sole positive marker for rMC isolation (see Fig. 4-1).

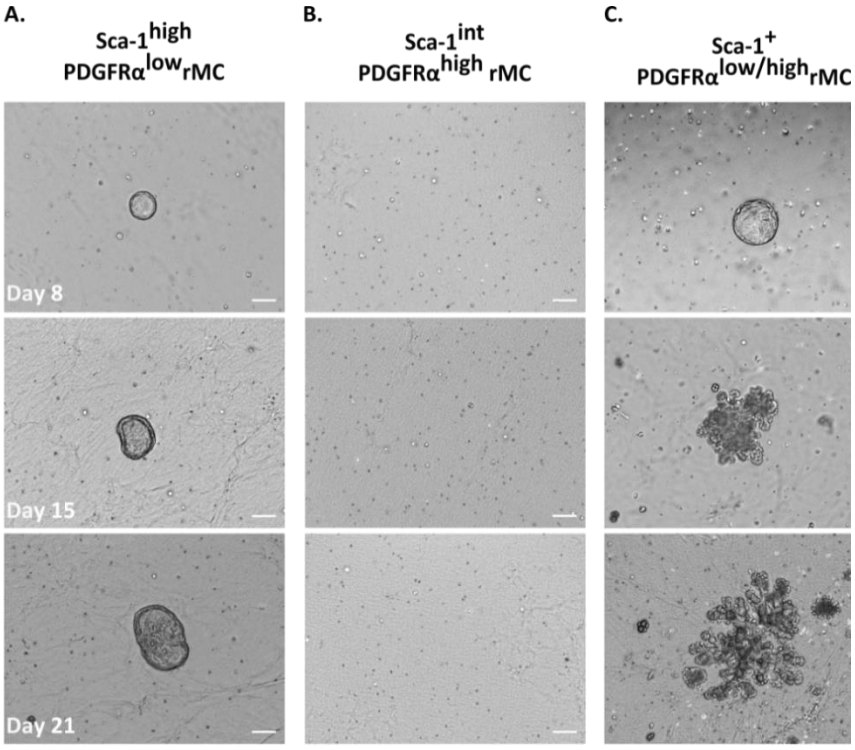

Figure 4-11. BALO development when cultured with different subsets of PDGFRα-expressing rMC. Both PDGFRα^{high} and PDGFRα^{low} rMC populations are necessary for organoid growth and formation. Representative images of BASC co-cultivation with (A) Sca-1^{high}PDGFRα^{low}, (B) Sca-1^{int}PDGFRα^{high}, and (C) Sca-1^{+}PDGFRα$^{low/high}$ rMC populations. Scale bars represent 100 µm.

Moreover, WT and PDGFRα-expressing rMC were analyzed by fluorescence microscopy. As previously observed, a part of rMC differentiated into lipid droplet-containing cells which is a characteristic feature of lipofibroblasts while other cells acquired spindle-shape, as typical for myofibroblasts[179,180]. To assess presence of lipofibroblasts and myofibroblasts, LipidTOX and αSMA stainings were performed in day 21 co-cultures. LipidTOX^{+} cells were detected nearby lung organoid structures whereas αSMA^{+} cells supported organoid structure by providing a scaffold within BALO (Fig. 4-12A-B). Moreover, several PDGFRα^{low} rMC were LipidTOX^{+} while a fraction of PDGFRα^{high} rMC was αSMA^{+} which confirmed the presence of lipofibroblasts and myofibroblasts, respectively (Fig. 4-12B). In accordance, αSMA^{+}PDGFRα^{high} myofibroblasts accumulate within BALO structure (Fig. 4-12C).

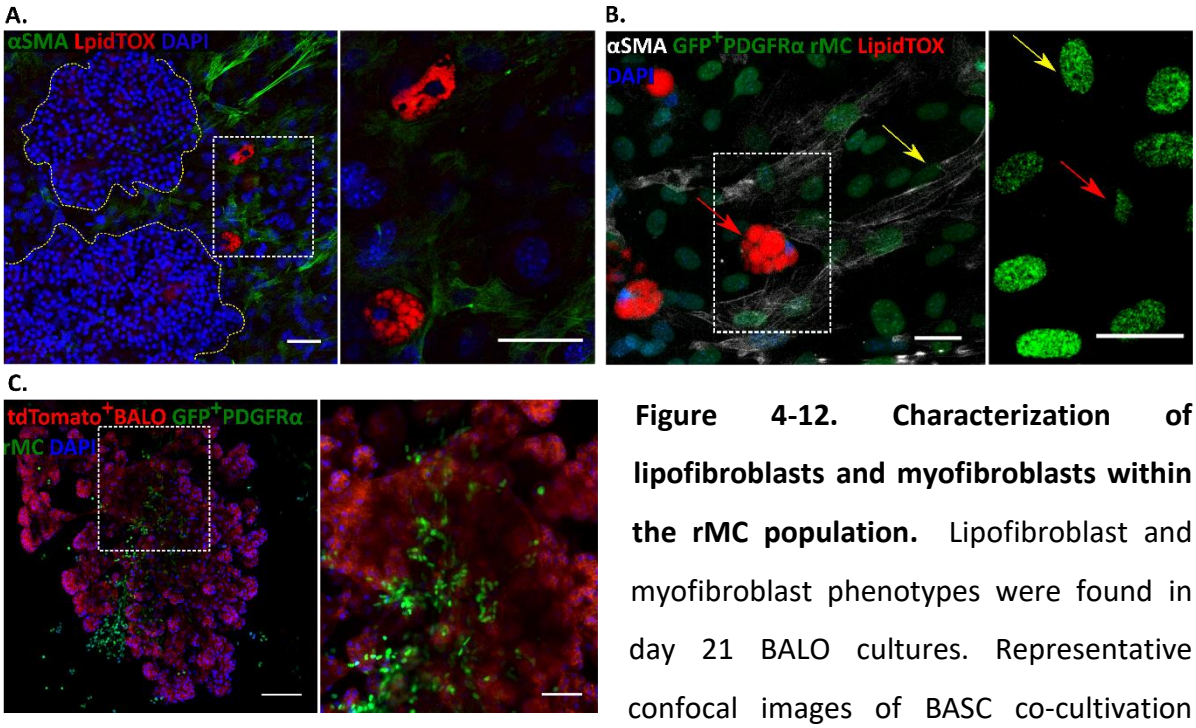

Figure 4-12. Characterization of lipofibroblasts and myofibroblasts within the rMC population. Lipofibroblast and myofibroblast phenotypes were found in day 21 BALO cultures. Representative confocal images of BASC co-cultivation with (A) WT or (B-C) PDGFRα-expressing rMC stained with αSMA antibody (yellow arrows) and/or LipidTOX (red arrows). The right panel in (B) only depicts PDGFRα-GFP to demonstrate that αSMA+ and LipidTOX+ cells are PDGFRα high and low, respectively. Scale bars for A-B represent 50 (left) and 25 (right) µm. Scale bars for C represent 100 (left) and 50 (right) µm.

Taken together, when co-cultured with BASC, cells within the rMC heterogeneous population are capable to differentiate into at least two cell types including lipofibroblasts and myofibroblasts which were shown to be vital for lung organoid formation.

4.6 BALO can be supplemented with TR-Mac

The reported BALO model has so far consisted of epithelial and mesenchymal cells but lack other cells present in the lung required for organ functionality. To add another layer of cellular complexity to the system, an experimental procedure to introduce a tissue-resident myeloid cellular component of the lung was established. Tissue-resident alveolar macrophages (TR-Mac) were isolated from the bronchoalveolar lavage of tdTomato-expressing reporter mice and microinjected into day 14 BALO using injection needles with 10 µm diameter (Fig. 4-13B). Prior to microinjection, TR-Mac surface expression signature ($CD45^+Ly6\text{-}G^-Gr1^-CD11c^+Siglec\text{-}F^+$) was confirmed by FACS (Fig. 4-13A). During BALO formation, TR-Mac remained within BALO and showed homing to the alveolar compartment (Fig. 4-13C). Moreover, preservation of TR-Mac phenotype was proven by positive staining with TR-Mac markers CD206 and Siglec-F 14 days after microinjection (Fig. 4-13D). Thus, this model offers the possibility to analyze defined TR-Mac gene products and AEC/TR-Mac signaling networks in the context of lung development and disease. The feasibility of microinjection into BALO may also allow analyzing and visualizing interactions of lung epithelial cells with other leukocyte populations during development and disease.

A.

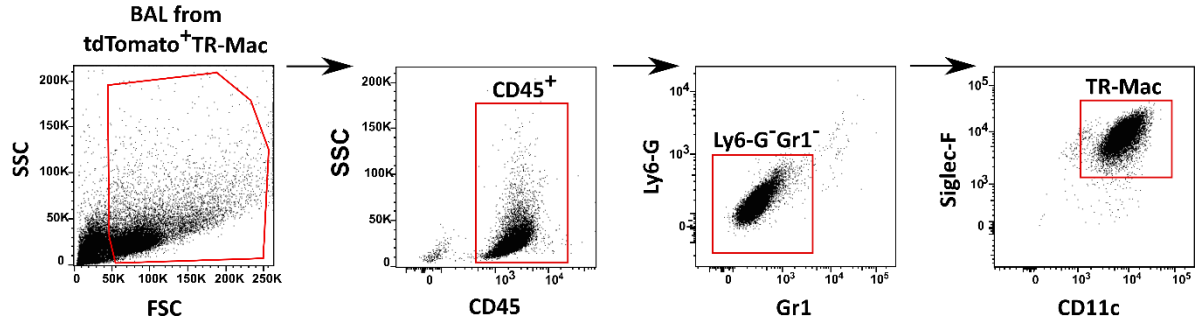

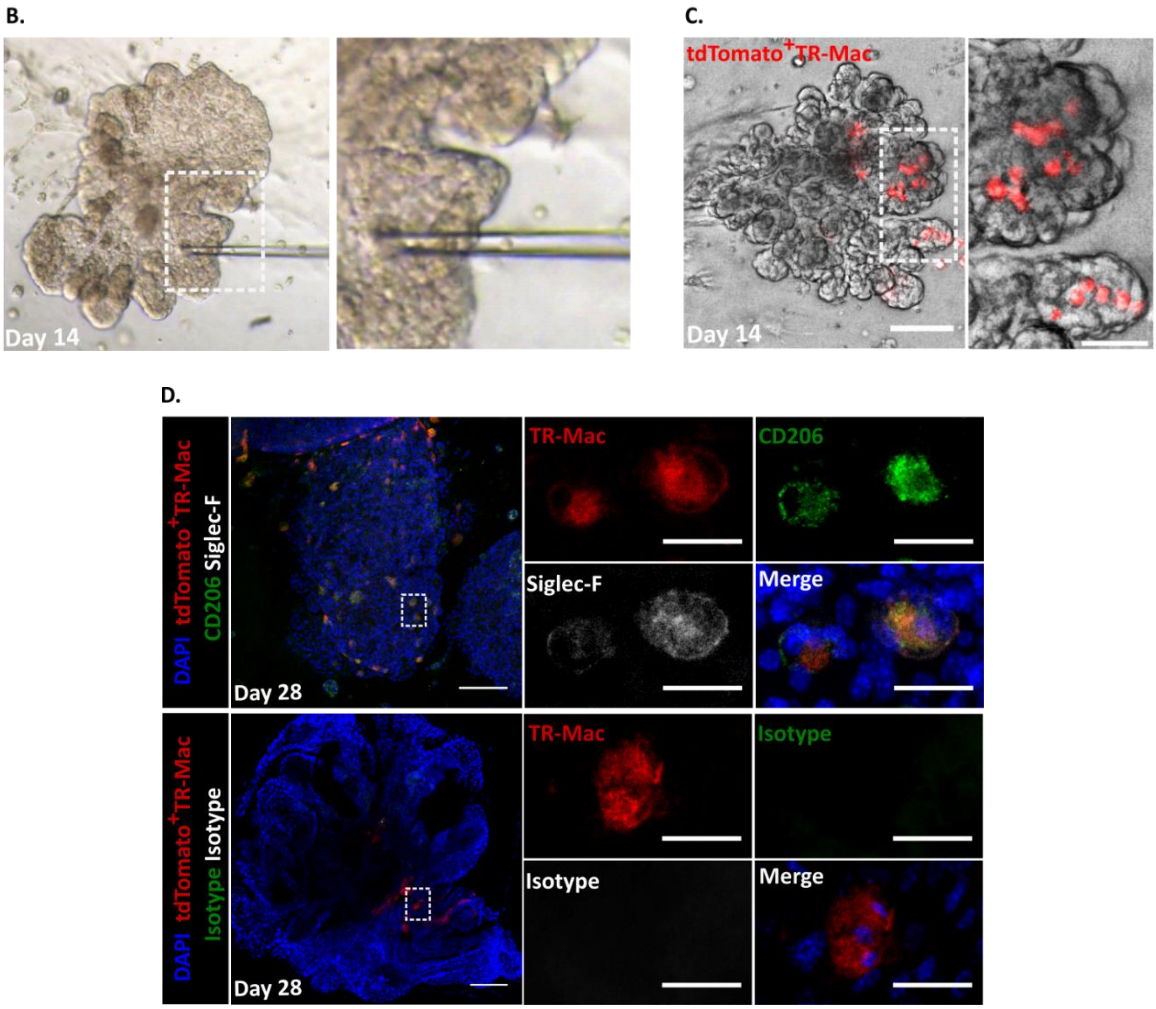

Figure 4-13. TR-Mac maintain alveolar identity after incorporation into BALO. BALO can be complemented with microinjected TR-Mac**.** (A) Gating strategy to define TR-Mac from bronchoalveolar lavage of adult tdTomato⁺ mice. (B) Representative images of tdTomato⁺ TR-Mac microinjection into day 14 BALO. (C) Representative images of day 14 BALO 6 h after microinjection of tdTomato⁺ TR-Mac. Scale bar represent 100 µm (left) and 50 µm (right). (D) Fluorescence confocal images of CD206, Siglec-F, or isotype stainings 14 days after tdTomato⁺ TR-Mac microinjection at day 28 BALO. Scale bars represent 100 µm (left) and 25 µm (right).

4.7 BALO as a model to study developmental questions of the alveolar epithelium

Having established a functional *in vitro* model for the murine distal lung, it was crucial to assess BALO applicability to study lung generation and regeneration processes including developmental aspects of bronchioalveolar formation.

Therefore, experiments directed to recapitulate *in vivo* findings described in the literature were performed using the BALO model. Carraro and co-workers have recently shown that microRNA 142-3p (*miR142-3p*) regulates WNT-dependent mesenchymal progenitor cell proliferation in the developing mouse lung[181]. In their work, morpholinos, oligos that bind to complementary RNA, were used to inhibit *miR142-3p* activity and maturation in embryonic lung explants. miR142-3p-specific morpholino (mo142-3p) not only decreased lung mesenchyme proliferation but also reduced lung growth and branching morphogenesis. Based on these observations, co-cultures were treated with mo142-3p to evaluate whether *miR142-3p* effects on lung development could be recapitulated in this BALO model. Notably, intermittent treatment with mo142-3p at an early culture stage prompted a significant decline in stem cell proliferation compared to scrambled morpholino (Scra) (Fig. 4-14A). Moreover, gene expression of epithelial and mesenchymal *miR142-3p* obtained from mo142-3p-treated BALO cultures was significantly downregulated in both compartments in comparison to Scra-treated cultures confirming *miR142-3p* loss of function (Fig. 4-14B).

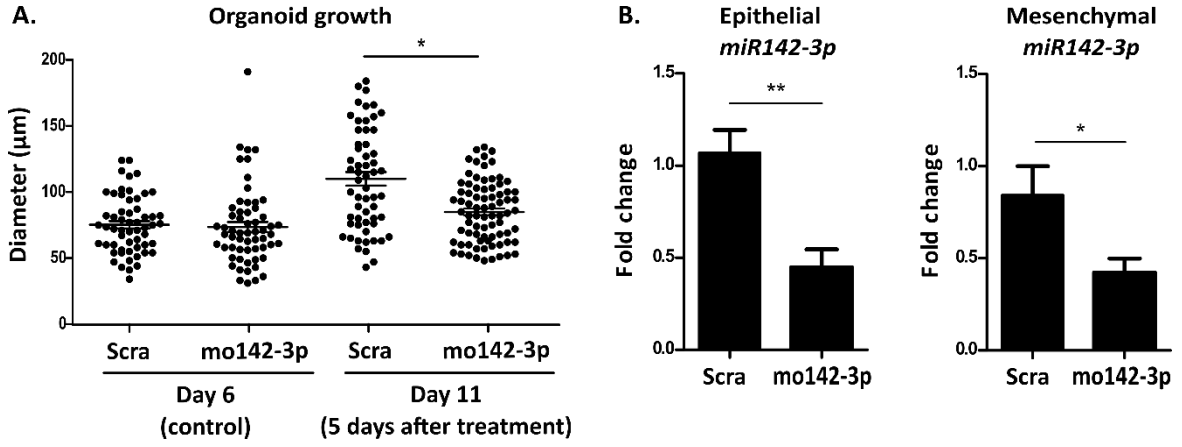

Figure 4-14. Effect of *miR142-3p* inhibition on BASC proliferation. mo142-3p addition to co-cultures led to organoid growth reduction. (A) Organoid diameter at day 0 and 5 days after treatment with Scra or mo142-3p. Mean ± SEM is depicted (n=3, P-value <0.05). (B) Gene expression analysis by qPCR of epithelial and mesenchymal *miR142-3p* in co-cultures after 5 days of treatment with Scra or mo142-3p. Mean ± SEM is depicted (n=3, P-value <0.05).

It has been previously shown that miR-142-3p controls canonical WNT signaling by targeting adenomatosis polyposis coli (APC), a main part of the β-catenin destruction complex[182]. To assess WNT signaling down-regulation in the model, BASC from TOPGAL mice were co-cultivated with WT rMC or vice versa, and treated with mo142-3p or Scra at day six of culture (Fig. 4-15A-B). TOPGAL mice express β-galactosidase controlled by the LEF/TCF-mediated signaling pathway and activated β-catenin[183]. Thus, TOPGAL activation is a direct indicator for active canonical WNT signaling in a cell. Before mo142-3p or Scra addition, comparable levels of WNT signaling expression were observed in BALO at day 6 of culture (Fig. 4-15A). Treatment of cultures with mo142-3p over five days resulted in a marked decrease in WNT signaling levels in BALO as compared to Scra. Similar observations were noted in TOPGAL rMC cultures (Fig. 4-15B). Remarkably, day six β-galactosidase$^+$ rMC were detected in clusters scattered throughout the Matrigel culture while day 11 β-galactosidase$^+$ rMC were mainly found within BALO, as described above.

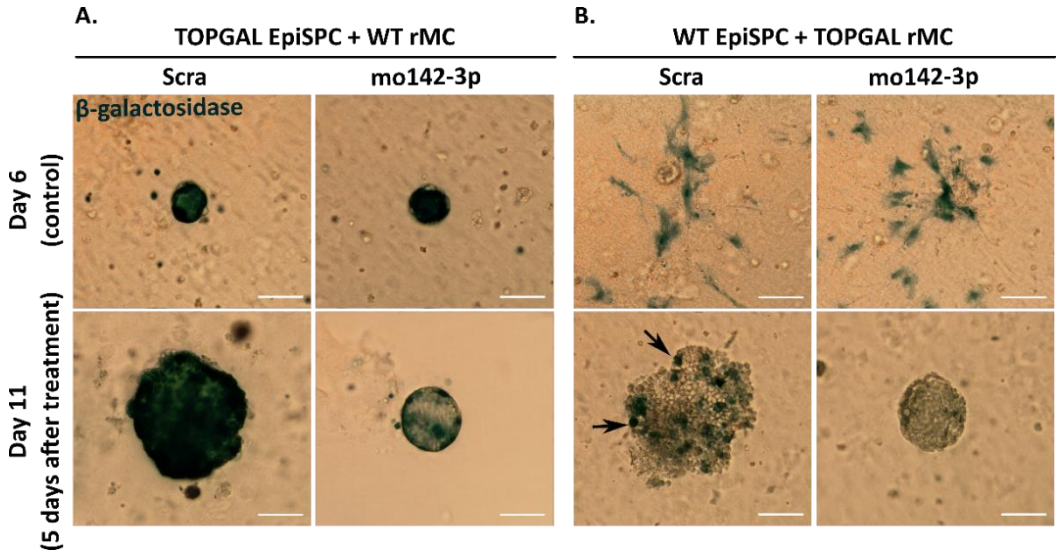

Figure 4-15. Active β-catenin expression in BASC and rMC after mo142-3p treatment. Active canonical WNT signalling was reduced in mo142-3p-treated cultures. Representative images of β-galactosidase staining in (A) TOPGAL BASC co-cultivated with WT rMC and (B) WT BASC co-cultivated with TOPGAL rMC at day 0 and 5 (arrows) after treatment with Scra or mo142-3p. Scale bars represent 100 µm.

Lastly, BALO formation was examined after 15 days of mo142-3p or Scra application. Not only were mo142-3p-treated BALO considerably smaller than Scra-treated BALO but also displayed impaired branching morphogenesis shown by the decreased number of branching points in mo142-3p-treated BALO. These data indicate that *miR142-3p* loss of function in BALO recapitulates the phenotype found in embryonic lung explants, as described in Carraro *et al.*, 2014[181](Fig. 4-16A and B).

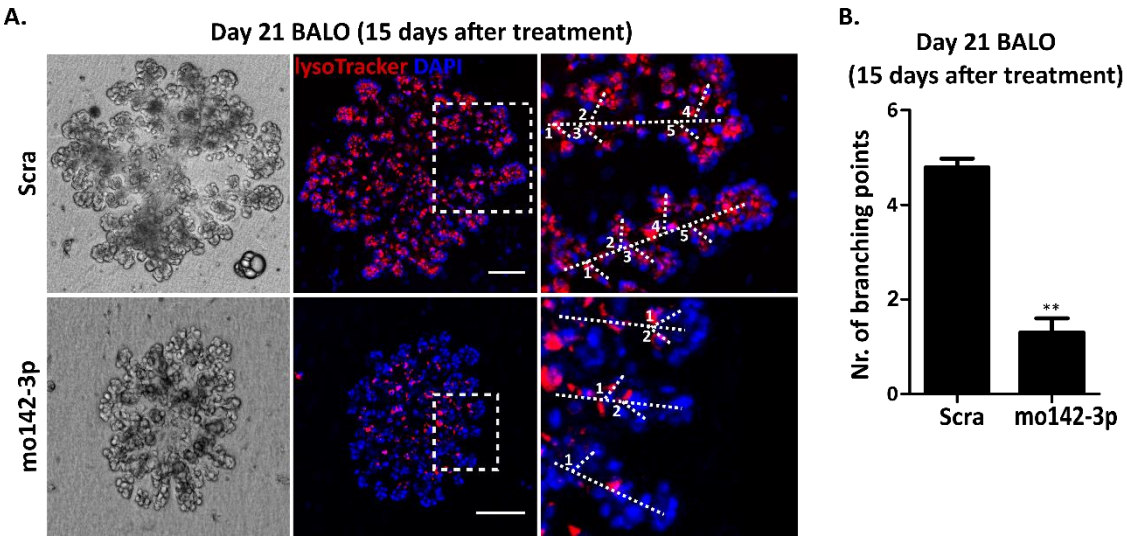

Figure 4-16. BALO formation after prolonged mo142-3p addition. Loss of *miR142-3p* caused a major defect in branching morphogenesis in BALO. (A) Representative images of bright field and LysoTracker staining of co-cultures at day 15 after treatment with Scra or mo142-3p. Scale bars represent 100 µm. (B) Number of branching points observed in BALO after 15 days of treatment by Scra or mo142-3p. Mean ± SEM is depicted (n=4 BALO, n=3 experiments P-value <0.05).

Altogether, *miR142-3p* positive regulation of canonical WNT signaling and its impact on lung growth and branching morphogenesis was confirmed in the BALO system, but these experiments also revealed that gene knockdown strategies can be efficiently applied to that system. These results indicate that the *in vitro* BALO model represents a functional tool to address cell-specific developmental questions, especially referring to epithelial-mesenchymal crosstalk during lung development.

4.8 Use of BALO model to study the effect of the soluble growth factor, GM-CSF, in BASC proliferation and differentiation

The BALO system was also employed to test if GM-CSF, a well-known differentiation factor for myeloid cells, was involved in lung epithelial stem cell proliferation and differentiation. In this regard, published and unpublished data acquired in our laboratory[184] demonstrated that GM-CSF expressed by the alveolar epithelium increases survival after IAV infection. To first evaluate the impact of GM-CSF on the AECII population *in vivo*, immunofluorescence of SFTPC and ki67 in mock and IAV-infected WT, GM-CSF$^{-/-}$, and SPC-GM lung sections was performed (Fig. 4-17A-B). Of note, SPC-GM mice have a GM-CSF$^{-/-}$ background but overexpress GM-CSF only in SFTPC^{+} cells. 7 days after IAV infection, the number of AECII in infected GM-CSF$^{-/-}$ lungs was considerably decreased in comparison with both WT and SPC-GM mice (Fig. 4-17A). In accordance, percentage of ki67^{+} cells was significantly reduced in infected GM-CSF-deficient mice compared to WT and SPC-GM mice (Fig. 4-17B). These data confirmed previous results indicating that the presence of GM-CSF in the alveolar epithelium is crucial for cell proliferation and restoration of the AECII pool after viral infection and suggest that GM-CSF may also mediate proliferation of epithelial progenitor cell subsets of the distal lung.

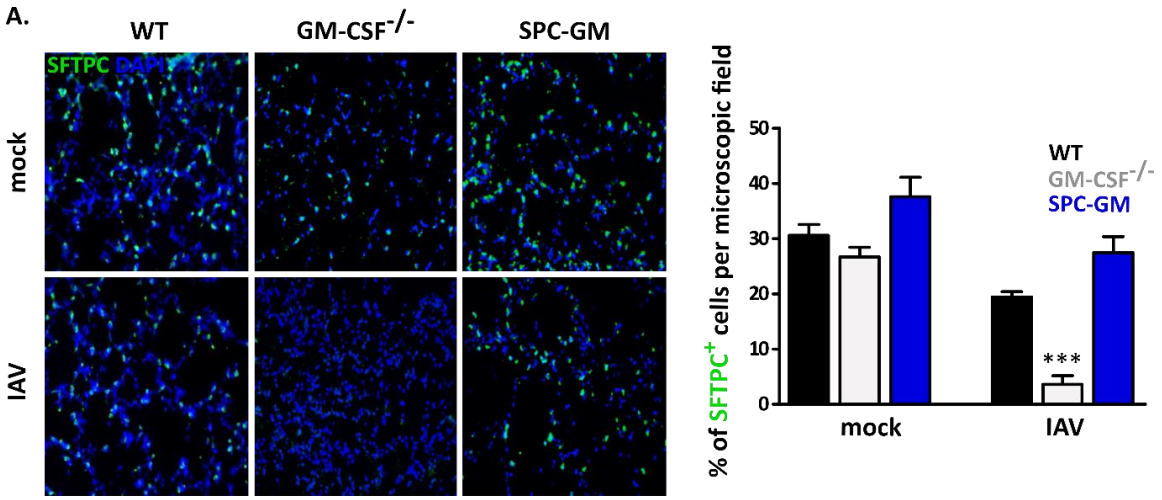

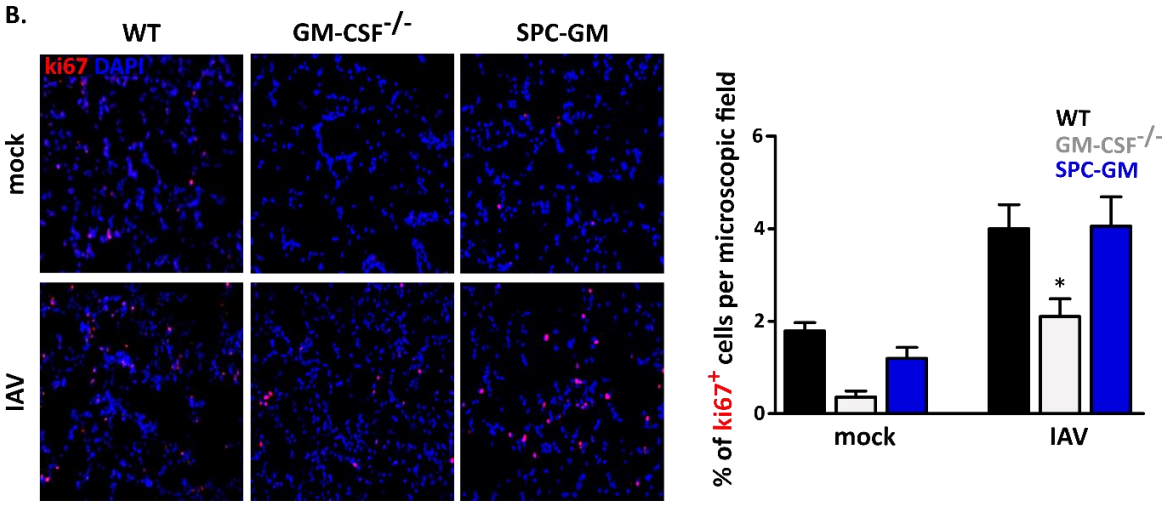

Figure 4-17. Effect of GM-CSF on AECII numbers and proliferation upon IAV infection. Presence or absence of GM-CSF has a significant influence on AECII pool and proliferation 7 days pi. Representative images and quantification of (A) SFTPC$^+$ and (B) ki67$^+$ cells in mock and IAV-infected WT, GM-CSF$^{-/-}$, and SPC-GM lung sections 7 days pi. Mean ± SEM is depicted (n=4 experiments P-value <0.05).

In this line, gene expression of important transcription factors involed in distal lung specification, Sex determining region Y-box 9 (*Sox9*)[185] and retinoic acid receptor beta (*Rarb*)[186], were downregulated in BASC isolated from GM-CSF$^{-/-}$ in comparison with WT BASC (Fig. 4-18A). Based on these data, the *in vitro* system was exploited to test if GM-CSF was involved in BALO formation. Thus, BASC and rMC derived from GM-CSF$^{-/-}$ and WT mice were co-cultivated and organoid growth was evaluated at day 6 and 11 of culture (Fig. 4-18B). Strikingly, BALO from GM-CSF$^{-/-}$-derived BASC were significantly smaller compared to WT cultures. Furthermore, BALO in GM-CSF$^{-/-}$co-cultures did not develop tubular and saccular structures (Fig. 4-18C). These data suggest that GM-CSF is not only important for BASC proliferation but also for lung specification during BALO development. Notably, endogenous GM-CSF release in WT BALO starts at day 6 of culture and peaks at day 11, coinciding with the beginning of organoid differentiation into BALO (Fig. 4-18D).

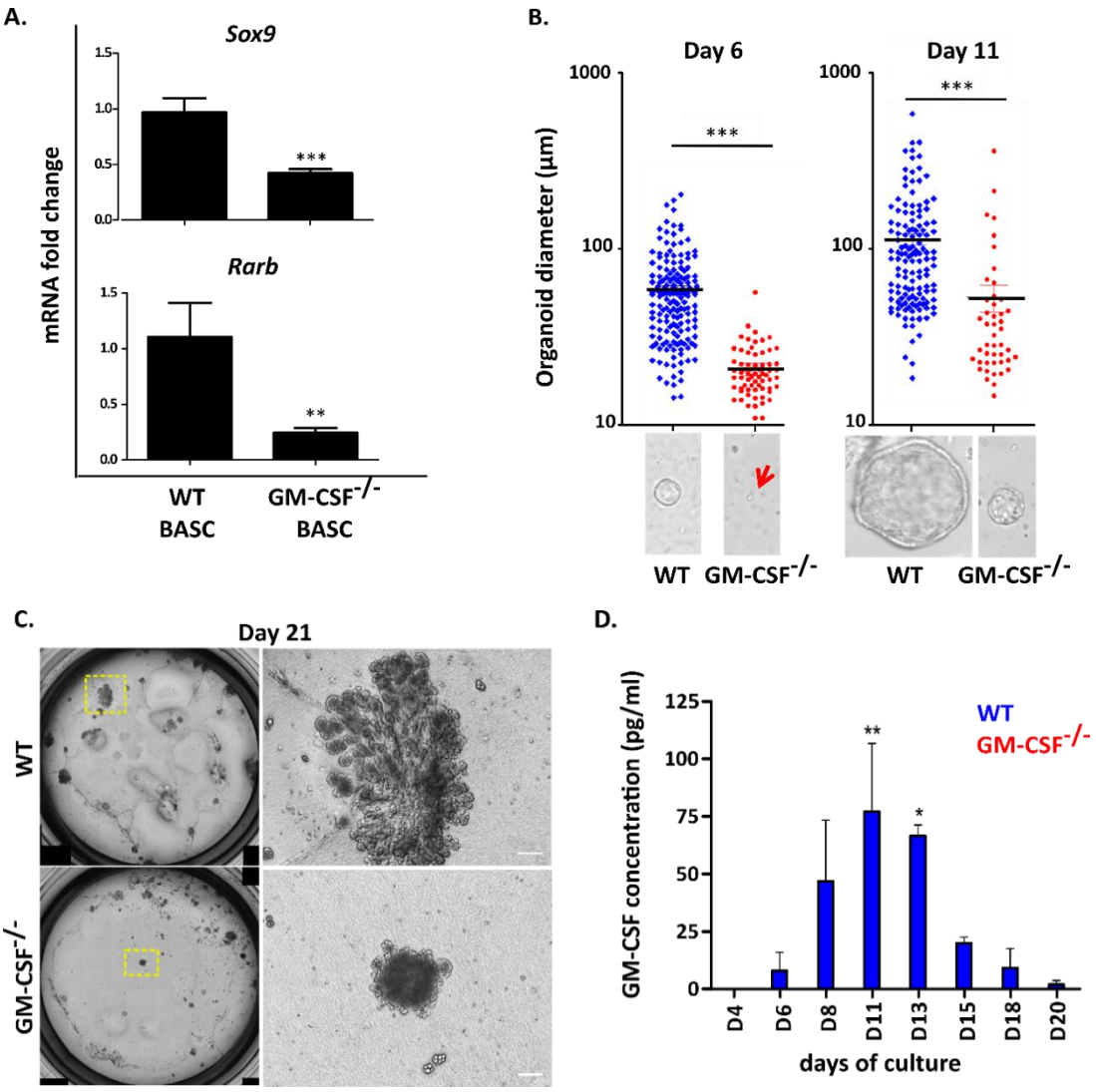

Figure 4-18. BASC proliferation and differentiation in GM-CSF$^{-/-}$ co-cultures. GM-CSF-deficient BASC show reduced proliferation and are not able to form BALO. (A) Gene expression analysis of Sox9 and *Rarb* in WT and GM-CSF$^{-/-}$ BASC by qPCR (n=3, P-value <0.05). (B) Organoid diameter in WT and GM-CSF$^{-/-}$ cultures at day 6 and 11. Red arrow indicates a small organoid. (C) Representative brightfield images of WT and GM-CSF$^{-/-}$ co-cultures at day 21. Scale bars represent 100 µm. (D) Time course of GM-CSF release in WT and GM-CSF$^{-/-}$ co-cultures by ELISA. Mean ± SEM is depicted (n=3, P-value <0.05).

To further examine the relevance of GM-CSF in BASC proliferation and BALO formation, GM-CSF neutralizing antibodies (Ab) or isotype control were added to WT co-cultures. Once again, BASC proliferation was evaluated at day 6 and 11 of culture (Fig. 4-19A). Although a similar effect on BASC proliferation was observed,

organoid growth reduction was only significant at day 11 of culture suggesting that the antibody does not fully neutralize GM-CSF. Nonetheless, as in GM-CSF$^{-/-}$ co-cultures, BALO formation was greatly reduced in anti-GM-CSF Ab treated cultures in comparison with isotype-treated cultures (Fig. 4-19B).

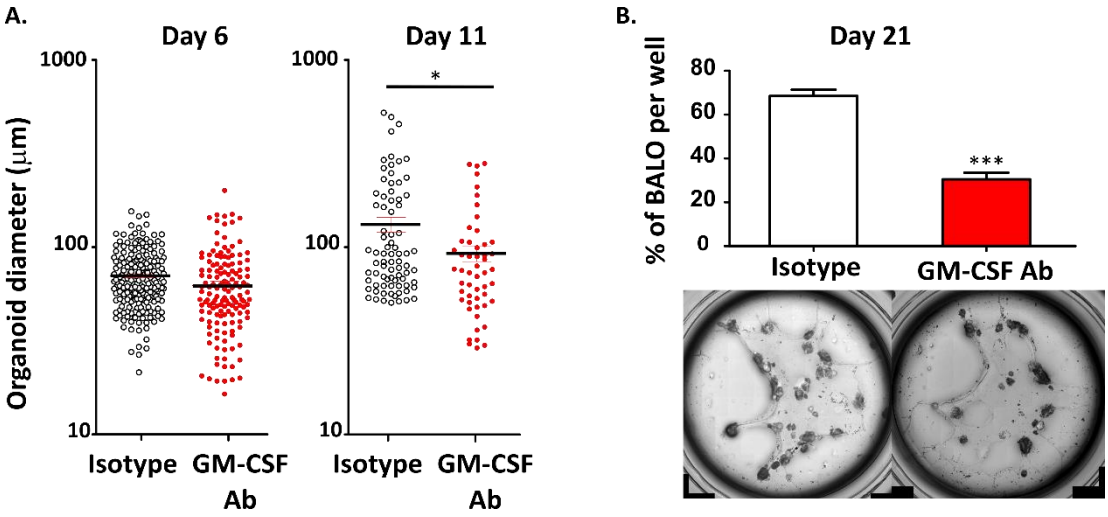

Figure 4-19. BASC proliferation and differentiation after GM-CSF Ab treatment. BASC treated with GM-CSF Ab are less proliferative and form fewer BALO**.** (A) Organoid diameter in isotype- and GM-CSF Ab-treated cultures at day 6 and 11. Mean ± SEM is depicted (n=3, P-value <0.05). (B) Percentage of Isotype- and GM-CSF Ab-treated BALO per well and representative images of whole-well brightfield at day 21 of culture. Mean ± SEM is depicted (n=4, P-value <0.05).

The GM-CSF receptor is a heterodimer composed of a ligand-binding subunit alpha (GM-CSFRα) and a beta subunit which mediates signal transduction (GM-CSFRβ). Hence, to further evaluate GM-CSF signalling pathway, BASC and rMC derived from GM-CSFRβ$^{-/-}$ and WT mice were co-cultivated. Reduced BASC growth was found in day 11 GM-CSFRβ$^{-/-}$ cultures when compared to WT (Fig. 4-20A). Interestingly, in GM-CSFRβ$^{-/-}$ day 21 cultures, BASC failed to form BALO with characteristic distal specification as verified by lack of distal tip saccular structures (Fig. 4-20B). In concordance, low numbers of differentiated AECII were found in GM-CSFRβ$^{-/-}$ BALO by confocal microscopy (Fig. 4-20C).

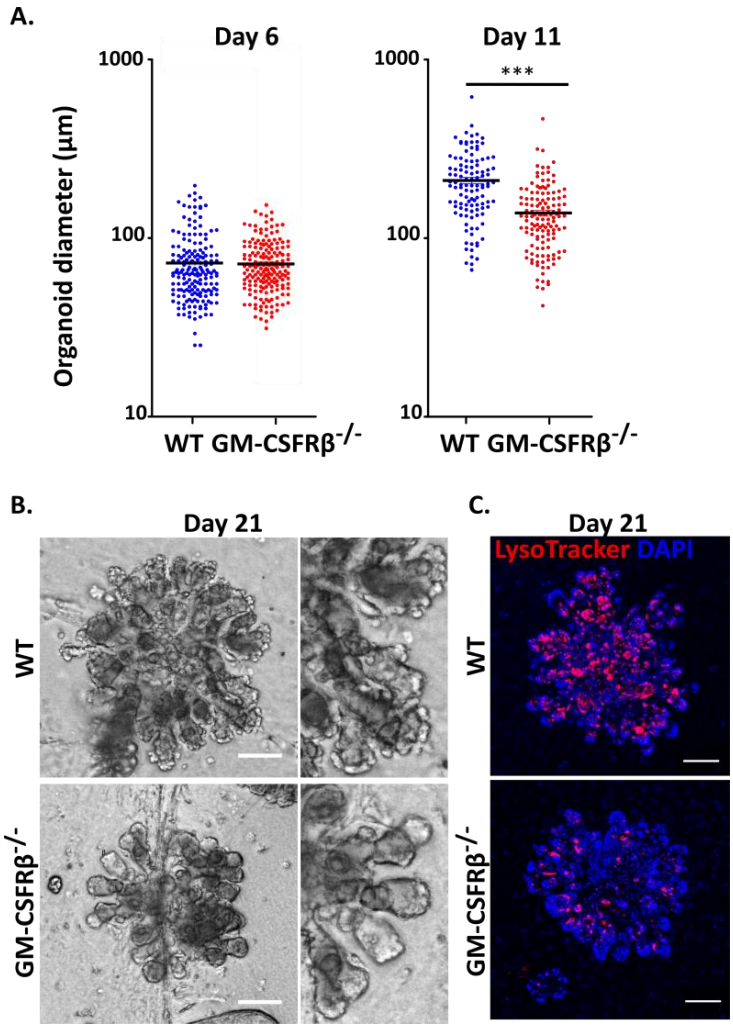

Figure 4-20. BASC proliferation and differentiation in GM-CSF Rβ$^{-/-}$ co-cultures. GM-CSF Rβ -deficient BASC proliferate less and form defective BALO. (A) Organoid diameter in WT and GM-CSFRβ$^{-/-}$ cultures at day 6 and 11 of culture. Mean ± SEM is depicted (n=3, P-value <0.05). (B) Representative brightfield images of WT and GM-CSFRβ$^{-/-}$ co-cultures at day 21. Scale bars represent 100 µm. (C) Representative confocal images of LysoTracker staining in GM-CSFRβ$^{-/-}$ co-cultures at day 21 of culture. Scale bars represent 100 µm.

In conclusion, the BALO *in vitro* model shows that GM-CSF is indispensable for BASC proliferation and differentiation into AECII and will now be further used to determine whether GM-CSF/GM-CSFR regenerative signaling pathway can drive lung tissue repair upon lung injury caused by pathogens such as influenza virus. The data also demonstrate that the BALO model is useful to study the role of growth factors on epithelial cell proliferation and survival, and specification during lung development.

4.9 BALO support IAV replication and can be used to model lung infection

The applicability of the BALO system for disease modeling was next tested in an influenza infection model, using a highly pathogenic H7N7 and a seasonal H1N1 strain. To directly visualize infected epithelial cells, a recently generated Influenza A reporter virus expressing Cre recombinase (SC35M-Cre) (H7N7)[154] was used. Identification of IAV-infected cells on a single-cell basis was achieved by using SC35M-Cre in combination with BALO derived from a reporter mouse expressing membrane-targeted tdTomato (mT) after Cre recombination. BALO were observed from 24 to 48 h pi to visualize cell infection, viral spread and virus-induced cell loss. BALO were infected by IAV as shown through microscopy. Moreover, viral spread was observed between 24 and 48 h pi, indicating that BALO support viral replication. Release of infectious influenza A virions from BALO was confirmed by plaque assay of cell culture supernatant at 48 h pi (Fig. 4-21B). In parallel, significant loss of tissue areas in BALO was observed at 48 h, which had been infected at 24 h, reflecting loss of cells observed in IAV-induced lung injury *in vivo*[187] (Fig. 4-21A).

H1N1 viral proteins, hemagglutinin (HA) and nucleoprotein (NP), are indispensable for successful viral infection and replication. For instance, HA binds on the surface of the host cell through its α-sialic acid receptor and mediates virus entry whereas NP is essential for viral replication as part of the ribonucleoprotein complex[176]. Therefore, to further demonstrate successful BALO infection in terms of generation of viral proteins in infected epithelial cells, gene expression analysis of NP was performed in flow-sorted infected and non-infected cells. Respectively, $EpCAM^+HA^+$ and $EpCAM^+HA^-$ cells were analyzed by qPCR, where, as expected, NP expression was detected only in the infected epithelial cell population (Fig. 4-21C). Additionally, the proportion of infected $EpCAM^+$ epithelial cells showing productive viral replication was determined by FACS analysis of intracellular NP expression. On average, 8% of BALO epithelial cells were infected (Fig. 4-21D). The $EpCAM^-$ mesenchymal cell population in BALO was not infected by IAV as previously

observed *in vivo*[85] (data not shown). To define cellular responses to infection in BALO, interferon beta (*Ifn*β) expression in non- and IAV-infected BALO cells was analyzed by qPCR. A significant upregulation of *Ifn*β was observed in IAV-infected $EpCam^{+}HA^{+}$ BALO cells, indicating that BALO epithelium not only supports IAV infection and spread, but is also functional with respect to mounting an antiviral response upon IAV infection and can therefore be used for viral infection disease modeling (Fig. 4-21E).

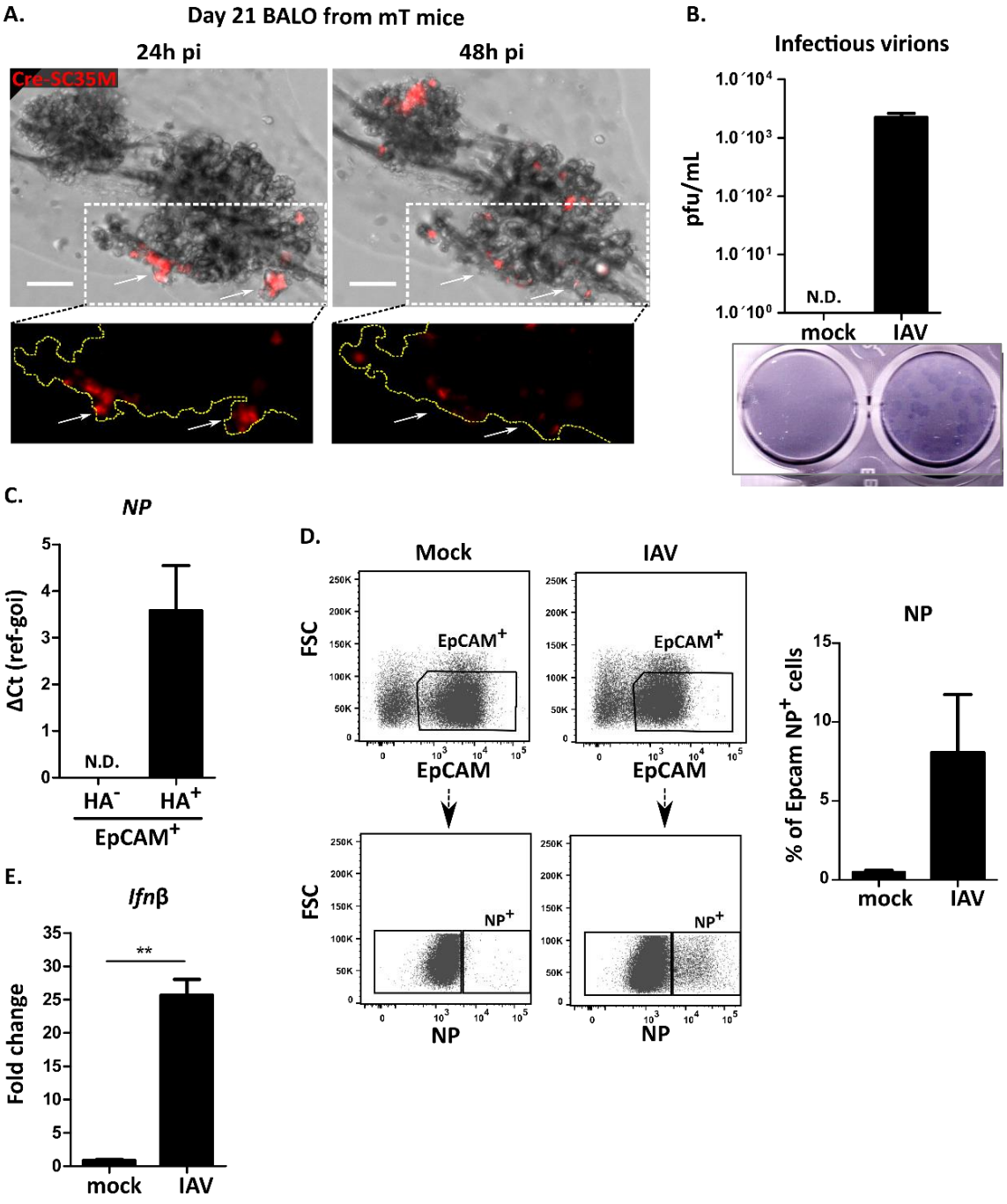

Figure 4-21. Analysis of IAV infection in BALO. BALO support IAV infection of alveolar epithelial cells. (A) Representative images of BALO infection by Cre-SC35M IAV (red) after 24 and 48 h. Cell loss was observed 48 h pi (white arrows). Scale bars represent 100 µm. (B) Plaque assay of mock and infected co-culture supernatants 48 h pi. Mean ± SEM is depicted (n=3). (C) Gene expression analysis of *NP* in mock and infected $EpCAM^+$ cells by qPCR. Mean ± SEM is depicted (n=3). (D) Percentage of NP in mock and infected $EpCAM^+$ cells by FACS. Mean ± SEM is depicted (n=3). (E) Gene expression analysis of *Ifn*β in non-infected and infected $EpCAM^+$ cells by qPCR. Mean ± SEM is depicted (n=3, P-value <0.05).

5 DISCUSSION

This thesis describes the establishment of a robust protocol for isolation and 3D culture of murine BASC and rMC giving rise to complete BALO, and possessing distinct proximo-distal specification with tubular and saccular lung structures after 21 days of culture. The system is easily amenable for various applications for organ development and disease modeling. The stem cell of origin contained in the previously-defined $EpCAM^{high}itg(\alpha6\beta4)^{+}CD24^{low}$ EpiSPC population[85] that generates BALO was characterized in detail. Cells with a "BASC" signature[134](Sca-$1^{+}SFTPC^{+}SCGB1A1^{+}$) were capable of multilineage differentiation which seems a prerequisite for successful BALO formation. 3D culture data indicate that a high BALO purity (>80%) can be achieved when both Sca-1 and CD24 markers are included to define the BASC population and a strict gating strategy (exclusion of alveolosphere- and bronchiolosphere-forming progenitor cells) is applied. Compared to other similar models, this approach represents a substantial improvement in organoid structural homogeneity. For instance, only ~20% of the forming organoids in previously reported models possess cell markers representing both bronchiolar and alveolar compartments[61,134]. These findings will be relevant for numerous future applications (e.g. drug screening), as single BASC could be easily deposited by automated single-cell sorting and generate a complete BALO per cell culture well.

Most of the established models for human lung development and disease are based on iPSC differentiated in 2D cultures, therefore lacking a robust 3D structure including branched airways and distal alveoli[48,135,141,171,172,188–191]. Recently, iPSC-derived human lung organoids were demonstrated to form airway-like structures, but maintain a relatively high number of undifferentiated epithelial progenitor cells and low numbers of differentiated bronchial and alveolar cells, particularly AECI[135,192,193]. In addition, generation of lung-like structures from human pluripotent

stem cells is relatively time-consuming and requires several months until final differentiation stages are reached (~180 days)[193]. In contrast, investigation of the cellular composition of BALO using qPCR, immunofluorescence and FACS provided evidence that all major cell types of the conducting airways as well as alveoli are present. In particular, FACS analysis of single-cell suspensions derived from BALO reproduced the cellular composition of adult mouse lungs, and AECII within the alveolar BALO compartment were capable of surfactant secretion. To my knowledge, the BASC-derived organoid model is the only one that offers this level of complexity and allows direct observation of stem cell proliferation and organ development.

The phenotype and spatial organization of co-cultured mesenchymal cells emerged as another important aspect of a successful lung organoid system. During development, mesenchyme-derived growth factors drive epithelial proliferation, differentiation, and branching morphogenesis[194]. Previous studies revealed that lipofibroblasts are located at the base of the alveoli and express low levels of PDGFRα, whereas non–lipid-containing myofibroblasts are PDGFRα^{high} and reside at the alveolar entry ring during development[195,196]. A previous study in which AECII were co-cultured with PDGFRα^{+} cells revealed that these cells are necessary for alveolosphere formation[73]. Accordingly, CD31^{-}EpCAM^{-}Sca-1^{+} rMC proved to be indispensable for proper BALO formation. Using rMC isolated from PDGFRα reporter mice, a PDGFRα fraction of sorted rMC was shown to represent progenitor cells for lipofibroblast and myofibroblast phenotypes. αSMA^{+}PDGFRα^{high} myofibroblasts were detected inside the organoid structures and seemed to provide a scaffold for tube formation. However, BASC cultured with myofibroblast precursors alone did not show any organoid formation. In contrast, rMC-derived LipidTOX^{+}PDGFRα^{low} lipofibroblasts supported BASC proliferation in the early organoid but did not support branching morphogenesis. These data indicate that both PDGFRα^{high} and PDGFRα^{low} mesenchymal cell subsets are indispensable components of the stem cell

niche and fulfill distinct tasks during BALO formation in absence of endothelial cells[134]. Emergence of distinct myofibroblast and lipofibroblast phenotypes from PDGFRα^{high} and PDGFRα^{low} rMC within the developing BALO will enable researchers to study epithelial-mesenchymal cross-talk mechanisms and the role of these subsets within the niche during organogenesis, injury and repair[197].

Another important component of the lung stem cell niche are TR-Mac. Macrophage precursors seed the organ as early as E10.5 in different waves and significantly contribute to lung development, branching morphogenesis, tissue regeneration and remodeling[198–201]. Establishment of a reliable microinjection protocol enabled us to introduce these cells into the alveolar BALO compartment to study and visualize these processes. It has been suggested recently that different subsets of macrophages might exert different roles for branching, alveolarization, and repair after injury[202]. Vice versa, it seems likely that the developing or repairing epithelium provides signals important for programming of macrophages into distinct phenotypes. It has been difficult to address the molecular cross-talk between immune cells and lung epithelia and to visualize such processes at single-cell resolution, particularly in developing embryonic lungs. The BALO model will facilitate future mechanistic studies in this field, including the role of different myeloid cell populations. Despite the evident advantages of BALO complemented with myeloid cells, the *in vitro* model lacks an endothelial compartment. Endothelial cells co-develop with the lung epithelium and it would be of great benefit to study endothelial/epithelial cross-talk *in vitro* or to model lung diseases confined to this compartment. Although, CD31^{+} endothelial cells from adult lung were found to drive organoid development from BASC, a proper spatially organized endo-epithelial network never developed in such studies[134]. The question remains whether better-defined endothelial progenitor cells such as cells derived from multi-potent cardiopulmonary mesoderm progenitors[203] will be helpful to increase the cellular complexity of the BALO model.

Current CRISPR/Cas9 protocols mostly rely on 2D growth of cells combined with single-cell cloning of respective mutant cells, which has hampered the generation of loss of function or gene corrected murine and human lung organoids[192]. Therefore, a knock-down strategy was applied in growing BALO. *miR142-3p*, a miRNA known to inhibit the canonical WNT β-catenin pathway, was suppressed by addition of morpholino oligos. This approach faithfully recapitulated developmental defects in BALO including reduced growth and impaired branching morphogenesis that were previously observed in embryonic lung explants treated with mo142-3p[181]. In sum, knock-down of target genes at different stages of BALO development is a powerful tool to dissect the function of individual genes without damaging the organoid and without the need for organoid dissociation[204].

As previously demonstrated, bacterial and viral lung infection stimulate the release of GM-CSF *in vivo* which acts as a growth factor driving cell-mediated repair mechanisms by inducing AECII proliferation and restoring the alveolar epithelial barrier after injury[113,205]. These observations were further confirmed *in vivo* by IAV infection of WT and transgenic mice. In these experiments, AECII pool and cell proliferation was markedly decreased in the absence of GM-CSF. Next, *in vitro* experiments with the newly established BALO model using BASC and rMC derived from GM-CSF- and GM-CSFRβ-deficient mice were performed. Interestingly, the model revealed that GM-CSF is indispensable for cell proliferation and alveologenesis of BALO. In concordance, gene expression of *Sox9* and *Rar*β, transcription factors involved in stem cell differentiation and proliferation, was downregulated in BASC isolated from GM-CSF-deficient mice. Laresgoiti and colleagues showed that STAT3 signalling pathway drives alveolar differentiation of *Sox9*$^{+}$ distal tip progenitor cells during lung development[206]. In this line, previous data showed that GM-CSF can signal through JAK/STAT pathway in hematopoietic cells[207] suggesting that STAT3 could represent a downstream target for GM-CSF signalling pathway during development and tissue repair in the lung. Notably,

recent single cell RNA sequencing data indicates that GM-CSF gene expression is highly upregulated in the epithelium and in SFTPC and SCGB1A1-expressing cells during murine lung development at E16.5 and E18.5, respectively[208]. Therefore, GM-CSF-dependent developmental programs might be re-activated during repair after IAV-induced injury. The BALO *in vitro* system will be of high relevance to further elucidate the underlying molecular pathways and cellular cross-talk mechanisms by which GM-CSF induces alveolar repair from stem cell pools of the distal lung in our future work.

In a recent study, human lung organoids derived for hPSC were infected with respiratory syncytial virus. After 48 h of infection, apoptosis and shedding of infected cells occurred, resembling to some extent morphological aspects observed in humans during viral infection[206]. However, in this model, organoids developed slowly (~170 days), forming only early alveolar structures, and are unlikely to be suitable to study infections affecting the bronchioalveolar compartment. Accordingly, BALO epithelium infected by different strains of IAV, supports viral replication and spread, and is capable of initiating an antiviral immune response. Moreover, compared to *in vivo* infection models, the BALO model facilitates live cell imaging of infected cells and - regarding further applications - drug library screens for antiviral drugs could be performed[146]. In this context, an example of the use of organoid models to study bacterial infection was given by Bartfeld and colleagues. This work showed successful infection of mouse and human gastric organoids by direct microinjection of *Helicobacter pylori* into the organoids lumen[209]. Besides the study of viral infections, BALO are well applicable to model other diseases that affect the distal lung, such as bacterial pneumonia caused by *Streptococcus pneumonia or Pseudomonas aeruginosa*[210].

Altogether, the *in vitro* model presented here generates predominantly BALO, that recapitulate the cellular and structural complexity of the bronchioalveolar lung

compartment. Similar models are scarce and observed organoids only possessed a minor degree of bronchiolar and alveolar specification. Moreover, BALO system reproduces lung developmental processes, permits viral infection and replication, and supports homing and persistence of injected tissue-resident myeloid cells such as TR-Mac. Thereby, this model opens several new avenues to study lung development, infection, and regenerative processes *in vitro*.

In the future, the BALO model might be used to: 1) visualize tissue regeneration after injury induced by infection or other insults at high resolution (up to single-cell level) and over time, and 2) pinpoint the role of cells of mesenchymal, epithelial and myeloid origin in these processes. The possibility to supplement the alveolar space of BALO with different tissue-resident or bone marrow-derived leukocyte populations of interest adds a further level of complexity that was not addressed in previously described models. The employment of BASC, rMC and/or leukocytes derived from transgenic mice with gain- or loss of function of defined genes, or from reporter mice, will enable characterization of cell-specific functions of individual of genes. Such feature is currently difficult to achieve using human lung organoid models derived from tissue-endogenous stem cells or iPSC. In this regard, deep sequencing of the murine BASC is currently employed to derive marker genes for identification of a comparable endogenous stem cell type in human lung tissue for development of human lung organoids with a high cellular and structural complexity.

6 SUMMARY

Organoid model systems derived from mouse and human stem cells have recently evolved as a powerful tool to study development and disease. A murine 3D bronchioalveolar lung organoid model was established based on FACS-sorting of a newly defined population of bronchioalveolar stem cells. Upon co-culture with subsets of lung mesenchymal cells, which model the stem cell niche of the developing lung, these stem cells underwent clonal expansion, followed by branching morphogenesis and self-organization into complete lung organoids, while retaining their tissue-of-origin commitment and their potential to differentiate into functional cells. Of note, organoids closely reproduced the 3D structure and cellular composition of the bronchioalveolar compartment of the lung. In addition, the 3D bronchioalveolar organoid structure allowed seeding of tissue-resident macrophages into the alveolar compartment, providing the possibility to study the contribution of the resident myeloid cell pool to developmental and regeneration processes within the alveolar microenvironment. Moreover, lung organoids derived from gene-deficient mice and selective inhibitor experiments revealed that the GM-CSF/GM-CSFR axis was necessary for BALO growth, survival, and alveolarization. Organoids were suitable for FACS-based single cell analyses, and for genetic manipulation as demonstrated by successful knockdown of genes involved in lung development and targeting miR142-3p/β-catenin signaling. Finally, organoids could be used to model lung infection, as demonstrated by use of reporter-tagged influenza viruses in conjunction with live cell imaging, gene expression and functional analyses. In summary, this is the first organoid model recapitulating the 3D structure and cellular composition of the bronchioalveolar lung compartment, opening up new avenues to model lung development, infection, and regeneration processes.

7 ZUSAMMENFASSUNG

In den letzten Jahren wurden zunehmend Organoid-Modelle beschrieben, die von murinen oder humanen Stammzellen ausgehen und Organe ex vivo simulieren. In der vorliegenden Arbeit wurde ein solches 3D Modellsystem für die murine Lunge etabliert, basierend auf FACS-Sortierung einer neu definierten Population bronchoalveolärer Stammzellen. Um die Stammzellnische einer sich entwickelnden Lunge zu rekapitulieren, wurden diese Zellen mit einer definierten Population mesenchymaler Zellen der Lunge ko-kultiviert. Unter diesen Bedingungen waren einzelne Lungenstammzellen in der Lage, klonal zu expandieren, und durch Selbstorganisation ein jeweils vollständiges Organoid der Lunge zu bilden. Von Bedeutung ist in diesem Zusammenhang, dass diese Organoide sowohl die drei dimensionale Struktur als auch die zelluläre Zusammensetzung des bronchoalveolären Kompartiments der Lunge vollständig widerspiegeln. Darüber hinaus gelang es, sich entwickelnde Alveolen der Organoide mit Alveolarmakrophagen zu besiedeln. Dies eröffnet die Möglichkeit, den Einfluss von Gewebe-ständigen myeloiden Zellen auf Entwicklungs- und Regenerationsprozesse in der Alveole zu untersuchen. Es besteht zudem die Möglichkeit, Organoide zu generieren, die von Gen-defizienten Zellen abstammen. Mit Hilfe solcher Organoide oder mittels Applikation von spezifischen Inhibitoren während der Organoid-entwicklung konnte gezeigt werden, dass die GM-CSF/GM-CSFR Achse für das Wachstum und die proximo-distale Spezifizierung von Lungenorganoiden von zentraler Bedeutung ist. Darüber hinaus konnten wir zeigen, dass Organoide sowohl das Ausschalten definierter Gene im epithelialen und mesenchymalen Kompartiment erlauben, als auch die Durchführung von Infektionsexperimenten mit Influenza Virus, was mittels Lebendzell-Imaging, Analyse der viralen Replikation, und der zellulären Immunantwort gezeigt werden konnte. Insgesamt beschreibt die vorliegende Arbeit das erste 3D-Modellsystem für die murine Lunge, das die Struktur und zelluläre Zusammensetzung des bronchioalveolären Kompartiments

vollständig rekapituliert. Dadurch eröffnen sich vielfältige Möglichkeiten, zukünftig Entwicklungs-, Regenerations- sowie Infektionsprozesse in der Lunge hochauflösend und auf Einzelzell-Ebene zu analysieren.

8 REFERENCES

1. Suarez, C. J., Dintzis, S. M. & Frevert, C. W. Respiratory. *Comp. Anat. Histol.* 121–134 (2012). doi:10.1016/B978-0-12-381361-9.00009-3
2. Gaughan, C. & Panos, A. L. in *Principles of Pulmonary Protection in Heart Surgery* 3–8 (Springer London, 2010). doi:10.1007/978-1-84996-308-4_1
3. Min, H. *et al.* Fgf-10 is required for both limb and lung development and exhibits striking functional similarity to Drosophila branchless. *Genes Dev.* **12,** 3156–61 (1998).
4. Rock, J. R., Randell, S. H. & Hogan, B. L. M. Airway basal stem cells: a perspective on their roles in epithelial homeostasis and remodeling. *Dis. Model. Mech.* **3,** 545–56 (2010).
5. Mercer, R. R., Russell, M. L. & Crapo, J. D. Alveolar septal structure in different species. *J. Appl. Physiol.* **77,** (1994).
6. Gehr, P., Bachofen, M. & Weibel, E. R. The normal human lung: ultrastructure and morphometric estimation of diffusion capacity. *Respir Physiol* 121–140 (1978).
7. Netter, F. H. (Frank H. *Atlas of human anatomy*. (Saunders/Elsevier, 2006).
8. Rawlins, E. L. The building blocks of mammalian lung development. *Dev. Dyn.* **240,** 463–476 (2011).
9. Morrisey, E. E. & Hogan, B. L. M. Preparing for the first breath: genetic and cellular mechanisms in lung development. *Dev. Cell* **18,** 8–23 (2010).
10. Que, J., Choi, M., Ziel, J. W., Klingensmith, J. & Hogan, B. L. M. Morphogenesis of the trachea and esophagus: current players and new roles for noggin and Bmps. *Differentiation* **74,** 422–437 (2006).
11. Wells, J. M. & Melton, D. A. Early mouse endoderm is patterned by soluble factors from adjacent germ layers. *Dev.* 1563–1572 (2000).
12. Burri, P. H. Fetal and Postnatal Development of the Lung. *Annu. Rev. Physiol.* **46,** 617–628 (1984).

13. Shannon, J. M., Nielsen, L. D., Gebb, S. A. & Randell, S. H. Mesenchyme specifies epithelial differentiation in reciprocal recombinants of embryonic lung and trachea. *Dev. Dyn.* **212,** 482–494 (1998).
14. Weaver, M., Yingling, J. M., Dunn, N. R., Bellusci, S. & Hogan, B. L. Bmp signaling regulates proximal-distal differentiation of endoderm in mouse lung development. *Development* **126,** 4005–4015 (1999).
15. Lu, M. M. *et al.* The bone morphogenic protein antagonist gremlin regulates proximal-distal patterning of the lung. *Dev. Dyn.* **222,** 667–680 (2001).
16. Mucenski, M. L. *et al.* beta-Catenin is required for specification of proximal/distal cell fate during lung morphogenesis. *J. Biol. Chem.* **278,** 40231–8 (2003).
17. Rackley, C. R. *et al.* Building and maintaining the epithelium of the lung. *J. Clin. Invest.* **122,** 2724–30 (2012).
18. Minoo, P., Su, G., Drum, H., Bringas, P. & Kimura, S. Defects in Tracheoesophageal and Lung Morphogenesis inNkx2.1(−/−) Mouse Embryos. *Dev. Biol.* **209,** 60–71 (1999).
19. Que, J. *et al.* Multiple dose-dependent roles for Sox2 in the patterning and differentiation of anterior foregut endoderm. *Development* **134,** (2007).
20. Metzger, R. J., Klein, O. D., Martin, G. R. & Krasnow, M. A. The branching programme of mouse lung development. *Nature* **453,** 745–750 (2008).
21. Sekine, K. *et al.* Fgf10 is essential for limb and lung formation. *Nat. Genet.* **21,** 138–141 (1999).
22. Rawlins, E. L., Ostrowski, L. E., Randell, S. H. & Hogan, B. L. M. Lung development and repair: contribution of the ciliated lineage. *Proc. Natl. Acad. Sci. U. S. A.* **104,** 410–7 (2007).
23. Sorokin, S. P., Hoyt, R. F. & Shaffer, M. J. Ontogeny of neuroepithelial bodies: Correlations with mitogenesis and innervation. *Microsc. Res. Tech.* **37,** 43–61 (1997).
24. Herriges, M. & Morrisey, E. E. Lung development: orchestrating the

generation and regeneration of a complex organ. *Development* **141,** 502–13 (2014).

25. Rawlins, E. L., Clark, C. P., Xue, Y. & Hogan, B. L. M. The Id2+ distal tip lung epithelium contains individual multipotent embryonic progenitor cells. *Development* **136,** (2009).
26. Desai, T. J., Brownfield, D. G. & Krasnow, M. A. Alveolar progenitor and stem cells in lung development, renewal and cancer. *Nature* **507,** (2014).
27. Wongtrakool, C. *et al.* Down-regulation of retinoic acid receptor alpha signaling is required for sacculation and type I cell formation in the developing lung. *J. Biol. Chem.* **278,** 46911–8 (2003).
28. Langston, C., Kida, K., Reed, M. & Thurlbeck, W. M. Human lung growth in late gestation and in the neonate. *Am. Rev. Respir. Dis.* **129,** 607–13 (1984).
29. Amy, R. W., Bowes, D., Burri, P. H., Haines, J. & Thurlbeck, W. M. Postnatal growth of the mouse lung. *J. Anat.* **124,** 131–51 (1977).
30. Rackley, C. R. & Stripp, B. R. Building and maintaining the epithelium of the lung. *J. Clin. Invest.* **122,** 2724–30 (2012).
31. Kotton, D. N. & Morrisey, E. E. Lung regeneration: mechanisms, applications and emerging stem cell populations. *Nat Med* **20,** 822–832 (2014).
32. Van Lommel, A. *et al.* Pulmonary neuroendocrine cells (PNEC) and neuroepithelial bodies (NEB): chemoreceptors and regulators of lung development. *Paediatr. Respir. Rev.* **2,** 171–6 (2001).
33. Liu, X. & Engelhardt, J. F. The glandular stem/progenitor cell niche in airway development and repair. *Proc. Am. Thorac. Soc.* **5,** 682–8 (2008).
34. Van Lommel, A., Lauweryns, J. M. & Berthoud, H. R. Pulmonary neuroepithelial bodies are innervated by vagal afferent nerves: an investigation with in vivo anterograde DiI tracing and confocal microscopy. *Anat. Embryol. (Berl).* **197,** 325–30 (1998).
35. Rock, J. R. & Hogan, B. L. M. Epithelial progenitor cells in lung development, maintenance, repair, and disease. *Annu. Rev. Cell Dev. Biol.* **27,** 493–512

(2011).

36. Chen, J., Knowles, H. J., Hebert, J. L. & Hackett, B. P. Mutation of the mouse hepatocyte nuclear factor/forkhead homologue 4 gene results in an absence of cilia and random left-right asymmetry. *J. Clin. Invest.* **102,** 1077–82 (1998).
37. Rawlins, E. L. *et al.* The role of Scgb1a1+ Clara cells in the long-term maintenance and repair of lung airway, but not alveolar, epithelium. *Cell Stem Cell* **4,** 525–34 (2009).
38. Williams, M. C. Alveolar Type I Cells: Molecular Phenotype and Development. *Annu. Rev. Physiol.* **65,** 669–695 (2003).
39. Matthay, M. A., Folkesson, H. G. & Clerici, C. Lung Epithelial Fluid Transport and the Resolution of Pulmonary Edema.
40. Whitsett, J. A., Wert, S. E. & Weaver, T. E. Alveolar surfactant homeostasis and the pathogenesis of pulmonary disease. *Annu. Rev. Med.* **61,** 105–19 (2010).
41. Pérez-Gil, J. Structure of pulmonary surfactant membranes and films: The role of proteins and lipid–protein interactions. *Biochim. Biophys. Acta - Biomembr.* **1778,** 1676–1695 (2008).
42. Burns, A. R., Smith, C. W. & Walker, D. C. Unique Structural Features That Influence Neutrophil Emigration Into the Lung. *Physiol. Rev.* **83,** 309–336 (2003).
43. Kapanci, Y., Ribaux, C., Chaponnier, C. & Gabbiani, G. Cytoskeletal features of alveolar myofibroblasts and pericytes in normal human and rat lung. *J. Histochem. Cytochem.* **40,** 1955–63 (1992).
44. Lindahl, P. *et al.* Alveogenesis failure in PDGF-A-deficient mice is coupled to lack of distal spreading of alveolar smooth muscle cell progenitors during lung development. *Development* **124,** (1997).
45. Morimoto, M. *et al.* Canonical Notch signaling in the developing lung is required for determination of arterial smooth muscle cells and selection of Clara versus ciliated cell fate. *J. Cell Sci.* **123,** 213–24 (2010).
46. Martin, U. Methods for studying stem cells: Adult stem cells for lung repair.

Methods **45,** 121–132 (2008).

47. Li, F., He, J., Wei, J., Cho, W. C. & Liu, X. Diversity of Epithelial Stem Cell Types in Adult Lung. *Stem Cells Int.* **2015,** 1–11 (2015).
48. Rock, J. R. *et al.* Basal cells as stem cells of the mouse trachea and human airway epithelium. *Proc. Natl. Acad. Sci. U. S. A.* **106,** 12771–5 (2009).
49. Rawlins, E. L. *et al.* The role of Scgb1a1+ Clara cells in the long-term maintenance and repair of lung airway, but not alveolar, epithelium. *Cell Stem Cell* **4,** 525–34 (2009).
50. Hegab, A. E. *et al.* Novel stem/progenitor cell population from murine tracheal submucosal gland ducts with multipotent regenerative potential. *Stem Cells* **29,** 1283–93 (2011).
51. Kim, C. F. B. *et al.* Identification of bronchioalveolar stem cells in normal lung and lung cancer. *Cell* **121,** 823–35 (2005).
52. Schoch, K. G. *et al.* A subset of mouse tracheal epithelial basal cells generates large colonies in vitro. *Am. J. Physiol. - Lung Cell. Mol. Physiol.* **286,** (2004).
53. Ghosh, M. *et al.* A single cell functions as a tissue-specific stem cell and the in vitro niche-forming cell. *Am. J. Respir. Cell Mol. Biol.* **45,** 459–69 (2011).
54. Tadokoro, T. *et al.* IL-6/STAT3 promotes regeneration of airway ciliated cells from basal stem cells. *Proc. Natl. Acad. Sci. U. S. A.* **111,** E3641-9 (2014).
55. Borthwick, D. W., Shahbazian, M., Todd Krantz, Q., Dorin, J. R. & Randell, S. H. Evidence for Stem-Cell Niches in the Tracheal Epithelium. *Am. J. Respir. Cell Mol. Biol.* **24,** 662–670 (2001).
56. Tata, P. R. *et al.* Dedifferentiation of committed epithelial cells into stem cells in vivo. *Nature* **503,** 218–23 (2013).
57. Hong, K. U., Reynolds, S. D., Giangreco, A., Hurley, C. M. & Stripp, B. R. Clara Cell Secretory Protein–Expressing Cells of the Airway Neuroepithelial Body Microenvironment Include a Label-Retaining Subset and Are Critical for Epithelial Renewal after Progenitor Cell Depletion. *Am. J. Respir. Cell Mol. Biol.* **24,** 671–681 (2001).

58. Reynolds, S. D. & Malkinson, A. M. Clara cell: progenitor for the bronchiolar epithelium. *Int. J. Biochem. Cell Biol.* **42,** 1–4 (2010).

59. Giangreco, A., Reynolds, S. D. & Stripp, B. R. Terminal bronchioles harbor a unique airway stem cell population that localizes to the bronchoalveolar duct junction. *Am. J. Pathol.* **161,** 173–82 (2002).

60. Teisanu, R. M., Lagasse, E., Whitesides, J. F. & Stripp, B. R. Prospective isolation of bronchiolar stem cells based upon immunophenotypic and autofluorescence characteristics. *Stem Cells* **27,** 612–22 (2009).

61. McQualter, J. L., Yuen, K., Williams, B. & Bertoncello, I. Evidence of an epithelial stem/progenitor cell hierarchy in the adult mouse lung. *Proc. Natl. Acad. Sci. U. S. A.* **107,** 1414–1419 (2010).

62. Zuo, W. *et al.* p63(+)Krt5(+) distal airway stem cells are essential for lung regeneration. *Nature* **517,** 616–620 (2014).

63. Kumar, P. A. *et al.* Distal airway stem cells yield alveoli in vitro and during lung regeneration following H1N1 influenza infection. *Cell* **147,** 525–538 (2011).

64. Vaughan, A. E. *et al.* Lineage-negative progenitors mobilize to regenerate lung epithelium after major injury. *Nature* **517,** 621–5 (2015).

65. Mahoney, J. E. & Kim, C. F. Tracing the potential of lung progenitors. *Nat. Biotechnol.* **33,** 152–154 (2015).

66. Zheng, D. *et al.* A Cellular Pathway Involved in Clara Cell to Alveolar Type II Cell Differentiation after Severe Lung Injury. *PLoS One* **8,** e71028 (2013).

67. Rock, J. R. *et al.* Multiple stromal populations contribute to pulmonary fibrosis without evidence for epithelial to mesenchymal transition. *Proc. Natl. Acad. Sci. U. S. A.* **108,** E1475-83 (2011).

68. Hegab, A. E. *et al.* Isolation and Characterization of Murine Multipotent Lung Stem Cells. *Stem Cells Dev.* **19,** 523–536 (2010).

69. McQualter, J. L. *et al.* Endogenous Fibroblastic Progenitor Cells in the Adult Mouse Lung Are Highly Enriched in the Sca-1 Positive Cell Fraction. *Stem Cells* **27,** 623–633 (2009).

70. Zacharek, S. J. *et al.* Lung stem cell self-renewal relies on BMI1-dependent control of expression at imprinted loci. *Cell Stem Cell* **9,** 272–81 (2011).

71. McQualter, J. L. & Bertoncello, I. Concise Review: Deconstructing the Lung to Reveal Its Regenerative Potential. *Stem Cells* **30,** 811–816 (2012).

72. Shiomi, T., Sklepkiewicz, P., Bodine, P. V. N. & D'Armiento, J. M. Maintenance of the bronchial alveolar stem cells in an undifferentiated state by secreted frizzled-related protein 1. *FASEB J.* **28,** 5242–9 (2014).

73. Barkauskas, C. et al. Type 2 alveolar cells are stem cells in adult lung. *J Clin Invest* **123,** 3025–3036 (2013).

74. Adamson, I. Y. & Bowden, D. H. The type 2 cell as progenitor of alveolar epithelial regeneration. A cytodynamic study in mice after exposure to oxygen. *Lab. Invest.* **30,** 35–42 (1974).

75. Evans, M. J., Cabral, L. J., Stephens, R. J. & Freeman, G. Transformation of alveolar Type 2 cells to Type 1 cells following exposure to NO2. *Exp. Mol. Pathol.* **22,** 142–150 (1975).

76. Reddy, R. *et al.* Isolation of a putative progenitor subpopulation of alveolar epithelial type 2 cells. *Am. J. Physiol. - Lung Cell. Mol. Physiol.* **286,** (2004).

77. Reynolds, S. D. *et al.* Airway injury in lung disease pathophysiology: selective depletion of airway stem and progenitor cell pools potentiates lung inflammation and alveolar dysfunction. *Am. J. Physiol. - Lung Cell. Mol. Physiol.* **287,** (2004).

78. Chapman, H. A. *et al.* Integrin α6β4 identifies an adult distal lung epithelial population with regenerative potential in mice. *J. Clin. Invest.* **121,** 2855–62 (2011).

79. Avril-Delplanque, A. *et al.* Aquaporin-3 Expression in Human Fetal Airway Epithelial Progenitor Cells. *Stem Cells* **23,** 992–1001 (2005).

80. Oeztuerk-Winder, F., Guinot, A., Ochalek, A. & Ventura, J.-J. Regulation of human lung alveolar multipotent cells by a novel p38α MAPK/miR-17-92 axis. *EMBO J.* **31,** 3431–3441 (2012).

81. Bravo, D. T. *et al.* Characterization of human upper airway epithelial progenitors. *Int. Forum Allergy Rhinol.* **3,** 841–847 (2013).

82. Kajstura, J. *et al.* Evidence for Human Lung Stem Cells. *N. Engl. J. Med.* **364,** 1795–1806 (2011).

83. Fuchs, E., Tumbar, T. & Guasch, G. Socializing with the neighbors: stem cells and their niche. *Cell* **116,** 769–78 (2004).

84. Volckaert, T. & De Langhe, S. Lung epithelial stem cells and their niches: Fgf10 takes center stage. *Fibrogenesis Tissue Repair* **7,** 8 (2014).

85. Quantius, J. *et al.* Influenza Virus Infects Epithelial Stem/Progenitor Cells of the Distal Lung: Impact on Fgfr2b-Driven Epithelial Repair. *PLoS Pathog.* **12,** (2016).

86. Guha, A. *et al.* Neuroepithelial body microenvironment is a niche for a distinct subset of Clara-like precursors in the developing airways. *Proc. Natl. Acad. Sci. U. S. A.* **109,** 12592–7 (2012).

87. Hong, K. U., Reynolds, S. D., Watkins, S., Fuchs, E. & Stripp, B. R. In vivo differentiation potential of tracheal basal cells: evidence for multipotent and unipotent subpopulations. *Am J Physiol Lung Cell Mol Physiol* **286,** L643-9 (2004).

88. Hong, K. U. In vivo differentiation potential of tracheal basal cells: evidence for multipotent and unipotent subpopulations. *AJP Lung Cell. Mol. Physiol.* **286,** 643L–649 (2003).

89. Griffiths, M. J., Bonnet, D. & Janes, S. M. Stem cells of the alveolar epithelium. *Lancet* **366,** 249–260 (2005).

90. Rehan, V. K. & Torday, J. S. PPARγ signaling mediates the evolution, development, homeostasis, and repair of the lung. *PPAR Research* **2012,** 1–8 (2012).

91. Orkin, S. H. & Zon, L. I. Hematopoiesis: An Evolving Paradigm for Stem Cell Biology. *Cell* **132,** 631–644 (2008).

92. Naito, M., Yamamura, F., Nishikawa, S. & Takahashi, K. Development,

differentiation, and maturation of fetal mouse yolk sac macrophages in cultures. *J. Leukoc. Biol.* **46,** 1–10 (1989).

93. Schneider, C. *et al.* Induction of the nuclear receptor PPAR-γ by the cytokine GM-CSF is critical for the differentiation of fetal monocytes into alveolar macrophages. *Nat. Immunol.* **15,** 1026–1037 (2014).
94. Guilliams, M. *et al.* Alveolar macrophages develop from fetal monocytes that differentiate into long-lived cells in the first week of life via GM-CSF. *J. Exp. Med.* **210,** (2013).
95. Ajami, B., Bennett, J. L., Krieger, C., Tetzlaff, W. & Rossi, F. M. V. Local self-renewal can sustain CNS microglia maintenance and function throughout adult life. *Nat. Neurosci.* **10,** 1538–1543 (2007).
96. Ginhoux, F. *et al.* Fate Mapping Analysis Reveals That Adult Microglia Derive from Primitive Macrophages. *Science (80-.).* **330,** 841–845 (2010).
97. Hashimoto, D. *et al.* Tissue-Resident Macrophages Self-Maintain Locally throughout Adult Life with Minimal Contribution from Circulating Monocytes. *Immunity* **38,** 792–804 (2013).
98. Goldstein, E., Lippert, W. & Warshauer, D. Pulmonary alveolar macrophage. Defender against bacterial infection of the lung. *J. Clin. Invest.* **54,** 519–28 (1974).
99. Westphalen, K. *et al.* Sessile alveolar macrophages communicate with alveolar epithelium to modulate immunity. *Nature* **506,** 503–6 (2014).
100. Ballinger, M. N. *et al.* Role of Granulocyte Macrophage Colony-Stimulating Factor during Gram-Negative Lung Infection with ***Pseudomonas aeruginosa*** . *Am. J. Respir. Cell Mol. Biol.* **34,** 766–774 (2006).
101. Paine, R. *et al.* Granulocyte-macrophage colony-stimulating factor in the innate immune response to Pneumocystis carinii pneumonia in mice. *J. Immunol.* **164,** 2602–9 (2000).
102. Gonzalez-Juarrero, M. *et al.* Disruption of granulocyte macrophage-colony stimulating factor production in the lungs severely affects the ability of mice

to control Mycobacterium tuberculosis infection. *J. Leukoc. Biol.* **77,** 914–22 (2005).

103. Schneider, C. *et al.* Induction of the nuclear receptor PPAR-γ by the cytokine GM-CSF is critical for the differentiation of fetal monocytes into alveolar macrophages. *Nat. Immunol.* **15,** 1026–37 (2014).
104. Shalaby, F. *et al.* Failure of blood-island formation and vasculogenesis in Flk-1-deficient mice. *Nature* **376,** 62–66 (1995).
105. Boström, H. *et al.* PDGF-A signaling is a critical event in lung alveolar myofibroblast development and alveogenesis. *Cell* **85,** 863–73 (1996).
106. Cardoso, W. V. Molecular Regulation of Lung Development. *Annu. Rev. Physiol.* **63,** 471–494 (2001).
107. Corne, J. *et al.* IL-13 stimulates vascular endothelial cell growth factor and protects against hyperoxic acute lung injury. *J. Clin. Invest.* **106,** 783–791 (2000).
108. Buch, S. *et al.* Basic fibroblast growth factor and growth factor receptor gene expression in 85% O2-exposed rat lung. *Am. J. Physiol.* **268,** L455-64 (1995).
109. Chen, G.-H. *et al.* Local GM-CSF-Dependent Differentiation and Activation of Pulmonary Dendritic Cells and Macrophages Protect against Progressive Cryptococcal Lung Infection in Mice. *J. Immunol.* **196,** 1810–21 (2016).
110. Ballinger, M. N. *et al.* Role of granulocyte macrophage colony-stimulating factor during gram-negative lung infection with Pseudomonas aeruginosa. *Am. J. Respir. Cell Mol. Biol.* **34,** 766–74 (2006).
111. Trapnell, B. C. & Whitsett, J. A. GM-CSF Regulates Pulmonary Surfactant Homeostasis and Alveolar Macrophage-Mediated Innate Host Defense. *Annu. Rev. Physiol.* **64,** 775–802 (2002).
112. Unkel, B. *et al.* Alveolar epithelial cells orchestrate DC function in murine viral pneumonia. *J. Clin. Invest.* **122,** 3652–64 (2012).
113. Cakarova, L. *et al.* Macrophage tumor necrosis factor-α induces epithelial expression of granulocyte-macrophage colony-stimulating factor: Impact on

alveolar epithelial repair. *Am. J. Respir. Crit. Care Med.* **180,** 521–532 (2009).

114. Huch, M. & Koo, B.-K. Modeling mouse and human development using organoid cultures. *Development* **142,** (2015).
115. Lancaster, M. a. & Knoblich, J. a. Organogenesis in a dish: modeling development and disease using organoid technologies. *Science* **345,** 1247125 (2014).
116. Murrow, L. M., Weber, R. J. & Gartner, Z. J. Dissecting the stem cell niche with organoid models: an engineering-based approach. *Development* **144,** 998–1007 (2017).
117. Huch, M., Knoblich, J. A., Lutolf, M. P. & Martinez-Arias, A. The hope and the hype of organoid research. *Development* **144,** (2017).
118. Eiraku, M. & Sasai, Y. Self-formation of layered neural structures in three-dimensional culture of ES cells. *Curr. Opin. Neurobiol.* **22,** 768–777 (2012).
119. Dontu, G. *et al.* In vitro propagation and transcriptional profiling of human mammary stem/progenitor cells. *Genes Dev.* **17,** 1253–70 (2003).
120. Long, M. W. *et al.* Three-dimensional cellular development is essential for ex vivo formation of human bone. *Nat. Biotechnol.* **18,** 954–958 (2000).
121. Sato, T. *et al.* Single Lgr5 stem cells build crypt–villus structures in vitro without a mesenchymal niche. *Nature* **459,** 262–265 (2009).
122. Spence, J. R. *et al.* Directed differentiation of human pluripotent stem cells into intestinal tissue in vitro. *Nature* **470,** 105–9 (2011).
123. Barker, N. *et al.* Lgr5+ve Stem Cells Drive Self-Renewal in the Stomach and Build Long-Lived Gastric Units In Vitro. *Cell Stem Cell* **6,** 25–36 (2010).
124. McCracken, K. W. *et al.* Modelling human development and disease in pluripotent stem-cell-derived gastric organoids. *Nature* **516,** 400–404 (2014).
125. Sato, T. *et al.* Long-term Expansion of Epithelial Organoids From Human Colon, Adenoma, Adenocarcinoma, and Barrett's Epithelium. *Gastroenterology* **141,** 1762–1772 (2011).
126. Huch, M. *et al.* Long-Term Culture of Genome-Stable Bipotent Stem Cells from

Adult Human Liver. *Cell* **160,** 299–312 (2015).

127. Takebe, T. *et al.* Vascularized and functional human liver from an iPSC-derived organ bud transplant. *Nature* **499,** 481–484 (2013).
128. Huch, M. *et al.* Unlimited in vitro expansion of adult bi-potent pancreas progenitors through the Lgr5/R-spondin axis. *EMBO J.* **32,** 2708–2721 (2013).
129. Eiraku, M. *et al.* Self-organizing optic-cup morphogenesis in three-dimensional culture. *Nature* **472,** 51–56 (2011).
130. Lancaster, M. A. *et al.* Cerebral organoids model human brain development and microcephaly. *Nature* **501,** 373–379 (2013).
131. Antonica, F. *et al.* Generation of functional thyroid from embryonic stem cells. *Nature* **491,** 66–71 (2012).
132. Stevens, K. R., Pabon, L., Muskheli, V. & Murry, C. E. Scaffold-Free Human Cardiac Tissue Patch Created from Embryonic Stem Cells. *Tissue Eng. Part A* **15,** 1211–1222 (2009).
133. Gao, D. *et al.* Organoid Cultures Derived from Patients with Advanced Prostate Cancer. *Cell* **159,** 176–187 (2014).
134. Lee, J. H. *et al.* Lung stem cell differentiation in mice directed by endothelial cells via a BMP4-NFATc1-thrombospondin-1 axis. *Cell* **156,** 440–455 (2014).
135. Dye, B. R. *et al.* In vitro generation of human pluripotent stem cell derived lung organoids. *Elife* **4,** e05098 (2015).
136. Hogan, B. L. M. *et al.* Repair and regeneration of the respiratory system: Complexity, plasticity, and mechanisms of lung stem cell function. *Cell Stem Cell* **15,** 123–138 (2014).
137. Hegab, A. E. *et al.* Mimicking the niche of lung epithelial stem cells and characterization of several effectors of their in vitro behavior. *Stem Cell Res.* **15,** 109–121 (2015).
138. Kleinman, H. K. & Martin, G. R. Matrigel: Basement membrane matrix with biological activity. *Semin. Cancer Biol.* **15,** 378–386 (2005).
139. Van Haute, L., De Block, G., Liebaers, I., Sermon, K. & De Rycke, M. Generation

of lung epithelial-like tissue from human embryonic stem cells. *Respir. Res.* **10,** 105 (2009).

140. Delgado, O. *et al.* Multipotent capacity of immortalized human bronchial epithelial cells. *PLoS One* **6,** e22023 (2011).
141. Nadkarni, R. R., Abed, S. & Draper, J. S. Organoids as a model system for studying human lung development and disease. *Biochem. Biophys. Res. Commun.* **473,** 675–682 (2016).
142. Vladar, E. K., Bayly, R. D., Sangoram, A. M., Scott, M. P. & Axelrod, J. D. Microtubules Enable the Planar Cell Polarity of Airway Cilia. *Curr. Biol.* **22,** 2203–2212 (2012).
143. Mou, H. *et al.* Dual SMAD Signaling Inhibition Enables Long-Term Expansion of Diverse Epithelial Basal Cells. *Cell Stem Cell* **19,** 217–231 (2016).
144. Tadokoro, T., Gao, X., Hong, C. C., Hotten, D. & Hogan, B. L. M. BMP signaling and cellular dynamics during regeneration of airway epithelium from basal progenitors. *Development* **143,** 764–73 (2016).
145. Butler, C. R. *et al.* Rapid Expansion of Human Epithelial Stem Cells Suitable for Airway Tissue Engineering. *Am. J. Respir. Crit. Care Med.* **194,** 156–168 (2016).
146. Danahay, H. *et al.* Notch2 Is Required for Inflammatory Cytokine-Driven Goblet Cell Metaplasia in the Lung. *Cell Rep.* **10,** 239–252 (2015).
147. Hild, M. & Jaffe, A. B. Production of 3-D Airway Organoids From Primary Human Airway Basal Cells and Their Use in High-Throughput Screening. *Curr. Protoc. Stem Cell Biol* **37915,** 1–15 (2016).
148. Guseh, J. S. *et al.* Notch signaling promotes airway mucous metaplasia and inhibits alveolar development. *Development* **136,** 1751–1759 (2009).
149. Rock, J. R. *et al.* Notch-dependent differentiation of adult airway basal stem cells. *Cell Stem Cell* **8,** 639–648 (2011).
150. Gao, X., Bali, A. S., Randell, S. H. & Hogan, B. L. M. GRHL2 coordinates regeneration of a polarized mucociliary epithelium from basal stem cells. *J. Cell Biol.* **211,** 669–682 (2015).

151. Chen, H. *et al.* Airway epithelial progenitors are region specific and show differential responses to bleomycin-induced lung injury. *Stem Cells* **30,** 1948–60 (2012).

152. Leeman, K. T., Fillmore, C. M. & Kim, C. F. Lung stem and progenitor cells in tissue homeostasis and disease. *Curr. Top. Dev. Biol.* **107,** 207–33 (2014).

153. Tropea, K. a *et al.* Bronchioalveolar stem cells increase after mesenchymal stromal cell treatment in a mouse model of bronchopulmonary dysplasia. *Am. J. Physiol. Lung Cell. Mol. Physiol.* **302,** L829-37 (2012).

154. Jain, R. *et al.* Plasticity of Hopx(+) type I alveolar cells to regenerate type II cells in the lung. *Nat. Commun.* **6,** 6727 (2015).

155. Gonzalez, R. F., Allen, L., Gonzales, L., Ballard, P. L. & Dobbs, L. G. HTII-280, a Biomarker Specific to the Apical Plasma Membrane of Human Lung Alveolar Type II Cells. *J. Histochem. Cytochem.* **58,** 891–901 (2010).

156. Takahashi, K. *et al.* Induction of Pluripotent Stem Cells from Adult Human Fibroblasts by Defined Factors. *Cell* **131,** 861–872 (2007).

157. Yu, J. *et al.* Induced Pluripotent Stem Cell Lines Derived from Human Somatic Cells. *Science (80-.).* **318,** 1917–1920 (2007).

158. Takahashi, K. & Yamanaka, S. Induction of Pluripotent Stem Cells from Mouse Embryonic and Adult Fibroblast Cultures by Defined Factors. *Cell* **126,** 663–676 (2006).

159. Mou, H. *et al.* Generation of multipotent lung and airway progenitors from mouse ESCs and patient-specific cystic fibrosis iPSCs. *Cell Stem Cell* **10,** 385–97 (2012).

160. Vladar, E. K., Nayak, J. V, Milla, C. E. & Axelrod, J. D. Airway epithelial homeostasis and planar cell polarity signaling depend on multiciliated cell differentiation. *JCI insight* **1,** (2016).

161. Wong, A. P. *et al.* Directed differentiation of human pluripotent stem cells into mature airway epithelia expressing functional CFTR protein. *Nat. Biotechnol.* **30,** 876–82 (2012).

162. Green, M. D. *et al.* Generation of anterior foregut endoderm from human embryonic and induced pluripotent stem cells. *Nat. Biotechnol.* **29,** 267–272 (2011).

163. Longmire, T. A. *et al.* Efficient derivation of purified lung and thyroid progenitors from embryonic stem cells. *Cell Stem Cell* **10,** 398–411 (2012).

164. Huang, S. X. L. *et al.* Efficient generation of lung and airway epithelial cells from human pluripotent stem cells. *Nat. Biotechnol.* **32,** 84–91 (2014).

165. Firth, A. L. *et al.* Generation of multiciliated cells in functional airway epithelia from human induced pluripotent stem cells. *Proc. Natl. Acad. Sci. U. S. A.* **111,** E1723-30 (2014).

166. McIntyre, B. A. S. *et al.* Expansive generation of functional airway epithelium from human embryonic stem cells. *Stem Cells Transl. Med.* **3,** 7–17 (2014).

167. Clevers, H. Modeling Development and Disease with Organoids. *Cell* **165,** 1586–1597 (2016).

168. Huang, S. X. L. *et al.* The in vitro generation of lung and airway progenitor cells from human pluripotent stem cells. *Nat. Protoc.* **10,** 413–25 (2015).

169. Mondrinos, M. J., Jones, P. L., Finck, C. M. & Lelkes, P. I. Engineering de novo assembly of fetal pulmonary organoids. *Tissue Eng. Part A* **20,** 2892–907 (2014).

170. Rosen, C. *et al.* Preconditioning allows engraftment of mouse and human embryonic lung cells, enabling lung repair in mice. *Nat Med* **21,** 869–879 (2015).

171. Dye, B. R. *et al.* A bioengineered niche promotes in vivo engraftment and maturation of pluripotent stem cell derived human lung organoids. *Elife* **5,** 3025–3036 (2016).

172. Gotoh, S. *et al.* Generation of alveolar epithelial spheroids via isolated progenitor cells from human pluripotent stem cells. *Stem cell reports* **3,** 394–403 (2014).

173. Herold, S. *et al.* Alveolar Epithelial Cells Direct Monocyte Transepithelial

Migration upon Influenza Virus Infection: Impact of Chemokines and Adhesion Molecules TL - 177. *J. Immunol.* **177 VN-,** 1817–1824 (2006).

174. Reuther, P. *et al.* Generation of a variety of stable Influenza A reporter viruses by genetic engineering of the NS gene segment. *Sci Rep* **5,** 11346 (2015).
175. Tang, F., Hajkova, P., Barton, S. C., Lao, K. & Surani, M. A. MicroRNA expression profiling of single whole embryonic stem cells. *Nucleic Acids Res.* **34,** 1–7 (2006).
176. Panganiban, R. A. M. & Day, R. M. Hepatocyte growth factor in lung repair and pulmonary fibrosis. *Acta Pharmacol. Sin.* **32,** 12–20 (2011).
177. Pozarska, A. *et al.* Stereological monitoring of mouse lung alveolarization from the early postnatal period to adulthood. *Am. J. Physiol. - Lung Cell. Mol. Physiol.* **312,** L882–L895 (2017).
178. Green, J., Endale, M., Auer, H. & Perl, A.-K. T. Diversity of Interstitial Lung Fibroblasts Is Regulated by Platelet-Derived Growth Factor Receptor α Kinase Activity. *Am. J. Respir. Cell Mol. Biol.* **54,** 532–545 (2016).
179. McGowan, S. E. & Torday, J. S. The pulmonary lipofibroblast (lipid interstitial cell) and its contributions to alveolar development. *Annu. Rev. Physiol.* **59,** 43–62 (1997).
180. El Agha, E. & Bellusci, S. Walking along the Fibroblast Growth Factor 10 Route: A Key Pathway to Understand the Control and Regulation of Epithelial and Mesenchymal Cell-Lineage Formation during Lung Development and Repair after Injury. *Scientifica (Cairo).* **2014,** 538379 (2014).
181. Carraro, G. *et al.* miR-142-3p balances proliferation and differentiation of mesenchymal cells during lung development. *Development* **141,** 1272–81 (2014).
182. Clevers, H. & Nusse, R. Wnt/B-catenin signaling and disease. *Cell* **149,** 1192–1205 (2012).
183. DasGupta, R. & Fuchs, E. Multiple roles for activated LEF/TCF transcription complexes during hair follicle development and differentiation. *Development*

126, 4557–68 (1999).

184. Cakarova, L. *et al.* Macrophage Tumor Necrosis Factor-α Induces Epithelial Expression of Granulocyte–Macrophage Colony-stimulating Factor. *Am. J. Respir. Crit. Care Med.* **180,** 521–532 (2009).
185. Nishizaka, T. *et al.* Position-dependent linkages of fibronectin- integrin-cytoskeleton. *Proc. Natl. Acad. Sci.* **97,** 692–697 (2000).
186. Maden, M. & Hind, M. Retinoic acid in alveolar development, maintenance and regeneration. *Philos. Trans. R. Soc. B Biol. Sci.* **359,** 799–808 (2004).
187. Herold, S. *et al.* Lung epithelial apoptosis in influenza virus pneumonia : the role of macrophage- expressed TNF-related apoptosis- inducing ligand. *J. Exp. Med.* **205,** 3065–3078 (2008).
188. Franzdóttir, S. R. *et al.* Airway branching morphogenesis in three dimensional culture. *Respir. Res.* **11,** 162 (2010).
189. Pageau, S. C., Sazonova, O. V, Wong, J. Y., Soto, A. M. & Sonnenschein, C. The effect of stromal components on the modulation of the phenotype of human bronchial epithelial cells in 3D culture. *Biomaterials* **32,** 7169–7180 (2011).
190. Fessart, D., Begueret, H., Delom, F. & Fessart, D. Three-dimensional culture model to distinguish normal from malignant human bronchial epithelial cells. *Eur Respir J* **42,** 1345–1356 (2013).
191. Kaisani, A. *et al.* Branching morphogenesis of immortalized human bronchial epithelial cells in three-dimensional culture. *Differentiation.* **87,** 119–26 (2014).
192. Barkauskas, C. E. *et al.* Lung organoids: current uses and future promise.*Development*. doi:10.1242/dev.140103
193. Chen, Y.-W. *et al.* A three-dimensional model of human lung development and disease from pluripotent stem cells. *Nat. Cell Biol.* **19,** 542–549 (2017).
194. Herriges, M. & Morrisey, E. E. Lung development: orchestrating the generation and regeneration of a complex organ. *Development* **141,** 502–513 (2014).

195. McGowan, S. E. & Torday, J. S. THE PULMONARY LIPOFIBROBLAST (LIPID INTERSTITIAL CELL) AND ITS CONTRIBUTIONS TO ALVEOLAR DEVELOPMENT. *Annu. Rev. Physiol.* **59,** 43–62 (1997).
196. Chen, L., Acciani, T., Le Cras, T., Lutzko, C. & Perl, A.-K. T. Dynamic Regulation of Platelet-Derived Growth Factor Receptor α Expression in Alveolar Fibroblasts during Realveolarization. *Am. J. Respir. Cell Mol. Biol.* **47,** 517–527 (2012).
197. Moiseenko, A. *et al.* Origin and characterization of alpha smooth muscle actin-positive cells during murine lung development. *Stem Cells* **35,** 1566–1578 (2017).
198. Jones, C. V *et al.* M2 macrophage polarisation is associated with alveolar formation during postnatal lung development. *Respir. Res.* **14,** 41 (2013).
199. Mass, E. *et al.* Specification of tissue-resident macrophages during organogenesis. *Science (80-.).* **353,** aaf4238-aaf4238 (2016).
200. Tan, S. Y. S. & Krasnow, M. A. Developmental origin of lung macrophage diversity. *Development* **143,** 1318–1327 (2016).
201. Wynn, T. A. & Vannella, K. M. Macrophages in Tissue Repair, Regeneration, and Fibrosis. *Immunity* **44,** 450–462 (2016).
202. Lechner, A. J. *et al.* Recruited Monocytes and Type 2 Immunity Promote Lung Regeneration following Pneumonectomy. *Cell Stem Cell* **21,** 120–134.e7 (2017).
203. Peng, T. *et al.* Coordination of heart and lung co-development by a multipotent cardiopulmonary progenitor. *Nature* **500,** 589–592 (2013).
204. Broutier, L. *et al.* Culture and establishment of self-renewing human and mouse adult liver and pancreas 3D organoids and their genetic manipulation. *Nat. Protoc.* **11,** 1724–1743 (2016).
205. Unkel, B. *et al.* Alveolar epithelial cells orchestrate DC function in murine viral pneumonia. *J. Clin. Invest.* **122,** 3652–3664 (2012).
206. Laresgoiti, U. *et al.* Lung epithelial tip progenitors integrate glucocorticoid-

and STAT3-mediated signals to control progeny fate. *Development* **143,** 3686–3699 (2016).

207. Al-Shami, A., Mahanna, W. & Naccache, P. H. Granulocyte-macrophage colony-stimulating factor-activated signaling pathways in human neutrophils. Selective activation of Jak2, Stat3, and Stat5b. *J. Biol. Chem.* **273,** 1058–63 (1998).
208. Du, Y., Guo, M., Whitsett, J. A. & Xu, Y. 'LungGENS': a web-based tool for mapping single-cell gene expression in the developing lung: Figure 1. *Thorax* **70,** 1092–1094 (2015).
209. Bartfeld, S. & Clevers, H. Organoids as Model for Infectious Diseases: Culture of Human and Murine Stomach Organoids and Microinjection of Helicobacter Pylori. *J. Vis. Exp.* e53359–e53359 (2015). doi:10.3791/53359
210. Barkal, L. J. *et al.* Microbial volatile communication in human organotypic lung models. *Nat. Commun.* **8,** 1770 (2017).

9 SUPPLEMENT

9.1 List of figures and tables

Table	**Page**

9.2 Materials

9.2.1. Chemicals and consumables

Chemical/consumable	Manufacturer
Avicel	AMC Biopolymers, Brüssel (BEL)
Biotin-binder magnetic beads	Life Technologies, Carlsbad (USA)
BSA	Sigma-Aldrich, Taufkirchen (GER)
Cell culture flasks 75cm^2	Greiner, Nürtingen (GER)
Cell culture inserts 12mm	Merck Millipore, Darmstadt (GER)
Cell culture plates, single- and multi-well	Greiner, Nürtingen (GER)
Cell nylon filters 20µM	Merck Millipore, Darmstadt (GER)
Cell scraper, 18cm handle	Greiner, Nürtingen (GER)
Cell strainer filters 40, 70 and 100µm	BD Biosciences, San Jose (USA)
DAPI	Life Technologies, Carlsbad (USA)
DMEM	Gibco BRL, Karlsruhe (GER)
dNTP's	Thermo Scientific, Waltham (USA)
EDTA	Roth, Karlsruhe (GER)
Ethanol	Sigma-Aldrich, Taufkirchen (GER)
FCS	Life Technologies, Carlsbad (USA)
Fluoromount-G	SouthernBiotech, Birmingham (USA)

GentleMACS C tubes	Miltenyi Biotec, Bergisch Gladbach (GER)
HBSS	Gibco BRL, Karlsruhe (GER)
HEPES	Merck Millipore, Darmstadt (GER)
HS	Sigma-Aldrich, Taufkirchen (GER)
Insulin-Transferrin-Selenium	Biozym Scientific, Hessisch Oldendorf (GER)
L-Glutamine [200mM]	Gibco BRL, Karlsruhe (GER)
LipidTOX™ red neutral lipid stain	Thermo Scientific, Waltham (USA)
LipidTOX™ red phospholipidosis detection reagent	Thermo Scientific, Waltham (USA)
LysoTracker® Red DND-99	Thermo Scientific, Waltham (USA)
Magnesium sulfate	Sigma-Aldrich, Taufkirchen (GER)
Matrigel matrix	Corning Life Sciences, Tewksbury (USA)
Parafilm	American National, Greenwich (USA)
Paraformaldehyde	Merck, Darmstadt (GER)
PBS	Life Technologies, Carlsbad (USA)
PBS^{++} (containing MgCl)	PAN-Biotech, Aidenbach (GER)
Penicillin/Streptomycin [5000 U/ml]	Gibco BRL, Karlsruhe (GER)
Pipettes 10 µm	BioMedical Instruments, Zöllnitz (GER)
Polystyrene round-bottom tubes 5ml	BD Biosciences, San Jose (USA)
Polystyrene tubes, 15ml and 50ml	Greiner, Nürtingen (GER)
Potassium chloride	Sigma-Aldrich, Taufkirchen (GER)
Reaction tubes 0.5ml and 1.5ml	Eppendorf, Hamburg (GER)

Sandoglobulin	Novartis, Basel (CH)
Saponin	Merck Millipore, Darmstadt (GER)
SYBR Green I	Life Technologies, Carlsbad (USA)
Syringe 1ml, 10ml and 20ml	Braun, Melsungen (GER)
TissueTek	Sakura, Alphen aan den Rijn (NL)
Triton-X-100	Roth, Karlsruhe (GER)
Tween 80	Sigma-Aldrich, Taufkirchen (GER)
αMEM	Gibco BRL, Karlsruhe (GER)

9.2.2. Enzymes and morpholino

Enzyme/morpholino	Manufacturer
Accutase	Corning Life Sciences, Tewksbury (USA)
Dispase	Corning Life Sciences, Tewksbury (USA)
DNase I	Serva, Heidelberg (GER)
***miR142-3p* Scra /morpholino**	Gene Tools, LLC, Philomath (USA)
MLV-RT	Life Technologies, Carlsbad (USA)
Trypsin-EDTA	Merck Millipore, Darmstadt (GER)
Trypsin-TPCK	Worthington Biochemical, Lakewood (USA)

9.2.3. Antibodies

Antibody	Manufacturer

Biotinylated rat anti-mouse CD16/32	BD Biosciences, San Jose (USA)
Biotinylated rat anti-mouse CD31	BD Biosciences, San Jose (USA)
Biotinylated rat anti-mouse CD45	BD Biosciences, San Jose (USA)
CD11c FITC (clone: N418)	BioLegend, San Diego (USA)
CD206 (clone:MR5D3)	Thermo Scientific, Waltham (USA)
CD206 Alexa Fluor® 488 (clone: MMR)	BioLegend, San Diego (USA)
CD24 PE/CY7 (clone: M1/69)	BioLegend, San Diego (USA)
CD31 Alexa Flour 488 (clone 390)	BioLegend, San Diego (USA)
CD31 PB (clone 390)	BioLegend, San Diego (USA)
CD31 PE (clone 390)	BioLegend, San Diego (USA)
CD326 APC/Cy7 (clone G8.8)	BioLegend, San Diego (USA)
CD326 APC-eF780 (clone G8.8)	Thermo Scientific, Waltham (USA)
CD45 APC/Cy7 (clone 30-F11)	BioLegend, San Diego (USA)
CD45 FITC (clone 30-F11)	BD Biosciences, San Jose (USA)
CD45 Horizon™ V450 (clone 30-F11)	BD Biosciences, San Jose (USA)
CD45 Horizon™ V500 (clone: 30-F11)	BD Biosciences, San Jose (USA)
Gr1 PE-Cy7 (clone: RB68C5)	BioLegend, San Diego (USA)
IgG Alexa Fluor 488, mouse	Merck Millipore, Darmstadt (GER)
Influenza A Virus, polyclonal (clone ab20841)	Abcam, Cambridge (UK)
Isotype control IgG1 (clone: CT6)	Abcam, Cambridge (UK)
Isotype control IgG2a (clone RTK2758)	BioLegend, San Diego (USA)
Isotype control Syrian hamster IgG	BioLegend, San Diego (USA)

(clone SHG-1)	
Isotype-matched normal goat IgG	Santa Cruz Biotechnology, Dallas (USA)
Ki67 (clone: SolA15)	Thermo Scientific, Waltham (USA)
Ly6G APC (clone: 1A8)	BioLegend, San Diego (USA)
mAb anti-GM-CSF	R&D Systems, Inc. Minneapolis (USA)
NP FITC (clone: 431)	Abcam, Cambridge (UK)
PDPN APC (clone: 8.1.1.)	BioLegend, San Diego (USA)
Sca-1 APC (Clone: D7)	BioLegend, San Diego (USA)
Sca-1 PB (clone: D7)	BioLegend, San Diego (USA)
SCGB1A1 (clone T-18)	Santa Cruz Biotechnology, Dallas (USA)
Secondary goat Alexa Flour 647	Life Technologies, Carlsbad (USA)
Secondary goat Alexa Fluor 488	Life Technologies, Carlsbad (USA)
Secondary mouse Alexa Fluor 488	Life Technologies, Carlsbad (USA)
Secondary rabbit Alexa Fluor 555	Life Technologies, Carlsbad (USA)
SFTPC (polyclonal)	Merck Millipore, Darmstadt (GER)
Siglec-F APC-CY7 (clone: E50-2440)	BD Biosciences, San Jose (USA)
Siglec-F eFluor 660 (clone: 1RNM44N)	Thermo Scientific, Waltham (USA)
αSMA APC (clone: 1A4)	R&D Systems, Inc. Minneapolis (USA)
αSMA FITC (clone: 1A4)	Sigma-Aldrich, Taufkirchen (GER)
β-IVtubulin (clone: ONS.1A6)	Abcam, Cambridge (UK)

9.2.4. ELISA Kit

ELISA kit	**Manufacturer**

mouse GM-CSF, detection limit 7 pg/ml	R&D Systems, Minneapolis (USA)

9.3 List of Abbreviations

Abbreviations	
°C	Celsius
ALDH1	Aldehyde dehydrogenase isoform 1
APC	Allophycocyanin
approx.	approximately
BMP	Bone morphogenetic protein
BrdU	Bromodeoxyuridine
BSA	Bovine serum albumin
CD	Cluster of differentiation
cDNA	Complementary DNA
CreER	Cre recombinase
CRISPR	Clustered regularly interspaced short palindromic repeats
CyP450-2F2	Cytochrome P450 2F2, CYP2F2
DAPI	4',6-Diamidin-2-phenylindol
dH_2O	Deionized water
DMEM	Dulbecco's modified Eagle's medium
DNA	Desoxyribonucleic Acid
EDTA	Ethylendinitrilotetraacetic acid
EGF	Epidermal growth factor
ELISA	Enzyme Linked Immunosorbent Assay
EpCAM	Epithelial cell adhesion molecule
FACS	Fluorescence activated cell sorting, flow cytometry
FCS	Fetal calf serum
$Fe(CN)_6$	Ferricyanide
FGF	Fibroblast growth factor
FGF10	Fibroblast growth factor 10
FGFR2	Fibroblast growth factor receptor 2
FITC	Fluorescein isothiocyanate
Foxj1	Forkhead transcription factor
FP	Forward primer

G	G-force
g	Grams
GFP	Green fluorescent protein
h	Hours
HBSS	Hank's buffered salt solution
Hoxp	Homeobox only protein 1
HS	Horse serum
ICAM-1	Intercellular cell adhesion molecule-1
ID2	DNA-binding protein inhibitor
IL6	Interleukin 6
Itgβ4	Integrin beta 4
l	Liter
LEF/TCF	Lymphoid enhancer binding factor 1/transcription factor 3
Lrg6	leucine rich repeat containing G protein-coupled receptor 6
m	Milli
M	Molar
m^2	Square meter
mAb	Murine antibody
MCDK	Madin darbey canine kidney
MEM	Minimal essential medium
$MgCl_2$	Magnesium chloride
min	Minute
miRNA	Micro ribonucleic acid
M-MLV	Moloney Murine Leukemia Virus
mRNA	Messenger RNA
n	Nano
$NaHCO_3$	Sodium bicarbonate
NFATc1	Nuclear factor of activated T cell c1
NH_4Cl	Ammonium chloride
NKX2.1	NK2 homeobox 1
PB	Pacific blue
PBS	Phosphate buffered saline
PCR	Polymerase chain reaction
PE	Phycoerythrin
PFA	Paraformaldehyde
pfu	Plaque forming units
PI	Propidium iodide

PR8	Influenza virus A/Puerto Rico/8/34 (H1N1)
qPCR	Quantitative real time polymerase chain reaction
RNA	Ribonucleic acid
RP	Reverse primer
rpm	Revolutions per minute
s	Seconds
Sca-1	Stem cell antigen-1
SEM	Standard error of the mean
SO_2	Sulfur dioxide
SOX2	Sex determining region Y-box 2
SOX9	Sex determining region Y-box 9
SP	Surfactant protein
STAT3	Signal transducer and activator of transcription 3
TGFβ	Transforming growth factor beta
TPCK	Tosyl phenylalanyl chloromethyl ketone
U	Unit
YFP	Yellow fluorescent protein
α-MEM	Alpha minimal essential medium
ΔCt	Delta Ct
µ	Micro

9.4 Curriculum vitae

9.5 Acknowledgements

I would like to thank my supervisor Prof. Susanne Herold for her invaluable support and advice during these four years. My gratitute to Prof. Lohmeyer for giving me the opportunity to enter the lab. Special thanks to Monika Heiner for her guidance and patience, she undoubtedly helped me to find the way to move my project forward and made me a better researcher in the process.

I would also like to express my gratitute to Thomas Braun and Saverio Bellusci for the constructive criticism and resources given towards my PhD work. Thanks to my labmates and friends, Christin Peteranderl, Carole Schmoldt, Lina Jankauskaite, Bala Selvakumar, Jennifer Quantius, Matt Ulrich, Learta Pervizaj-Oruqaj, Christina Malainou, Margarida Barroso, and Ludmilla Sperling for the scientific advice, ideas and aid when I needed assistance but specially thank you for the fun and good memories outside the workplace.

Thank you to all the technicians: Julia Rupp, Julia Bespalowa, Maria Koch, Elena Roth, Margit Lohmeyer, Stefanie Jarmer, Larissa Hamann for the immense help I continuously got from them. Specially, my total gratitude to Steffi and Julia, I really could not have done all this work without their assistance.

Thanks to my MBML-friends for their constant encouragement that made every problem easier to surpass. Without them my experience here would have not been as memorable. Also, special thanks to Isabelle Salwig and Elie El Agha for their vital assistance, advice and friendship throughout this process.

A mi familia y amigos en México, gracias por su incondicional amor y apoyo durante cada etapa de mi vida. En especial, muchas gracias a mis padres, Ruben y Blanca, por su ejemplo. De ustedes aprendí a amar mi trabajo, a luchar incansablemente por lo que quiero lograr en la vida y a nunca tener miedo de soñar en grande.

Gracias por siempre haber creído en mi y en mis locos sueños. Todos mis logros tambien son suyos. Los amo.

My whole gratitude to my beloved husband and best friend Alberto for his enourmous support troughtout these years. Thank you for making me believe that I can achieve everything I want in life. You are my rock and I could not have done it without your endless love and encouragement.

¡Sí se pudo!

9.6 Affirmation

"I declare that I have completed this dissertation single-handedly without the unauthorized help of a second party and only with the assistance acknowledged therein. I have appropriately acknowledged and referenced all text passages that are derived literally from or are based on the content of published or unpublished work of others, and all information that relates to verbal communications. I have abided by the principles of good scientific conduct laid down in the charter of the Justus Liebig University of Giessen in carrying out the investigations described in the dissertation."

Giessen, 26th September 2018

Ana Ivonne Vázquez Armendariz